

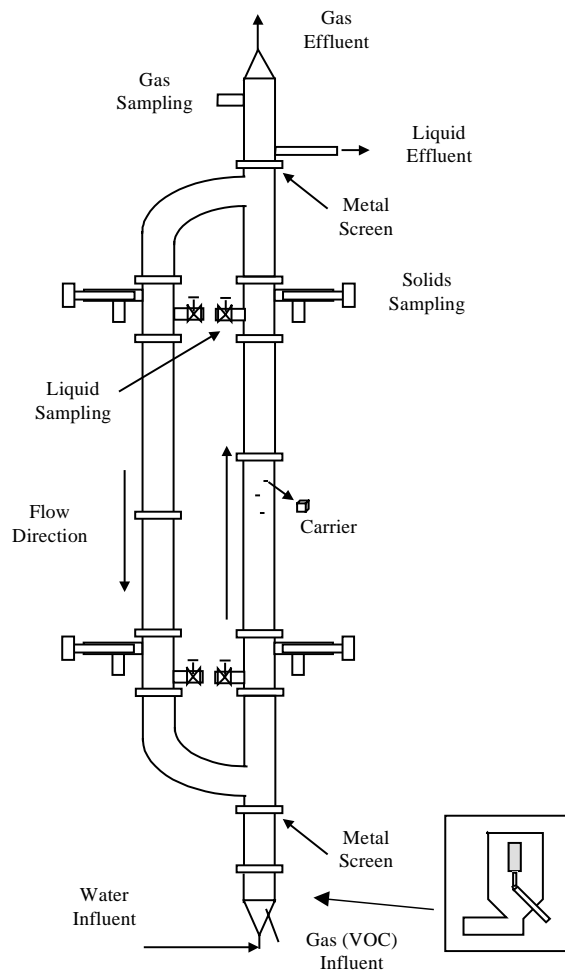


US Army Corps
of Engineers®
Engineer Research and
Development Center

Treatment of Volatile Organic Compounds From Gas Streams Using a Three-Phase Circulating-Bed Biofilm Reactor

by Byung J. Kim, Haibo Yu, and Bruce E. Rittmann

April 2000



Foreword

This study was conducted for the Directorate of Research and Development, Headquarters, U.S. Army Corps of Engineers under 622720D048, "Industrial Operations Pollution Control (6.2 Exploratory Development), Work Unit U29, "Biofilter Technology for Munitions Productions VOCs." The technical reviewer was Chris Vercautren, Industrial Operations Command.

The work was performed by the Environmental Processes Branch (CN-E) of the Installations Division (CN), Construction Engineering Research Laboratory (CERL). The CERL Principal Investigator was Dr. Byung J. Kim. Dr. Haibo Yu is a research engineer with Amoco, and Dr. Bruce E. Rittmann is a professor with the Civil Engineering Department, Northwestern University, Evanston, IL. The technical editor was Linda L. Wheatley, Information Technology Laboratory. Dr. Ilker Adiguzel is Chief, CN-E, and Dr. John T. Bandy is Chief, CN. The Acting Director of CERL is Dr. Alan W. Moore.

CERL is an element of the U.S. Army Engineer Research and Development Center (ERDC), U.S. Army Corps of Engineers. The Acting Director of ERDC is Dr. Lewis E. Link and the Commander is COL Robin R. Cababa, EN.

DISCLAIMER

The contents of this report are not to be used for advertising, publication, or promotional purposes. Citation of trade names does not constitute an official endorsement or approval of the use of such commercial products. All product names and trademarks cited are the property of their respective owners.

The findings of this report are not to be construed as an official Department of the Army position unless so designated by other authorized documents.

DESTROY THIS REPORT WHEN IT IS NO LONGER NEEDED. DO NOT RETURN IT TO THE ORIGINATOR.

Contents

Foreword	2
List of Figures and Tables	5
1 Introduction	9
Background	9
Objectives	12
Approach	13
Scope	14
Mode of Technology Transfer.....	14
Units of Weight and Measure.....	14
2 The Circulating-Bed Biofilm Reactor	15
Reactor Design	15
Analytical Techniques and Calibrations	20
Hydrodynamics and Gas-Liquid Mass Transfer.....	30
3 BTX Removal Experiments	35
General Approaches	35
Toluene as the Sole Substrate	35
Dual Substrates.....	38
4 Kinetic Analysis	39
Kinetics of BTX Degradation.....	39
Basic Mechanisms of Biofilm Removal.....	39
Removals in the Circulating-Bed Biofilm Reactor	42
5 Results	48
Gas-Liquid Mass Transfer.....	48
Biomass in the Circulating-Bed Biofilm Reactor	49
Removals of Toluene as the Sole Substrate.....	51
Removals of Toluene and Benzene as Dual Substrates.....	66
Removals of Toluene and <i>p</i> -Xylene as Dual Substrates.....	76
6 Nitroglycerin Removal	81
Introduction	81
Experiments	85

Results and Discussion.....	87
Summary.....	90
7 Conclusions and Practical Implications	92
References.....	95
CERL Distribution.....	99

List of Figures and Tables

Figures

1	Design of the circulating-bed biofilm reactor	16
2	Nutrient feeding system for the biofilm reactor	16
3	BTX feeding system for the biofilm reactor	18
4	Sampling port for carriers	19
5	Calibration relationship between biomass concentration and Net OD.....	21
6	A typical COD standard calibration curve for 0-40 mg/l COD vials	22
7	DO-probe calibration apparatus	26
8	Flowpath of dissolved oxygen measurement	27
9	Apparatus for gas-flow calibration	28
10	Gas flowmeter calibrations	29
11	Circulation velocities of carriers in the circulating-bed reactor.....	30
12	Gas holdup in the riser	31
13	Detailed drawing of the gas feed system	32
14	Gas-liquid mass-transfer coefficient in the circulating-bed reactor	34
15	Typical concentration profile of a VOC (S) in a gas-liquid-solid three-phase biofilm reactor.....	41
16	Relationship between toluene concentrations in the gas and liquid phases	48
17	Relationship between (a) benzene and (b) <i>p</i> -xylene concentrations in the gas and liquid phases.....	49
18	Average weight of biomass per porous carrier.....	50
19	Measured and average biomass concentrations in the bulk liquid during steady states Ss1-Ss3 and their short-term experiments	51
20	DO concentrations in the bulk liquid during Ss1-Ss3.....	52
21	Toluene concentrations in the gas effluent during Ss1-Ss3.....	53
22	COD concentrations in the bulk liquid during Ss1-Ss3	53
23	COD concentrations in the bulk liquid during Ss1-Ss3	54
24	The fraction of COD in the liquid that was toluene during Ss1-Ss3.....	54
25	Toluene removal from the circulating bed during Ss1-Ss3.....	56
26	COD removal from the circulating bed during Ss1-Ss3	56
27	COD removals at various concentrations of toluene and DO from the circulating bed during Ss1-Ss3	57

28	Percentages of toluene removal by the suspended biomass to the total toluene removal during steady states Ss1-Ss3 and their short-term experiments	58
29	Percentages of toluene intermediate removal by the suspended biomass to its total removal during steady states Ss1-Ss3 and their short-term experiments	58
30	Percentages of oxygen consumed by the suspended biomass to its total consumption during steady states Ss1-Ss3 and their short-term experiments.....	59
31	Relationship between total toluene/oxygen loading rates and their biofilm removals during steady states Ss1-Ss3 and their short-term experiments	60
32	Relationship between toluene/oxygen fluxes and the total effectiveness factors for toluene during steady states Ss1-Ss3 and their short-term experiments	60
33	Relationship between total toluene/oxygen loading and the mass fluxes of toluene intermediate into the biofilm during steady states Ss1-Ss3 and their short-term experiments	61
34	Mass fluxes of toluene intermediate into the biofilm at various ratios of toluene and oxygen fluxes	62
35	Dependency of toluene fluxes into the biofilm on the concentrations of toluene and oxygen in the liquid.....	63
36	Dependency of intermediate fluxes into the biofilm on the concentrations of toluene and oxygen in the liquid.....	64
37	Dependency of oxygen fluxes into the biofilm on the concentrations of toluene and oxygen in the liquid.....	64
38	Concentrations of toluene and benzene in the gas effluent during Ss4-Ss6	66
39	Concentrations of toluene and benzene in the liquid effluent during Ss4-Ss6	67
40	DO and COD concentrations in the bulk liquid during Ss4-Ss6.....	68
41	Toluene and benzene removals from the circulating bed during Ss4-Ss6.....	68
42	COD removals from the circulating bed during Ss4-Ss6	69
43	Percentages of toluene and benzene intermediates removed by suspended biomass during Ss4-Ss6	70
44	Effect of benzene loading on toluene and benzene removal during Ss4-Ss6	71
45	Effect of benzene loading on COD removals and during Ss4-Ss6	72
46	Percentages of toluene and benzene removals caused by suspended biomass during Ss4-Ss6	73
47	Percentages of toluene and benzene intermediate removals caused by suspended biomass during Ss4-Ss6.....	74
48	Relationship between toluene/benzene loading rates and the their mass fluxes into the biofilm during Ss4-Ss6.....	74
49	Relationship between total toluene/benzene loading and the mass fluxes of their intermediates into the biofilm during Ss4-Ss6.....	75
50	Toluene and <i>p</i> -xylene concentrations in the gas effluent during Ss7-Ss8	76
51	Toluene and <i>p</i> -xylene concentrations in the liquid effluent during Ss7-Ss8.....	77

52	DO and COD concentrations in the bulk liquid during Ss7-Ss8.....	77
53	Toluene and <i>p</i> -xylene removal from the circulating bed during Ss7-Ss8.....	78
54	COD Removals from the circulating bed during Ss7-Ss8.....	79
55	Relationship between toluene/benzene loading and the their mass fluxes into the biofilm during Ss4-Ss6	79
56	Biological pathway of NG denitration	84
57	Possible denitration mechanisms (a) hydrolytic reaction followed by nitrate reduction; (b) direct reductive reaction.....	85
58	Dynamic responses of NG, GDN, and GMN (estimated) in the liquid effluent of circulating-bed biofilm reactor fed with 22.0 μM of NG	87
59	Steady-state concentrations of NG, GDN, and GMN (estimated) in the liquid effluent of the circulating-bed biofilm reactor fed with 22.0 μM of NG	88
60	NG removal and GDN/GMN production in the circulating-bed biofilm reactor during the steady state and pseudo-steady-states experiments.....	89
61	Transformation of NG during the steady state and pseudo-steady-states experiments.....	89

Tables

1	List of VOCs defined as priority pollutants by the USEPA	9
2	Summary of VOC control technologies.....	11
3	Total cost comparison of several VOC-abatement technologies	11
4	Composition of the minimal mineral medium	17
5	Gas flowrate setup for the GC/FID system	23
6	Temperature programs of GC and BTX retention times (RT)	23
7	Values of parameters <i>a</i> and <i>b</i> in GC standard calibration curves.....	24
8	Typical retention times (RT) in the HPLC column	25
9	Reactor loading conditions when toluene was the sole carbon source	36
10	Reactor loading conditions when toluene and benzene were supplied.....	37
11	Reactor loading conditions when toluene and <i>p</i> -xylene were supplied	37
12	Summary of kinetic parameters for BTX degradation	40
13	New groups of the runs of Ss4-Ss6	71
14	Studies of bacterial biodegradation of nitroglycerin	82
15	Circulating-bed reactor performance during two identical steady states	86
16	Circulating-bed reactor performance during NG-removal experiments	90

1 Introduction

Background

Volatile Organic Compounds

Volatile organic compounds (VOCs) are organic chemicals that have a boiling point ≤ 100 °C and/or a vapor pressure ≥ 1 mmHg at 25 °C (Tchobanoglous and Burton 1991). They include alkane gases (e.g., methane), alcohols (e.g., methanol), low-molecular-weight petroleum hydrocarbons (e.g., benzene and toluene), halogenated aromatics (e.g., chlorobenzenes), and halogenated solvents (e.g., TCA and TCE). Table 1 lists the 31 (out of the 129) priority pollutants designated by the U.S. Environmental Protection Agency (USEPA) as volatile organic compounds. They are of particular environmental interest because they are very mobile, especially in the vapor phase, may affect the human senses through odor, may exert a narcotic effect, and may be toxic and even carcinogenic. VOCs also react with nitrogen oxides and other airborne chemicals photochemically to form ground level ozone, which is a primary component of smog. Recently, especially after the passage of the Clean Air Act Amendments of 1990 (CAAA), emission of VOCs to the atmosphere is receiving close scrutiny and becoming a greater concern to regulatory agencies, industry, and the general public.

Table 1. List of VOCs defined as priority pollutants by the USEPA.

1. Acrolein	17. 1,2-Dichloropropane
2. Acrylonitrile	18. 1,3-Dichloropropylene
3. Benzene	19. Ethylbenzene
4. Bis (Chloromethyl) Ether	20. Methyl Bromide
5. Bromoform	21. Methyl Chloride
6. Carbon Tetrachloride	22. Methylene Chloride
7. Chlorobenzene	23. 1,1,2,2-Tetrachloroethane
8. Chlorodibromomethane	24. Tetrachloroethylene
9. Chloroethane	25. Toluene
10. 2-Chloroethyl vinyl Ether	26. 1,2-Trans-Dichloroethylene
11. Chloroform	27. 1,1,1-Trichloroethane
12. Dichlorobromomethane	28. 1,1,2-Trichloroethane
13. Dichlorodifluoromethane	29. Trichloroethylene
14. 1,1-Dichloroethane	30. Trichlorofluoromethane
15. 1,2-Dichloroethane	31. Vinyl Chloride
16. 1,1-Dichloroethylene	

Among the gas streams containing VOCs are off-gases from air strippers, aerobic biological treatment, anaerobic treatment, and bioremediation by bioventing and air sparging (Webster et al. 1996; Ruddy and Carroll 1993). Other sources include direct emissions/leakage from manufacturing and storage facilities, such as refineries and gasoline-storage tanks; landfills; motor vehicles; and commercial use (Jutras et al. 1997). At Army installations, VOC sources include ammunition plant, depot, and arsenal activities and clean-up operations. Because of the risk they pose, contaminated gas streams may need to be treated to remove the VOCs before being released into the atmosphere.

Table 2 lists the many technologies developed to control the emission of VOCs. Although each VOC-abatement method has its unique advantages and applications, biological treatment systems have several advantages over other treatment methods that make them very appealing. Table 3 illustrates that low capital and operating costs are the main benefits of biological processes. Furthermore, since many VOCs can be biodegraded into H₂O, CO₂, and mineral salts, no secondary pollutants or residues require further treatment.

Biological processes have been found most successful in treating large volumes of gas streams that contain only low concentrations (typically ≤ 1000 ppm or roughly 1000 mg/m³) of organic target pollutants. VOC removal rates of 50 to 94 percent have been reported, depending on the chemical and biological reactivity of the chemicals and operating conditions (Leson and Winer 1991). When biological processes are limited by a high concentration of VOCs in gas streams or poor biodegradability of some components, they can be combined with other treatment methods to obtain a satisfactory system from capital, operating, and efficiency stand-points (Standefer and van Lith 1993).

Three groups of biological treatment systems have been developed to remove VOCs from gas streams, as well as oxidizable inorganic compounds such as H₂S and NH₃. The treatment systems are bioscrubbers, trickling filters, and biofilters (Ottengraf 1987). In a bioscrubber, the microbial flora are dispersed in the aqueous phase, which countercurrently contacts the gas stream through a spray column. In trickling filters and biofilters, the microbial flora are immobilized on a carrier or packing material. In most cases, the liquid (water) flows down the reactor, while gas streams flow countercurrently upward to achieve better contact between the gas and liquid phases. These two processes differ from a biofilter in that sufficient water is circulated so that the aqueous phase is continuously moving downward in a trickling filter. The water circulation is very small (if any) in the biofilter, and it can be viewed as essentially stationary.

Table 2. Summary of VOC control technologies.

Technology	VOC Category	Emission Stream Flow Rate, scfm	VOC Concentration, ppmv
Thermal oxidation	AHC, HHC, A, K	< 20,000 w/o heat recovery	20-1,000 w/o heat recovery
		≥ 20,000 w/ heat recovery	≥ 1,000 w/ heat recovery
Catalytic oxidation	AHC, HHC†, A, K	Unlimited	50-10,000
Flaring	AHC, A, K		
Condensation	AHC, HHC†, A, K	≤ 2,000	5,000-12,000
Adsorption	AHC, HHC, A	≥ 300	20-20,000
Absorption	A, K	≥ 1,000	1,000-20,000
Boilers and process heaters	AHC, A, K		
Biological processes	AHC, HHC†, A, K	Unlimited	500-20,000
Membrane separation	AHC, HHC, A, K		0-1,000
Ultraviolet oxidation	AHC, HHC, A, K		

Legend: AHC = aliphatic and aromatic hydrocarbons; HHC = halogenated hydrocarbons († = limited applicability); A = alcohols, glycols, ethers, epoxides, and phenols; K = ketones and aldehydes.

Source: Moretti and Mukhopadhyay (1993). Reproduced with permission of the American Institute of Chemical Engineers ©1993 AIChE. All rights reserved.

Table 3. Total cost comparison of several VOC-abatement technologies.

	Total cost per 10 ⁶ ft ³ of air*	
Incineration		\$130
Chlorine		\$60
Ozone		\$60
Activated Carbon (with regeneration)		\$20
Biofiltration		\$8
*Costs obtained from Jaeger and Jager (1978) and converted to 1991 dollars.		
	Operation Cost	
	Fuel/chemical consumption	Power
Incinerator**	\$15 per cfm	Negligible
Wet Chemical Scrubbing	Up to \$8 per cfm	1 W per cfm
Soil Beds	0	0.6 W per cfm
**Costs obtained from Vaart, Vatavuk, and Wehe (1991).		

Source: Bohn (1992). Reproduced with permission of the American Institute of Chemical Engineers ©1992 AIChE. All rights reserved.

Biological treatment for removing VOCs from gas streams has been accepted in Europe and Japan as an effective technique to treat VOCs and odor-containing industrial exhaust (Fouhy 1992; Leson and Winer 1991). In the United States, it was until recently still considered a new and untested technology (Fouhy 1992; Bohn 1992), but has since been receiving increasing attention because of its effectiveness and low costs (Swanson and Loehr 1997). However, fundamental

research is needed in areas such as: reaction kinetics for the rate-limiting steps of biodegradation in a biofilm system; substrate interactions during microbial degradation; the special role of oxygen; and the impact of metabolic intermediates. This research focuses on these four areas.

Selection of Model VOCs and Bacterial Species

Most of the commonly encountered VOCs are biodegradable. However, because of the variability in structures and biological reactivity of the organic compounds, they are biodegraded at different rates and under different conditions. Under aerobic conditions, the VOCs that can be degraded rapidly include alcohols, aldehydes, ketones, ethers, esters, organic acids, amines, and thiols. Aliphatic and aromatic hydrocarbons, phenols, and methylene chloride generally are degraded at a slower speed, while aliphatics degrade faster than aromatics such as toluene, benzene, xylene, and styrene. Polyaromatic hydrocarbons and highly halogenated hydrocarbons, such as trichloroethylene, trichloroethane, carbon tetrachloride, and pentachlorophenol, have the slowest degradation rate among the VOCs (Bohn 1992). For highly halogenated hydrocarbons, anaerobic biodegradation, such as reductive dehalogenation, is a successful alternative (Parsons, Barrio-Lage, and Rice 1985).

For VOCs in gas streams, the reactions will be aerobic in most cases. One reason is that the gas stream to be treated usually is air contaminated with relatively low concentrations of VOCs. The 21 percent oxygen content of air means that establishing anaerobic conditions will be difficult and costly. In addition, most of the key VOCs are best or only degraded under aerobic conditions. This situation is particularly true for the petroleum hydrocarbons and alkane gases.

Although a large number of VOCs were available for study, it was decided that benzene, toluene, and *p*-xylene (BTX) would be the model VOCs. BTX are the most frequently found aromatic hydrocarbons in soil and groundwater at sites contaminated by petroleum products. A well-studied aromatics-degrading bacterial species, *Pseudomonas putida* F1, was used as the model biomass.

Objectives

This report summarizes the results of a performance evaluation of a three-phase circulating-bed reactor, a modified bioscrubber. The three-phase circulating-bed reactor is one of three biofilter configurations that the U.S. Army Engineer Research and Development Center (ERDC) is working on. The performances of two

other systems (i.e., biotrickling filter and mechanized biofilter) are being evaluated and will be reported in future ERDC technical reports.

The objectives of this study were to:

1. Analyze the effects of pollutants and oxygen loading rates on biological treatment of VOCs and hazardous air pollutants (HAPs).
2. Investigate biological treatment kinetics in terms of mass transfer and reaction rate.
3. Understand competitive treatment when the number of pollutants in air emissions is two or more.
4. Analyze the effects of intermediate products and biomass accumulation on the treatment efficiencies.
5. Test the feasibility of treating energetic compounds, specifically NG, in the three-phase circulating-bed reactor.

Approach

This study presents the design, hydrodynamic studies, and biofilm experiments of a three-phase circulating-bed biofilm reactor for gas-phase BTX removal. The reactor uses gas flow to create an airlift pump that circulates liquid and solids phases. Mass-transfer and hydrodynamic experiments were performed to characterize the circulating bed. The main work involved a series of steady-state and pseudo-steady-state experiments to assess the removal kinetics of BTX in the circulating-bed biofilm reactor. The various trends in reactor performance for removing BTX from gas streams are interpreted with the aid of kinetic analysis of the transport/reaction processes in all three phases. The following questions are answered. First, how do BTX and oxygen loading rates affect the removal efficiency of the fluidized bed? Second, how do mass transfer and reaction control the process? Third, how does the presence of a second substrate affect the overall reactor performance? Fourth, how does intermediate formation affect liquid effluent quality and biofilm accumulation?

Finally, the circulating fluidized-bed biofilm reactor is applied to remove nitroglycerin (NG) from contaminated liquid. At this time, practical treatment technology for NG in air is not available.

Scope

This technical report attempted a bench scale evaluation of a new generation bioscrubber, three-phase circulating-bed biofilm reactor. Although this study proved the biofilm reactor was a promising technology to treat contaminated air streams, the Army needs to refine technology for implementation.

Mode of Technology Transfer

The Construction Engineering Research Laboratory (CERL) is evaluating three innovative biofilter technologies: the three-phase circulating-bed biofilm reactor reported here, a ceramic media trickling bed biofilter, and a rotary drum biofilter. In FY2003, CERL plans to demonstrate one biofilter technology out of these three technologies based on the bench scale experimental data gathered during each evaluation.

Units of Weight and Measure

U.S. standard units of measure are used throughout this report. A table of conversion factors for Standard International (SI) units is provided below.

SI conversion factors		
1 in.	=	2.54 cm
1 ft	=	0.305 m

2 The Circulating-Bed Biofilm Reactor

Reactor Design

Figure 1 illustrates the three-phase circulating-bed biofilm reactor constructed for this study. The reactor was constructed with glass-tubing segments of 40-mm inner diameter (ID), 8 in. or 4 in. long. This design allowed the adjustment of reactor height easily by adding or removing segments from the column. Two special Y-shaped joints connected the glass-tubing segments used for the fluidized-bed biofilm reactor to form a loop. The carriers were loaded inside the loop, and stainless steel screens were installed at both ends. The reactor working volume between the metal screens was 2.78 L. When the gas flow was turned on, the gas bubbles moved up the column on the right-hand-side (the riser), because the gas bubbles caused the liquid in the riser to have a lower overall density than the left column (the downcomer). Consequently, liquid circulation within the loop (counter-clock-wise) kept the particles in a constant circulating motion. The volume of the riser was almost identical to that of the downcomer (1.39 L). The ratios of riser-to-downcomer diameter for most circulating-bed reactors are larger than one in order to increase the volumetric fraction of the riser, where gas-liquid mass transfer occurs. The ratio in this study was exactly one in order to minimize the chance of carrier clogging in the downcomer due to their relative large size compared to the reactor.

The gas flow was introduced into the reactor via a fritted tube (pore-size: 200 - 220 μm) flared into the bottom of the reactor. The headspace of the bottle was connected to the gas exhaust line, which was directed into the hood. This configuration prevented the VOC-containing gas flow from entering the room and maintained atmospheric pressure in the headspace.

Figure 2 shows the nutrient feeding systems for the reactor. It included two 8-L nutrient bottles (50X-A and 50X-B), a 30-L water tank, and pumps. Bottles 50X-A and 50X-B were filled with 50 times the base concentration of group A and B chemicals (Table 4). Reverse osmosis (RO) water was fed to the tank continuously and overflows into a sink. The concentrated stock solutions were fed directly into the reactor via two of the spare liquid sampling ports, while RO water (48 times the flowrates of 50X-A/B) entered the reactor from the bottom. The pH in the reactor was maintained at 6.8 throughout the experiments. The temperature of the lab was maintained at a constant 22 °C.

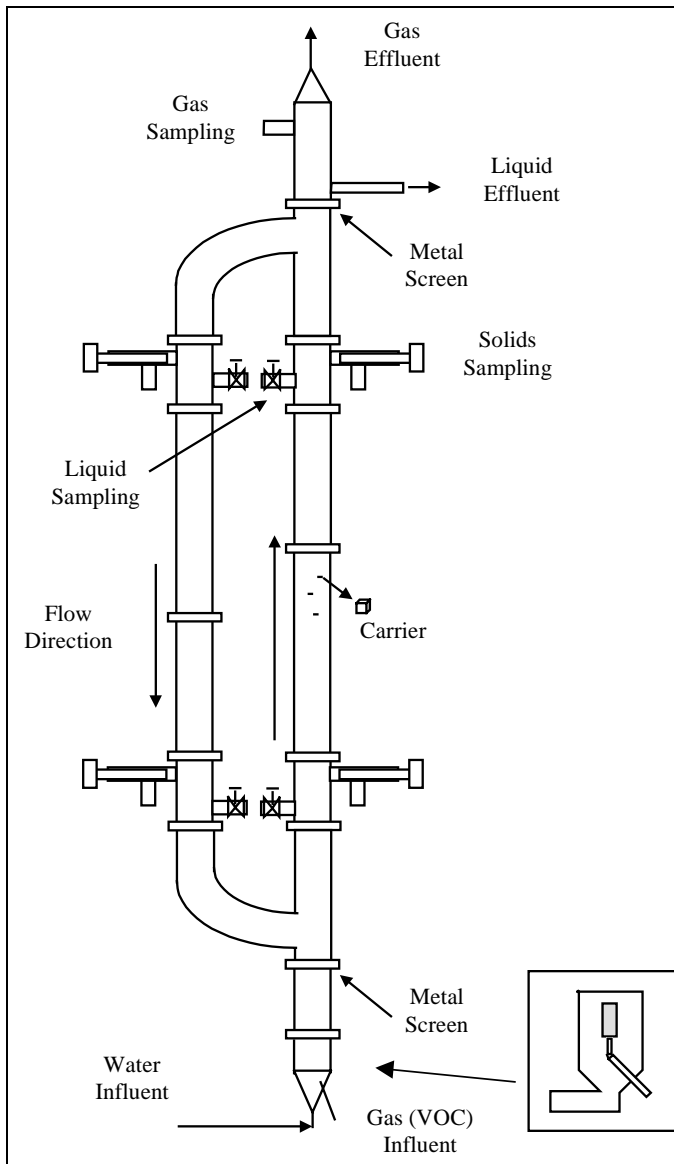


Figure 1. Design of the circulating-bed biofilm reactor. Insert: Bottom segment of the reactor.

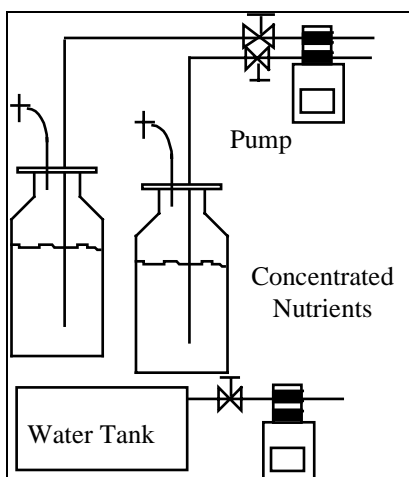


Figure 2. Nutrient feeding system for the biofilm reactor.

Table 4. Composition of the minimal mineral medium.

Group	Compound	Concentration (mg/L)
A	KH ₂ PO ₄	2040.0
	Na ₂ HPO ₄	2130.0
	(NH ₄) ₂ SO ₄	1000.0
B	CaCl ₂ ·2H ₂ O	11.0
	MgSO ₄ ·7H ₂ O	200.0
	FeSO ₄ ·7H ₂ O	7.0
	EDTA	2.50
	ZnSO ₄ ·7H ₂ O	2.00
	MnSO ₄ ·H ₂ O	1.54
	CuCl ₂	0.21
	CoCl ₂ ·6H ₂ O	0.404
	H ₃ BO ₃	0.11
	Na ₂ MoO ₄ ·2H ₂ O	0.25

Source: Seagren 1994, used with permission.

Flowing upward at the bottom of the reactor, the influent RO water facilitated the upward motion of gas bubbles from the fritted tube. Since clogging of the fritted tube can block the flow of the VOC-contaminated gas, it was important to keep the bottom segment of the reactor (below the metal screen) relatively free of bacterial growth. Because the mineral medium stock was fed directly into the circulating-bed reactor, the liquid in the reactor segment below the bottom screen lacked nutrients for bacteria to grow. In addition, about 50 pieces of 3-mm plastic pellets (density 0.98 – 1.01) were added to the bottom segment. These pellets were fluidized in the segment by the liquid and gas flows, thus abrading any possible biofilm attached to the glass wall and fritted tube.

The three-phase circulating-bed biofilm reactor is an ideal system for fundamental studies, as well as for practical applications. On the practical side, it maximizes biofilm accumulation due to its high surface area, avoids bed clogging due to its fluidized nature, and minimizes mass-transfer resistance due to its turbulent regime. As a vehicle for kinetic studies, such as this one, the three-phase circulating-bed biofilm reactor offers completely independent control of liquid velocity, contaminant loading, dissolved-oxygen concentration, and biofilm accumulation. Hence, it has maximum flexibility for experimental design.

The circulating-bed biofilm reactor has several advantages compared to a conventional fluidized bed, in which up-flowing gas and liquid fluidize the solid carriers. First, bed stratification, commonly found in the fluidized-bed reactors, is eliminated. Second, no liquid recycle is needed, which results in energy and equipment savings. Third, with solids moving in a circulation pattern, particle-particle collisions are decreased, which decreases detachment and improves bio-

mass accumulation. Fourth, the liquid mixing in the reactor is excellent. Based on a relationship published by Chisti, Halyard, and Moo-Young (1988), circulation velocity was computed to be as high as 32 cm/s for the gas flowrates used. At that velocity, the liquid circulates every 7 seconds. The fast liquid mixing improves gas-liquid mass-transfer efficiency, thereby improving the removal efficiency of the process. It also makes the reactor more completely mixed, which simplifies data interpretation.

Figure 3 illustrates the BTX feeding system. It included compressed house air with an inline air-filter, pure oxygen gas tank, pure nitrogen gas tank, five flow-meters connected two gas proportioners, micro-liter syringe pumps, and heating wire. The pressures of the air, oxygen, and nitrogen were all maintained at 10 psig before passing through the check valves and entering the gas flowmeters. By changing the flowrates of air, oxygen, and nitrogen, a gas flow of any oxygen concentration could be obtained. The volatile substrates — benzene, toluene, and *p*-xylene — were added to the gas flow through a syringe pump. Two syringes could be loaded to the pump, which could deliver flowrates from 7.3×10^{-6} to $467 \mu\text{l}/\text{min}$ by varying the syringe size (10 μl to 50 ml) and/or gear position (1 to 30).

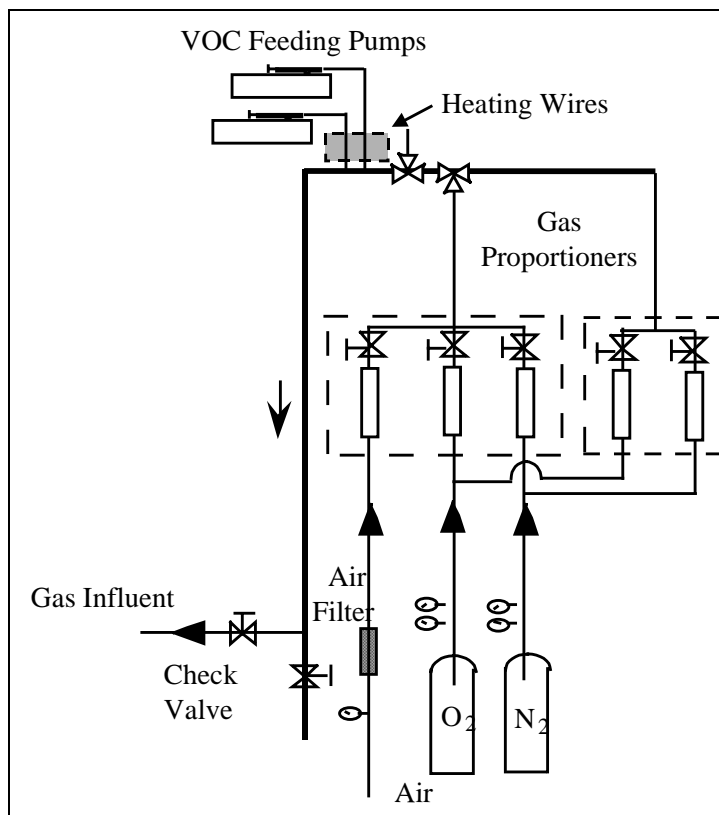


Figure 3. BTX feeding system for the biofilm reactor.

In this study, two 10-ml Hamilton gas-tight syringes with size 28 standard thread were used. The flowrates obtainable were from 0.00728 to 126 $\mu\text{l}/\text{min}$ per syringe. Because it took the pump an hour to reach a stable flowrate, the BTX mixtures were premixed in 165-ml serum bottles to desired compositions and then loaded into the syringes. To facilitate the evaporation of BTX, the 1/16-in. stainless steel tubing (0.01 in. ID) that carried the chemicals was heated to 140 $^{\circ}\text{C}$ by a heating wire. Because the gas line was not heated, the temperature of the influent gas flow was not affected. With this gas feeding system, the influent gas could be of any flowrate, oxygen concentration, BTX composition, and BTX concentrations. The syringe pump was located in the ventilation hood to improve the safety for handling and to minimize human exposure.

Each of the 4-in. segments on the reactor had two liquid sampling ports. They were sealed with Teflon-faced septa and penetrated by a 12-gauge needle. A Lure Lock 2-way valve was connected to each needle. During sampling, the valve was connected to a gas-tight syringe to withdraw samples. These ports also could be connected to the dissolved oxygen (DO) probe to measure the DO concentration. Each of the 4-in. segments also had one solids sampling port (Figure 4). An Ace Glass threaded tube was fit onto the side arm of the sampling port when carrier particles were sampled. Once the O-ring sealed plunger was pulled out about 1 in., the carriers passed into the water-filled tube. Sampling was stopped when the plunger was pushed back 1 in. The carriers were then removed from the tube bottom for characterization. This sampling method introduced minimum disturbance to the biofilm, which could otherwise be stripped of the particles.

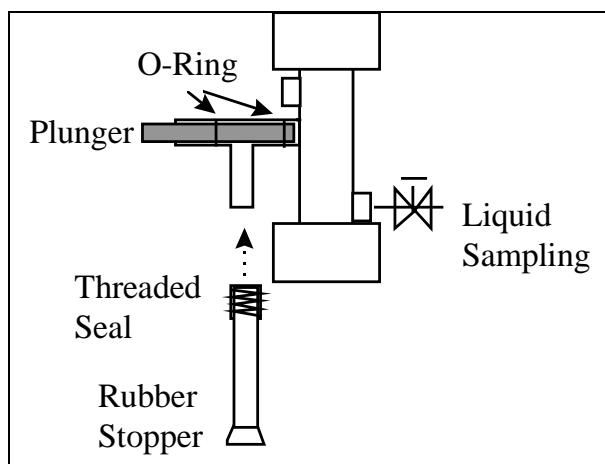


Figure 4. Sampling port for carriers.

One of the characteristics of biofilm processes is that bacteria are attached to micro carrier particles. Almost anything attachable by bacteria can be used as a carrier. In industrial biofiltration processes, sand, peat, compost, or their mixtures are commonly used as biofilm carriers. This study used a non-absorbent porous carrier in the circulating-bed reactor. The macro-porous cellulose carrier, AQUACEL (Ecomat, Inc, Hatward, CA), were used to immobilize nitrifying and denitrifying bacteria. The carriers were 4-mm (dry) cubes with an average porosity of 0.93 and wet density of 1.04 g/cm³. The average dry weight and wet volume of one of these carriers were 7.41 mg and 94.52 mm³, respectively.

Analytical Techniques and Calibrations

Suspended Biomass

The amount of biomass in the suspended phase was measured by its optical density, which was calibrated to dry weight per liquid volume (mg/l). During sampling, 3-5 ml of liquid sample was loaded into a clean standard cuvette. The absorbance of the sample was measured at 540 nm using a spectrophotometer (Spectronic 21D, Milton Roy Co., Ivyland, PA). The sample was then filtered with a 25-mm 0.45- μ m syringe filter or centrifuged at 14,000 rpm for 16 min. The absorbance of the filtered/centrifuged sample was measured. The difference between the two values (Net OD) was calculated and related to the biomass in the liquid through a calibration curve.

The calibration curve was specifically developed for the bacterial culture used in this study. *P. putida* F1 was grown in a flask with toluene supplied from the headspace. The absorbance at 540 nm was measured periodically until its value reached approximately one. The high value of absorbance was necessary to ensure a sufficiently high concentration of cells present and, thus, accurate measurement of cell dry-weight. A sample of 105 ml was then collected. Then 5 ml of the sample was measured for absorbance (Net OD) following the same procedure as described in the previous paragraph. The rest of the 100-ml sample was filtered through a pre-weighed filter paper (47-mm, 0.2- μ m). The filter paper was then dried at 104 °C and weighed. The dry weight of the biomass was calculated from the two measurements. Meanwhile, an additional 25 ml sample was collected from the flask, and a series of dilutions was made to the sample. The Net OD of each sample was measured. Because the biomass concentration of the undiluted sample was known, the biomass concentrations of the diluted samples were calculated from the dilution ratios. All the measurements of cell absorbance and dry weight were performed in duplicates to obtain average values. The

sampling process was repeated twice as the biomass in the flask reactor continuously grew.

This calibration was repeated four times throughout this study. Figure 5 includes results from all four sets of standards, which were consistent with each other over time. The log-log relationship between the biomass concentration in mg-dry weight/L and its Net OD at 540 nm was:

$$\text{Ln}(\text{Concentration, mg Dry Weight/L}) = 0.9551 \text{ Ln}(\text{Net OD}) + 6.1044$$

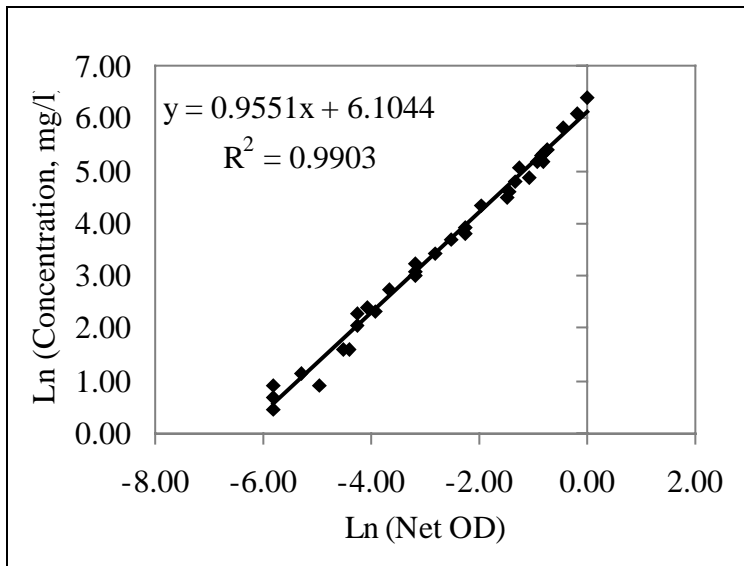


Figure 5. Calibration relationship between biomass concentration and Net OD.

Fixed Biomass on Carriers (Biofilm)

For the porous carrier, AQUACEL, biomass was immobilized inside the pores and difficult to remove. Therefore, the biomass in the carriers was measured as the weight difference between the carriers taken from the reactor and clean carriers. During sampling, the carriers taken from the reactor were first dried at 104 °C for 2 h and then weighed immediately.

Chemical Oxygen Demand (COD)

The COD test measures the oxygen demand equivalent of organic matter that can be oxidized using a strong chemical oxidizing agent in an acidic medium. Usually, potassium dichromate is used as the agent. In this study, standard COD vials of two COD ranges, 0-40 mgCOD/L and 0-150 mgCOD/L were obtained from Hach Co. (Loveland, CO). During a COD test, 2 ml of liquid sample

were added to the vial containing the chemical oxidizing agent and reacted at 150 °C on a Hach COD Reactor for 2 h. The vials were then cooled at room temperature for 2 h and measured for absorbance using a spectrophotometer. The wavelengths used for the 0-150 mg/L and 0-40 mg/L COD vials were 420 and 350 nm, respectively. The COD value of the sample was then obtained from a prepared standard calibration curve (Figure 6). The curve was slightly different for each batch of vials supplied by Hach; thus, calibration was repeated for each batch of 150 vials.

The COD standards were prepared following the protocol provided by Hach Co. A 1,000 mg/L COD standard was first prepared by dissolving 850 mg of oven-dried (120 °C, overnight) potassium acid phthalate (KHP) in ultra-high purity water and diluting to 1 L with ultra-high purity water. Standards of lower concentrations were then made from serial dilutions.

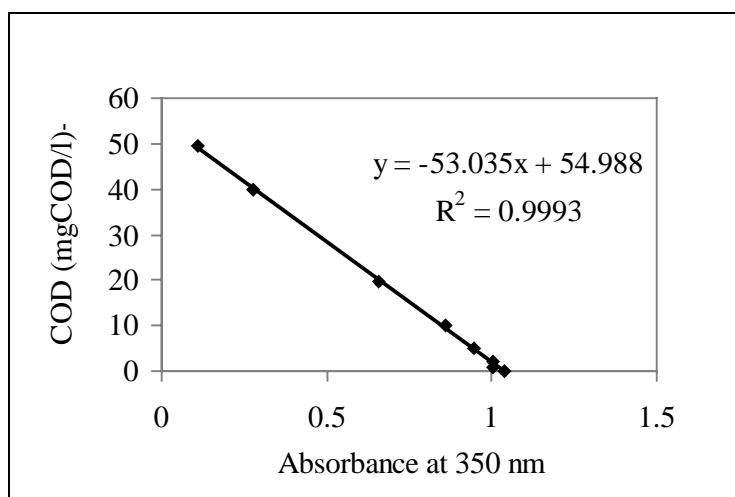


Figure 6. A typical COD standard calibration curve for 0-40 mg/l COD vials.

GC Analysis of BTX

In this study, an HP 5890 gas chromatography (GC) equipped with a flame-ionization detector (FID) and a glass capillary column (Model DB-5, J&W Scientific, Inc., Folsom, CA) was used to analyze the concentrations of toluene, benzene, or *p*-xylene in the gas or liquid phase. The GC/FID output signals were analyzed by an HP integrator (Model 3396). Table 5 shows the flowrate setup for the GC/FID system.

Table 5. Gas flowrate setup for the GC/FID system.

		Flowrate (ml/min)
GC Column	Septum Purge, H ₂	0.7
	Column Carrier Gas, H ₂	6.1
FID Detector	Flame-Oxidant, Air	374
	Flame-Combustible, H ₂	39
	Make-up Gas, N ₂	33

Table 6 shows the temperature programs used for this analysis and the residence times for toluene, BTX at each condition. The temperature history for the liquid phase was determined by the organic solvent used in this study, methylene chloride (DCM), which has a boiling point of 36 °C. The temperature histories of gas samples were determined by the boiling points of the chemicals analyzed. In general, the initial temperature needs to be at least 5 °C below the samples' boiling points.

Table 6. Temperature programs of GC and BTX retention times (RT).

Method	Liquid Sample	Toluene (gas)	Benzene (gas)	Benzene Toluene (gas)	Toluene <i>p</i> -xylene (gas)
Initial Temp (°C)	30	100	60	60	100
Initial Time (min)	1	1	1	1	1
First Temperature Ramp					
Rate (°C/min)	10	10	10	10	10
Final Temp (°C)	120	120	90	120	150
Final Time (min)	0	0	0	0	0
Second Temperature Ramp					
Rate A (°C/min)	35	45	45	45	45
Final A Temp (°C)	250	250	250	250	250
Final A Time (min)	0	0	0	0	0
Injector/Detector Temperature					
Injector (°C)	150	150	150	150	150
Detector (°C)	300	300	300	300	300
RT (min)	4.1/6.0/8.1 [†]	2.3	2.6	2.6/3.8 [‡]	2.5/3.3 [‡]
[†] Data for benzene/toluene/ <i>p</i> -xylene [‡] Data for benzene/toluene or toluene/ <i>p</i> -xylene.					

GC analysis of gas samples.

Researchers first drew 20-25 µl of gas sample from the reactor headspace into a 25-µl Hamilton gas-tight syringe. The syringe plunger was then pushed to the 10-µl mark and immediately injected into the GC column for analysis. Two or three injections were used for each gas sample.

GC analysis of liquid sample.

Using a gas-tight syringe, 2 mL of sample was first retrieved from the reactor. A 1-mL sample was then filtered through a 13-mm 0.2- μm syringe filter into a 3-ml conical vial containing 1.5 mL of DCM. The vial was then sealed tightly and shaken vigorously on a mixing vortex for 1.5 min. The DCM phase (bottom layer) was then withdrawn with a clean gas-tight syringe equipped with a 16-gauge needle and transferred into a 2-mL standard HP auto-sampler vial and analyzed by the GC-FID. Unlike the gas samples, the liquid samples were injected using an HP automated injector (Model 6890). Three 1- μL injections were made for each liquid sample.

The masses or concentrations of BTX in the samples were calculated from their peak areas on the GC/FID spectra based on standard calibration curves. Standards of toluene, benzene, and *p*-xylene were purchased from AccuStandards (New Haven, CT) or made directly following the protocols described in American Public Health Association (APHA) Methods 6210 and 6220 (APHA 1995). The high concentration standards were diluted into varied concentrations and analyzed by the GC. Since liquid samples underwent liquid-liquid extraction prior to GC analysis, their peak areas were multiplied by 1.5 before they were applied to the calibration correlation. Similar to the biomass calibration curve, log-log relationships were used for the calibrations:

$$\text{Gas sample: } \text{Ln}(\text{mass, } \mu\text{g}) = a \cdot \text{Ln}(\text{peak area}) - b$$

$$\text{Liquid sample: } \text{Ln}(\text{concentration, mg/L}) = a \cdot \text{Ln}(\text{peak area} \cdot 1.5) - b$$

in which *a* and *b* were fitted parameters for the calibration curves. The values of *a*, *b*, and the R-squared values for each fit are shown in Table 7.

Table 7. Values of parameters *a* and *b* in GC standard calibration curves.

Compound	Phase	A	b	R ²
Toluene	Gas	0.9953	15.7701	0.9968
	Liquid	0.9864	8.5222	0.9951
Benzene	Gas	1.0056	16.007	0.9997
	Liquid	1.0150	9.0112	0.9989
<i>p</i> -Xylene	Gas	0.8925	14.5540	0.9956
	Liquid	0.9331	7.9111	0.9968

High Performance Liquid Chromatography (HPLC) Analysis of Liquid Samples

In this study, an HPLC system (Hitachi Instruments, Inc., San Jose, CA) equipped with a diode-array detector (Hitachi L-4500) was used to identify the intermediates formed during BTX degradation. An HP-Hypersil column (C-18, 5 μm , 2.1-mm ID, and 10-cm length) was used to separate the compounds. The mobile phase was similar to that used by Shields et al. (1989) (i.e., acetonitrile:10 mM KH_2PO_4 buffer (pH 2.88) = 20:80 (volume:volume)). Initially, the flowrate used was 0.2 ml/min. A guard column was later installed in front of the HP-Hypersil column, and the flowrate was increased to 0.5 ml/min for better flowrate stability. The spectra were collected at 207 nm. The HPLC analysis in this study was mostly qualitative. Therefore, no calibration curves were made. However, if necessary, quantification of any specific compound could be made by comparing the HPLC peaks with standards of known concentrations. Table 8 lists the residence times for BTX and their potential intermediates. Since the retention times varied slightly due to flow rate/ column pressure during each run, standards were analyzed to confirm the peaks.

For collecting an HPLC sample, a Teflon syringe filter (13-mm, 0.45- μm PTFE) was first wetted and rinsed with 2 ml of acetonitrile. About 2 ml of liquid sample was then collected from the reactor using a 2.5-ml Hamilton gas-tight syringe. 1 ml of the sample was then filtered into a 2-ml HPLC auto-sampler vial. 0.2 ml of acetonitrile was added to the vial. The vial was finally sealed with a Teflon-faced septum and loaded onto the HPLC auto-sampler for analysis.

Table 8. Typical retention times (RT) in the HPLC column.

Name	RT (minutes)
Toluene	30.9
Benzene	12.2
<i>p</i> -Xylene	8.4
Catechol	1.6 (3.9)
3-Methylcatechol	3.1 (8.5)
Phenol	3.0 (7.7)
<i>o</i> -Cresol	6.3 (18.2)
<i>m</i> -Cresol	5.79 (17.0)
<i>p</i> -Cresol	5.82
3,6-Dimethylcatechol	4.4

Dissolved Oxygen

Concentration of DO in the liquid phase was measured with a high-resolution digital DO meter and probe (Martek Instruments, Inc., Raleigh, NC; Model Mark

XVIII). Because the electrolyte in the probe was consumed continuously during measurements, the probe needed to be calibrated before each usage. The probe was calibrated in water-saturated air using the apparatus shown in Figure 7. A beaker filled with water was placed in a rectangular chamber with a hole on top. When the probe was not calibrated, a rubber stopper was placed in the hole, and the water was saturated with oxygen by the air sent through a pipette. Since the chamber was closed, the air in it became saturated with water vapor. During calibration, the stopper and pipette were quickly replaced by the probe, which rested 3-5 mm above the liquid surface. Once the DO probe reading stabilized, the probe was set according to the standard DO value in water-saturated air at room temperature. Once calibrated, the probe could be immersed into the liquid to measure the DO concentration, or it could be used to read the partial pressure of oxygen in the gas phase.

To measure the DO in the biofilm reactor, the probe was seated in a flow chamber, which was connected to the reactor as shown in Figure 8. The liquid was drawn from the reactor top to minimize the possibility of withdrawing particles and gas bubbles into the DO flow chamber, sent through the chamber containing the DO probe, and then sent back to the reactor. Because the probe consumes oxygen during measurement, a continuous flow through the chamber (100-150 ml/min) is suggested by the manufacturer. In this study, a pump was used to maintain a constant flowrate of 105 ml/min through the chamber during DO measurement. To minimize bacterial growth on the probe membrane, the pump was stopped when no DO measurement was performed. The probe was removed from the chamber, rinsed, and stored in a 2 percent Na_2SO_3 solution between DO measurements.

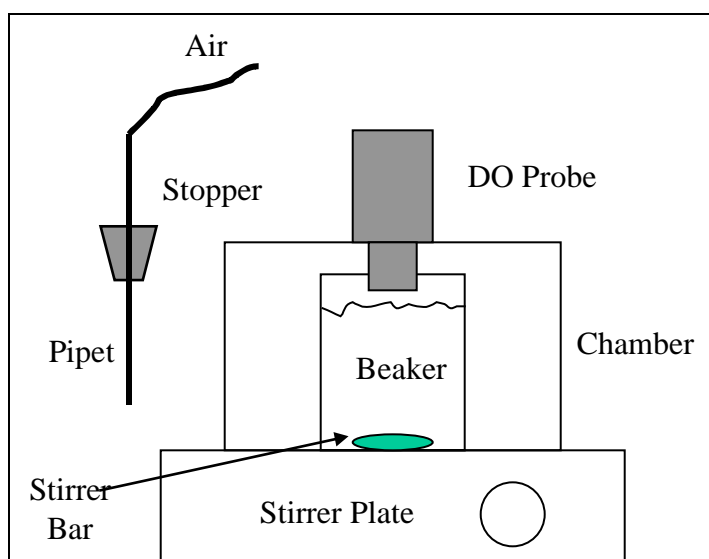


Figure 7. DO-probe calibration apparatus.

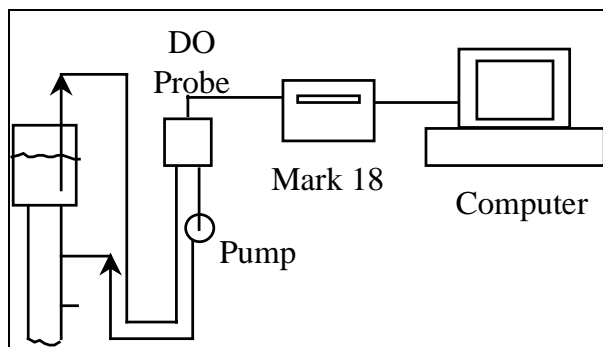


Figure 8. Flowpath of dissolved oxygen measurement.

The Mark XVIII DO meter was connected to an IBM-compatible personal computer. Data sampling software was used to record the DO reading every 3-5 seconds. Sampling data were saved into a text file as long as the continuous monitoring of DO was required.

Gas Holdup

Gas holdup is the volumetric fraction of the gas phase in the three-phase fluidized bed. It has significant impact on the gas-liquid mass transfer and the extent of fluidization. A liquid-displacement experiment was designed to measure the gas holdup independently in this study. The reactor, containing the desired amount of glass beads, was first started up in the liquid-solid circulation mode. After a stable circulating bed was established, gas flow was turned on, and the liquid volume displaced from the reactor at this gas/liquid flowrate was measured using a volumetric cylinder. The volume of gas bubbles inside the fluidized bed was then corrected based on the average pressures inside and above the fluidized bed. The gas holdups of the bed were calculated as the ratio of gas to fluidized-bed volumes. The calculation assumed that the axial mass distribution of the gas bubbles inside the reactor was constant.

BTX Flowrates

The syringe pump used to deliver single BTX component or mixture was extremely precise and stable over the long period of continuous operation. A flowrate table was supplied by the manufacturer (Harvard Apparatus, Inc., South Natick, MA). Numerous calibrations showed that the flowrates provided by the table were always within 2 percent of the measured data. Thus, flowrate values from the table supplied by the manufacturer were used.

Liquid Flowrates

The flowrates of dilution water and minimum mineral medium were calibrated daily by noting the amount of time needed for the pumps to deliver a certain amount of liquid. Because all the peristaltic pumps have digital displays, the flowrates could be adjusted easily by changing the rpm settings.

Gas Flowrates

The flowmeters in the gas proportioners came with factory-supplied calibration curves. However, because of the back pressure caused by the liquid and glass beads in the reactor (3.635 ~ 3.915 psig), these flowmeters had to be calibrated taking the back pressure into account. A device was designed to use three three-way valves to control the direction of gas flow after it exited the reactor top and to maintain the same back pressure to the gas flowmeters (Figure 9).

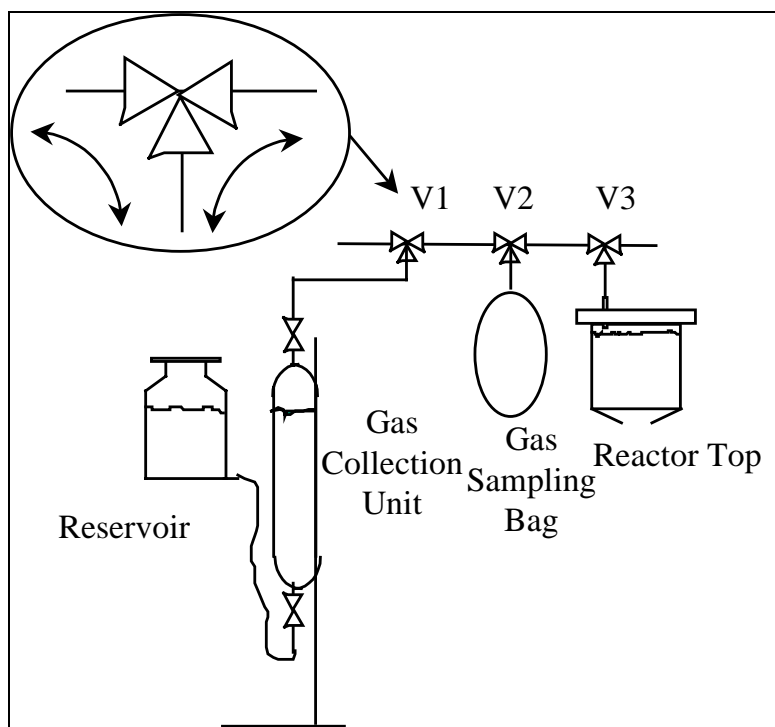


Figure 9. Apparatus for gas-flow calibration.

Before gas collection, valve V1 was open to the left (so the headspace of the gas collection unit was open to the atmosphere), and valves V2 and V3 were open to the right. To start collecting gas at any flowmeter setting, V3 was turned to the left, and gas was sent into the Teflon gas-sampling bag. To stop collecting the gas sample, V3 was turned to the right again. The sampling period was recorded. To measure the volume of gas collected, V1 was first turned to the right, and then V2 was turned to the left. By lowering the reservoir, the gas in the gas-sampling bag was drawn into the gas collection unit, which had had its volume calibrated. Once all the gas was drawn from the gas-sampling bag, V2 was turned to the right. The water levels in the reservoir and gas-sampling unit were equalized before the volume of gas collected was read from the calibration marks on the gas-collection unit. Finally, V1 was turned to the left, and gas in the gas collection unit was released into the atmosphere. The gas flowrate at any flowmeter setting was then calculated based on the volume of gas at atmosphere pressure passing through the reactor over a specific amount of time.

Figure 10 shows the relationships between the gas flowrate and flowmeter setting for the three gases that were used in the experiments. They were almost identical when different types of carriers were loaded. These curves can be fitted nicely by the following equations:

$$\begin{aligned} \text{N}_2: \text{Flowrate (ml/min)} = & -1.2345\text{E-}04 \text{ Setting}^3 + 3.4623\text{E-}02 \text{ Setting}^2 \\ & + 1.4036 \text{ Setting} + 15.572 \quad R^2 = 0.9996 \end{aligned}$$

$$\begin{aligned} \text{Air: Flowrate (ml/min)} = & -1.5671\text{E-}04 \text{ Setting}^3 + 4.1582\text{E-}02 \text{ Setting}^2 \\ & + 9.2453\text{E-}01 \text{ Setting} + 22.193 \quad R^2 = 0.9995 \end{aligned}$$

$$\begin{aligned} \text{O}_2: \text{Flowrate (ml/min)} = & -1.0000\text{E-}04 \text{ Setting}^3 + 0.0293 \text{ Setting}^2 \\ & + 1.3046 \text{ Setting} + 9.744 \quad R^2 = 0.9988 \end{aligned}$$

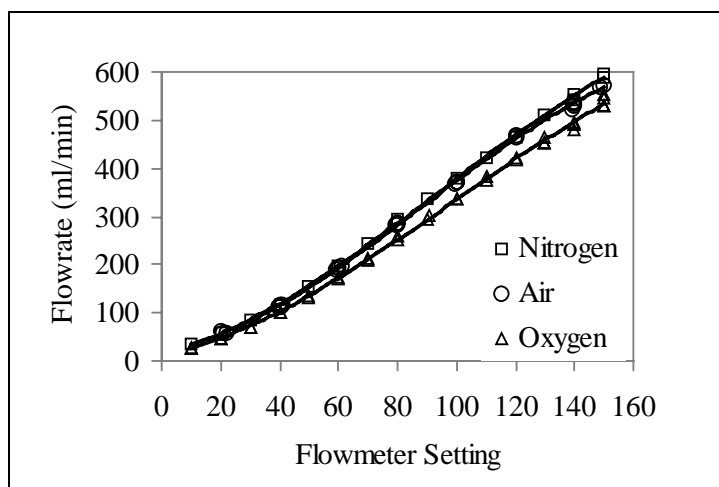


Figure 10. Gas flowmeter calibrations.

Hydrodynamics and Gas-Liquid Mass Transfer

Hydrodynamics Experiments

Before the reactor was inoculated, hydrodynamic experiments were conducted. The total flowrate of the liquid influent used for the hydrodynamic study was the same as the one for the biofilm studies. First, several pieces of carrier were loaded, and their circulation velocities were measured from circulation time determined with a stopwatch. Then, the amount of carriers to be used in this study (43.59 g) was loaded, and the carrier velocities were measured by tracking the movement of several darker-colored particles. Figure 11 compares the carrier velocities at various gas superficial velocities. The results show that the amount of carriers had an effect on the carrier velocity. At low superficial gas velocity ($U_g < 0.5$ cm/s), higher carrier concentration (overall $\epsilon_s = 0.2$) caused the average carrier velocity to decrease. However, at high gas velocity ($U_g > 0.5$ cm/s), the difference caused by the carrier concentration was minimal. In addition, the difference in circulating velocity in the riser and downcomer also diminished. The carrier velocity eventually reached a plateau (25 cm/sec).

Figure 12 shows the gas holdup (ϵ_g) in the riser part of the circulating bed before and after the carriers were loaded. It indicates that the gas void fraction in the riser increased linearly with gas flowrate and was slightly lower when the carriers were present. The fitted equation shown in Figure 12 is for data when the bed was loaded with carriers. Since the whole reactor volume was twice that of the riser and the downcomer was almost free of bubbles, the overall gas holdup in the circulating bed was half of that in the riser:

$$\epsilon_g = 0.01816 * U_g \text{ (cm/s)} + 0.00218 \quad (\text{Eq 1})$$

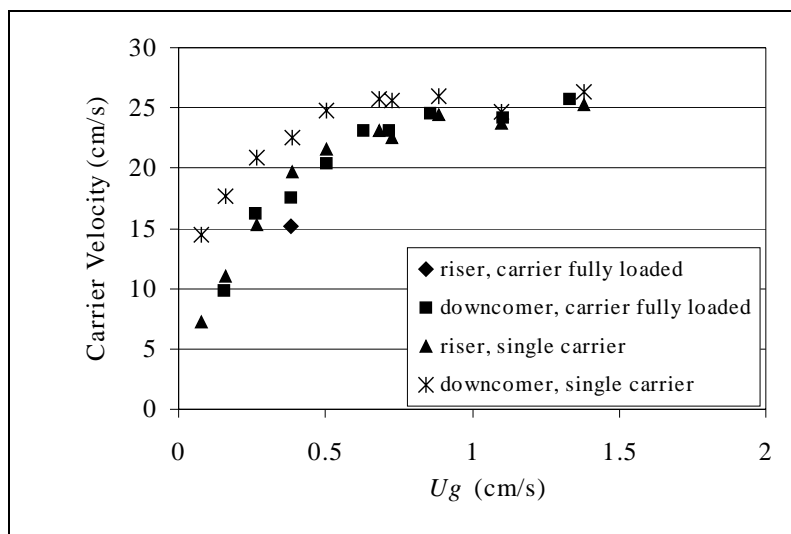


Figure 11. Circulation velocities of carriers in the circulating-bed reactor.

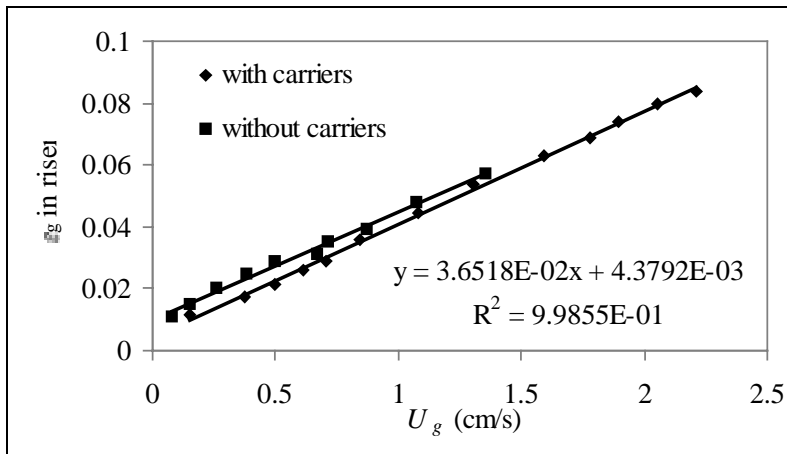


Figure 12. Gas holdup in the riser. The correlation shown was fitted only for data with carriers fully loaded.

Gas-Liquid Mass Transfer

Because the substrates for the biofilm system were supplied from the gas phase in this study, knowledge of the volumetric gas-liquid mass-transfer coefficient, k_La , was crucial. Since k_La was affected not only by process variables, such as gas superficial velocity, but also by system-dependent variables, such as gas-distribution design, the value of k_La for the three-phase fluidized biofilm reactor was obtained experimentally.

Many factors affect k_La , including gas/liquid superficial velocities, gas/liquid properties, particle properties, gas distribution system, reactor size and configuration, and phase holdups. Thus, a large number of system-specific k_La equations can be found in literature. However, all the studies suggest that, in a three-phase fluidized bed, the superficial gas velocity, U_g , is the single most significant factor that determines k_La , while the superficial liquid velocity, U_l , has a smaller or no effect on k_La . In this study, the k_La correlation is developed as a function of U_g , since other factors such as gas distribution and reactor size/configuration are fixed for the reactor used.

For a given system, k_La for a specific compound with diffusivity D can be related to another compound with known $(k_La)_0$ and diffusion coefficient, D_0 (Fan 1989):

$$k_La = (k_La)_0 \left(\frac{D}{D_0} \right)^{0.5} \quad (\text{Eq 2})$$

A traditional approach is to measure k_La for DO, which is easy to measure (Miyahara, Lee, and Takahashi 1993; Muroyama, Mitani, and Yasunishi 1985; and Koide, Sato, and Iwamoto 1983a, 1983b). Because the three-phase circulating-bed

reactor used in this study had a high liquid recycle flowrate (recycle ratio >1000:1), it could be treated as a completely mixed reactor when the physical absorption method was used to evaluate the values of k_a for oxygen.

The experimental setup for the k_a measurement is shown in Figure 8, which shows the DO meter setup, and Figure 13, which shows the detailed gas feed system. The seven valves and five flowmeters controlled the gas flow fed into the reactor. For example, leaving valves 1 and 5 open and valves 2, 3, and 4 closed made it possible to switch the gas flow between air-only and nitrogen-only modes by switching valve 6.

Before a k_a experiment, the reactor was loaded with the same size and amount of carriers to be used in biodegradation experiments. To start a k_a experiment, the liquid flow was first turned on to establish a stable fluidized bed. Then nitrogen flow, at the same rate as the air to be used, was supplied to the reactor. After the dissolved oxygen concentration inside the reactor approached zero (< 0.01 ppm), nitrogen was switched to air using valve 6. The DO concentrations during nitrogen- and air-feeding periods were recorded, as were the gas and liquid flowrates and the fluidized-bed height.

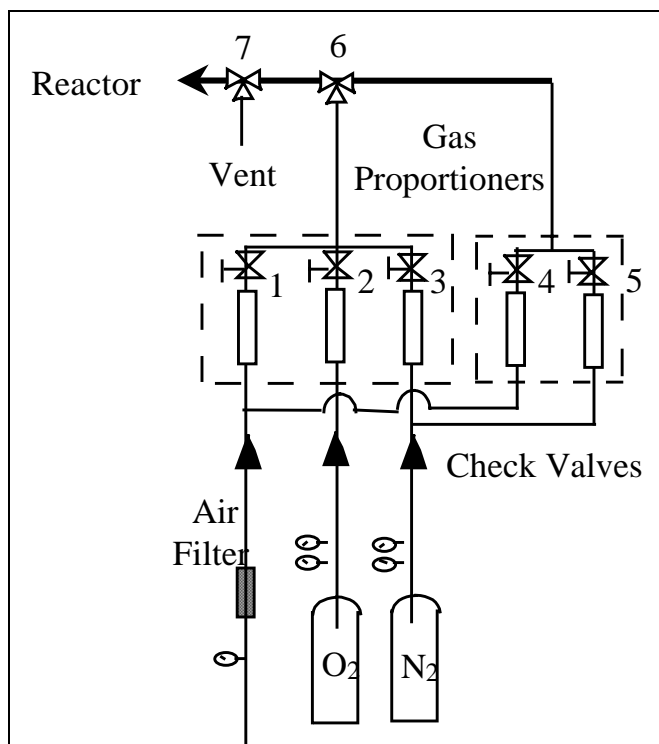


Figure 13. Detailed drawing of the gas feed system.

The oxygen-concentration history displayed on the Mark 18 DO meter and recorded by the PC was related to k_1a from the integrated mass balance on oxygen (Koide et al. 1983a, 1983b):

$$\frac{O^* - O(t)}{O^* - O_0} = \exp\left(-\frac{k_1a}{\varepsilon_l} t\right) \quad (\text{Eq 3})$$

where $O(t)$ is the oxygen concentration at time t , O^* is the oxygen concentration at the gas-liquid interface (zero for nitrogen feed, and 8.8 mg/L for air feed at the constant reactor liquid temperature 22 °C), O_0 is the initial oxygen concentration (mg/L), and ε_l is the volumetric fraction of the liquid phase in the fluidized bed. The value of k_1a was fit using a non-linear curve fitting routine once ε_l was calculated by subtracting ε_g and ε_s values from one. Since the carriers' large pores (0.5 mm in size) were filled with water when biofilm was absent, the ε_l values were adjusted to include the water in those pores.

The gas-liquid mass-transfer coefficient, k_1a , was measured after the carriers were loaded. Figure 14 shows that the value of k_1a increased with the superficial gas velocity within the range measured and followed Equation 4:

$$(k_1a)_o = 0.232U_g^{0.768} \quad (\text{Eq 4})$$

where the units of k_1a and U_g are in s⁻¹ and m/s, respectively. The exponent of 0.768 is similar to the exponent in correlation equations obtained by other researchers in various circulating beds or bubble columns (0.8 – 1.0) (Miyahara, Lee, and Takahashi 1993; Heijnen et al. 1993; Goto, Matsumoto, and Gaspillo 1989; Chisti and Moo-Young 1987; and Deckwer, Burckhart, and Zoll 1974). Lower exponent values were obtained in related, but different systems. In a bubble column containing suspended phenol-degrading bacteria, an exponent of 0.74 was reported (Shishido and Toda 1996). In a three-phase fluidized bed, Nore et al. (1992) reported an exponent of 0.59 for superficial gas velocity.

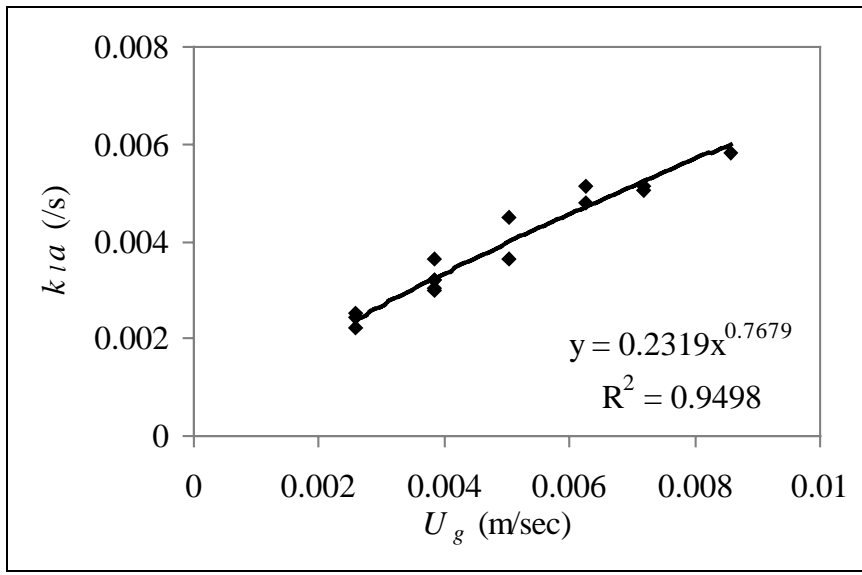


Figure 14. Gas-liquid mass-transfer coefficient in the circulating-bed reactor.

3 BTX Removal Experiments

General Approaches

The circulating-bed biofilm reactor was inoculated with *P. putida* F1. Because of the protective nature of the porous carriers, biofilm developed rapidly in the carriers. The total flowrate of the liquid influent (nutrient stock solution plus dilution water) was maintained at 42 ml/min, which gave a liquid dilution rate of 22 day⁻¹. The gas flowrate was maintained between 535-540 ml/min, which gave a U_g value of 0.71-0.72 cm/s.

The reactor was operated continuously for more than 6 months without loss of toluene reactivity. During the 6-mo period, extensive tests were conducted to study the performance of the circulating-bed biofilm reactor under various substrate and oxygen loading conditions. The experiments conducted were divided into three main groups, which are tabulated in Tables 9-11. The BTX conditions are identified by the total surface-loading rate. For example, the total surface loading for toluene equaled $r_{\text{pump,T}} \cdot \rho_T / A$, in which $r_{\text{pump,T}}$ was the syringe pump's volumetric feeding rate of pure toluene (L³T⁻¹), ρ_T was the density of toluene (M_{tol}L³) and is known for a given temperature, and A was the total surface area of biofilm in the circulating-bed biofilm reactor, which was a constant and equaled 0.73 m². The oxygen conditions are represented by O*, the DO concentration at the gas-liquid interface that was in equilibrium with the oxygen in the gas phase (Equation 3).

Toluene as the Sole Substrate

In the first group of experiments (Table 9), toluene was the sole electron donor and carbon source. Three steady states were established with air as the gas stream and different toluene loading rates. For each steady state, two types of short-term experiments were performed. In the first type of short-term experiments (e.g., Ss1-1 to Ss1-6 in Table 9), the gas stream was air, while the toluene loading was varied. In the second type of short-term experiments (e.g., Ss1-7 to Ss1-10 in Table 9), the toluene loading was maintained at the steady-state level, while the oxygen concentration in the gas stream was changed by mixing air with nitrogen or oxygen.

Table 9. Reactor loading conditions when toluene was the sole carbon source.

Run Name	Toluene Loading (mol/m ² -day)	O* (mg-O ₂ /L)	Comments	Loading Varied
Ss1	0.030	8.8	Steady State 1	
Ss1-1	0.015	8.8	Short Term	Toluene
Ss1-2	0.021	8.8	Short Term	Toluene
Ss1-3	0.042	8.8	Short Term	Toluene
Ss1-4	0.059	8.8	Short Term	Toluene
Ss1-5	0.082	8.8	Short Term	Toluene
Ss1-6	0.115	8.8	Short Term	Toluene
Ss1-7	0.030	7.0	Short Term	Oxygen
Ss1-8	0.030	5.3	Short Term	Oxygen
Ss1-9	0.030	3.5	Short Term	Oxygen
Ss1-10	0.030	1.8	Short Term	Oxygen
Ss2	0.042	8.8	Steady State 2	
Ss2-1	0.021	8.8	Short Term	Toluene
Ss2-2	0.030	8.8	Short Term	Toluene
Ss2-3	0.059	8.8	Short Term	Toluene
Ss2-4	0.082	8.8	Short Term	Toluene
Ss2-5	0.042	7.0	Short Term	Oxygen
Ss2-6	0.042	5.3	Short Term	Oxygen
Ss2-7	0.042	3.5	Short Term	Oxygen
Ss2-8	0.042	1.8	Short Term	Oxygen
Ss3	0.059	8.8	Steady State 3	
Ss3-1	0.030	8.8	Short Term	Toluene
Ss3-2	0.042	8.8	Short Term	Toluene
Ss3-3	0.082	8.8	Short Term	Toluene
Ss3-4	0.115	8.8	Short Term	Toluene
Ss3-5	0.059	7.0	Short Term	Oxygen
Ss3-6	0.059	5.3	Short Term	Oxygen
Ss3-7	0.059	3.5	Short Term	Oxygen
Ss3-8	0.059	1.8	Short Term	Oxygen
Ss3-9	0.059	15	Short Term	Oxygen
Ss3-10	0.059	22	Short Term	Oxygen

Table 10. Reactor loading conditions when toluene and benzene were supplied.

Run Name	Toluene (mol/m ² day)	Benzene (mol/m ² day)	Total COD (gCOD/m ² day)	Comments	Loading Varied
Ss4	0.056	0.0034	17.0	Steady State 4	
Ss4-1	0.029	0.0017	8.6	Short Term	Total COD
Ss4-2	0.040	0.0024	12.1	Short Term	Total COD
Ss4-3	0.078	0.0047	23.7	Short Term	Total COD
Ss4-4	0.11	0.0066	33.2	Short Term	Total COD
Ss5	0.052	0.0080	17.0	Steady State 5	
Ss5-1	0.027	0.0041	8.6	Short Term	Total COD
Ss5-2	0.037	0.0057	12.1	Short Term	Total COD
Ss5-3	0.073	0.011	23.7	Short Term	Total COD
Ss5-4	0.10	0.016	33.2	Short Term	Total COD
Ss6	0.046	0.015	17.0	Steady State 6	
Ss6-1	0.024	0.0077	8.6	Short Term	Total COD
Ss6-2	0.033	0.011	12.1	Short Term	Total COD
Ss6-3	0.065	0.021	23.7	Short Term	Total COD
Ss6-4	0.091	0.030	33.2	Short Term	Total COD

Table 11. Reactor loading conditions when toluene and *p*-xylene were supplied.

Run Name	Toluene (mol/m ² day)	<i>p</i> -Xylene (mol/m ² day)	Total COD (gCOD/m ² day)	Comments	Loading Varied
Ss7	0.055	0.0033	16.7	Steady State 7	
Ss7-1	0.028	0.0017	8.5	Short Term	Total COD
Ss7-2	0.039	0.0023	11.8	Short Term	Total COD
Ss7-3	0.077	0.0046	23.3	Short Term	Total COD
Ss7-4	0.11	0.0064	32.6	Short Term	Total COD
Ss8	0.050	0.0077	16.2	Steady State 8	
Ss8-1	0.025	0.0039	8.3	Short Term	Total COD
Ss8-2	0.036	0.0055	11.5	Short Term	Total COD
Ss8-3	0.070	0.011	22.7	Short Term	Total COD
Ss8-4	0.098	0.015	31.8	Short Term	Total COD

To ensure that steady states were reached before the short-term experiments began, the reactor was fed at the first steady-state condition for more than 1 mo before the first short-term experiment was conducted. For every other steady state, constant loading was maintained for about 2 wk. Before the short-term experiments, the gas and liquid effluent quality was measured for three consecutive days to confirm the steady states. Before each 1-h short-term experiment, the toluene or oxygen loading was changed to a desired value for nearly 3 h. The liquid retention time for the circulating-bed biofilm reactor was about 1 h. Therefore, the reactor was sampled after three liquid retention times. Since the time was too short for the biomass to change dramatically, but long enough for the substrate concentrations to stabilize, short-term experiments were at pseudo-steady states (i.e., the steady states of various toluene or oxygen loading

with a constant biomass concentration in the reactor). The toluene or oxygen loading was returned to its steady-state value between each short-term experiment.

Dual Substrates

After experiments with toluene as the sole substrate were completed, the second and third groups of experiments were conducted using toluene/benzene (Table 10) and toluene/*p*-xylene (Table 11) as substrate combinations, respectively. The total COD for the toluene/benzene or toluene/xylene mixtures for Ss4-Ss8 was maintained the same, while the composition of toluene/benzene or toluene/xylene was varied. Because changes in VOC loading rates during the short-term experiments were accomplished by changing the gears of the syringe pump, the composition of toluene/benzene or toluene/xylene was the same within one steady state and its short-term experiments. The approach taken for the second and third groups of experiments was similar to that for the first group. After a steady state was developed, series of short-term experiments were conducted. Three and two steady states were developed for the second and third groups of experiments, respectively. However, only the substrate loading was changed during the short-term experiments. The gas feed was always 100 percent air to maintain constant oxygen loading. Kinetic studies (Yu 1998) showed that *P. putida* F1 could grow on benzene, but not on *p*-xylene. Thus, benzene was a primary co-substrate, but *p*-xylene a cometabolic cosubstrate.

4 Kinetic Analysis

Kinetics of BTX Degradation

A recent study (Yu 1998) showed that biodegradation of toluene and benzene is described well as a two-step process. The first step does not support the biomass growth and does not generate electrons and carbons for cell synthesis. Biomass growth is supported by the second-step reactions, which are the oxidation of catechol intermediates. When oxygen is not limiting, the intermediates of toluene, benzene, and *p*-xylene are 3-methylcatechol, catechol, and 3-6-dimethylcatechol, respectively. Toluene or benzene inhibits the degradation of its intermediate non-competitively. Degradation of *p*-xylene occurs cometabolically. When toluene and benzene or toluene and *p*-xylene are degraded simultaneously, they inhibited each other's degradation competitively.

All the kinetic parameters associated to the fully aerobic degradation of BTX as a single substrate, and the parameters associated with the degradation of toluene-benzene or toluene-xylene as dual substrates have been obtained in independent experiments (Yu 1998). The final values of these kinetic parameters are summarized in Table 12.

Basic Mechanisms of Biofilm Removal

To be oxidized by the biomass attached to the carriers in the circulating bed, the VOCs in the gas stream take the following steps: (1) transfer from the gas phase into the liquid phase, (2) transport from the liquid phase to the surface of the biofilm, and (3) simultaneously diffuse and react within the biofilm. When the biodegradation reaction is negligible in the liquid phase, the typical concentration profiles of a VOC in such a system are illustrated schematically in Figure 15. Since cosubstrate oxygen also was supplied from the gas stream, it goes through the same steps.

Since BTX and oxygen are poorly soluble in water, the gas-phase film resistance is negligible (Doran 1995), making $SG = SG,i$. Thus, the mass transfer from the gas to the liquid phase is dominated by the liquid-film resistance at the interface. The transport rate is then:

$$N_g = k_l a \left(\frac{S_G}{H} - S_L \right) \quad (\text{Eq 5})$$

in which N_g is the volumetric rate of mass transfer of the gas component ($\text{ML}^{-3} \text{T}^{-1}$), $k_l a$ is the volumetric gas-liquid mass-transfer coefficient (T^{-1}), and H is the Henry's constant for the gas transferred.

Table 12. Summary of kinetic parameters for BTX degradation.

	Toluene	Benzene	<i>p</i> -Xylene
Y_2 (mg- X_a /mgCOD)	0.38	0.32	
$q_{2,max}$ (mgCOD/mg- X_a -day)	29	27	
K_2 (mg-COD/L)	3.7	2.7	
$q_{1,max}$ (mg-VOC/mg- X_a -day)	26	25	
K_1 (mg-VOC/L)	1.1	4.2	
$K_{i,12}$ (mg-VOC/L)	3.6	6.8	
β_2 (mg-xylene/mg- X_a)			4.1
K_P (mg-xylene/L)			0.51
K_{BT} (mg-benzene/L)	0.51		
K_{TB} (mg-toluene/L)	0.49		
β_1 (mg-xylene/mgCOD)			0.21
K_{PT} (mg-xylene/L)		0.87	
K_{TP} (mg-toluene/L)		25	
b (day^{-1})	0.06		

Y_2 = biomass true yield for the intermediate

$q_{2,max}$ = maximum specific rate of intermediate utilization

K_2 = half-maximum-rate concentration of intermediate

$q_{1,max}$ = maximum specific rate of toluene/benzene utilization

K_1 = half-maximum-rate concentration of toluene/benzene

$K_{i,12}$ = inhibition constant for toluene/benzene to their intermediates

β_2 = amount of *p*-xylene transformed per unit of biomass oxidized

K_P = half-maximum-rate concentration for *p*-xylene

K_{BT} = competitive inhibition constant of benzene to toluene

K_{TB} = competitive inhibition constant of toluene to benzene

β_1 = amount of *p*-xylene transformed per unit of toluene intermediate consumed

K_{PT} = competitive inhibition constant of *p*-xylene to toluene

K_{TP} = competitive inhibition constant of toluene to *p*-xylene

b = endogenous decay coefficient

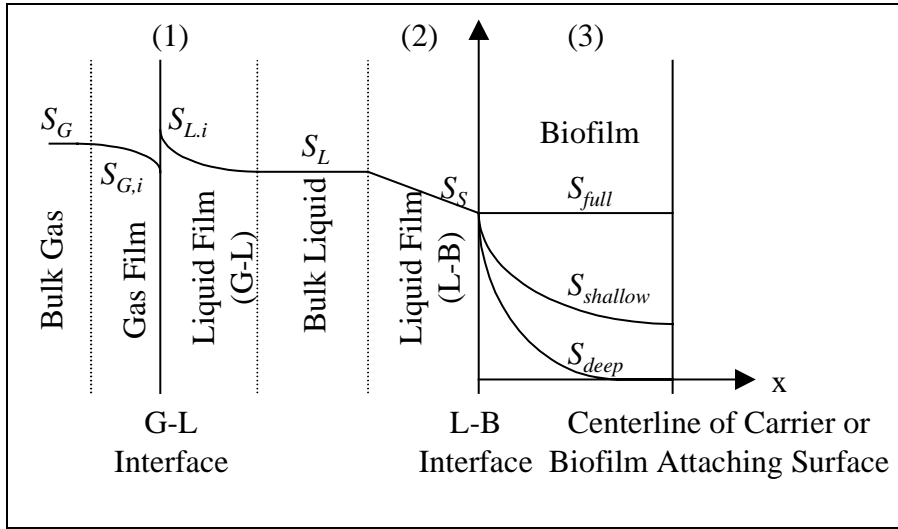


Figure 15. Typical concentration profile of a VOC (S) in a gas-liquid-solid three-phase biofilm reactor.

The flux of substrate across the liquid film at the liquid-biofilm interface is usually described by Fick's first law:

$$J = -D \frac{dS}{dx} = \frac{D}{L} (S_L - S_s) \quad (\text{Eq 6})$$

where J is the substrate flux into the biofilm ($M_s L^{-2} T^{-1}$), L is the thickness of the liquid film (L), D is the molecular diffusion coefficient in water ($L^2 T^{-1}$), and S_L and S_s are the substrate concentrations in the bulk liquid and at the liquid-solid interface, respectively ($M_s L^{-3}$).

Under steady-state conditions, the diffusion rates in processes (1) and (2) should balance if the degradation of the VOC by suspended biomass is negligible. Then $N_g * V = J * A + Q_L * S_L$, where V is the volume of the reactor (L^3), A is the total area of the liquid-biofilm interface (L^2), and Q_L is the flowrate of the liquid effluent ($L^3 T^{-1}$).

The reaction processes inside the biofilm drive the flux into the biofilm. Reactions in the biofilm lower the surface concentrations and create the gradients during the diffusion process. Rittmann and McCarty (1981) defined three-types of substrate concentration profiles in biofilm. In a fully penetrated biofilm, the substrate concentration in the biofilm has a negligible decrease from the surface concentration ($S_{full} = S_s$). In a deep biofilm, the substrate concentration (S_{deep}) reaches zero before the centerline of porous carrier or the biofilm attachment

surface. The case between these two extremes is a shallow biofilm (S_{shallow}). Due to the large amount of biomass accumulated in the carriers and the relatively rapid degradation kinetics for the BTX, the biofilm developed in this study is not likely a fully penetrated one, but it may be deep.

Removals in the Circulating-Bed Biofilm Reactor

Mass Balances in the Gas Phase

Because the BTX substrates were fed into the reactor through the gas stream, their mass balances in the gas phase are expressed as the following equation with toluene as an example:

$$M_{GL,T} = r_{\text{pump},T} \rho_T - S_{1,T,G} Q_G \quad (\text{Eq 7})$$

where $M_{GL,T}$ is the rate of toluene mass transferred from the gas into the liquid phase ($M_{\text{tol}} T^{-1}$), $S_{1,T,G}$ is the toluene concentration in the gas effluent ($M_{\text{tol}} L^{-3}$), and Q_G is the volumetric gas flowrate ($L^3 T^{-1}$). Since all the variables on the right-hand side of Equation 7 were experimentally measured or are known for a given temperature, $M_{GL,T}$ can be calculated directly.

The mass balance for oxygen is expressed as:

$$M_{GL,O} = (k_1 a)_O (O_{L,i}^* - O_L) V \quad (\text{Eq 8})$$

where $M_{GL,O}$ is the rate of oxygen mass transferred from the gas into the liquid phase ($M_{\text{oxy}} T^{-1}$), $(k_1 a)_O$ is the oxygen gas-liquid mass-transfer coefficient (T^{-1}), V is the reactor volume (L^3), $O_{L,i}^*$ is the liquid-phase concentration that would be in equilibrium with the bulk gas phase (S_G/H in Figure 15) ($M_{\text{oxy}} L^{-3}$), and O_L is the oxygen concentration in the bulk liquid phase (S_L in Figure 15) ($M_{\text{oxy}} L^{-3}$). The value $(k_1 a)_O$ can be computed using Equation 5, and $O_{L,i}^*$ can be computed using the known oxygen concentration in the gas stream and its Henry's constant. Therefore, $M_{GL,O}$ can be calculated from O_L , which was measured in this study.

Removals in the Bulk Liquid

The substrate and oxygen transferred from the gas into the liquid phase were removed by the suspended biomass in the bulk liquid, the biofilm in the carriers, or advected out of the reactor in the liquid effluent. In this study, the suspended biomass was always less than 1 percent of the total amount of biomass in the

reactor. However, its contribution to the substrate removal could be greater than 1 percent due to greater mass-transfer resistance in the biofilm. Therefore, the substrate removals by the suspended biomass were calculated using the concentrations of substrate, intermediates, and biomass in the liquid phase and the kinetic parameters shown in Table 12. In this study, it was assumed that the liquid regime in the circulating bed was completely mixed by the high recirculation rate and the carriers did not adsorb VOCs or oxygen.

Toluene as a single substrate.

When toluene was fed into the reactor as the sole substrate, the rates of removals for toluene, $R_{1,T,L}$ ($M_{\text{tol}} T^{-1}$) and its intermediate, $R_{2,T,L}$ ($M_{\text{mcat}} T^{-1}$), by the suspended biomass are expressed as:

$$R_{1,T,L} = \frac{q_{1,\text{max},T} S_{1,T,L}}{K_{1,T} + S_{1,T,L}} X_a \frac{O_L}{K_O + O_L} V_L \quad (\text{Eq 9})$$

$$R_{2,T,L} = \frac{q_{2,\text{max},T} S_{2,T,L}}{1 + \frac{S_{1,T,L}}{K_{1,12,T}}} \frac{S_{2,T,L}}{K_{2,T} + S_{2,T,L}} X_a \frac{O_L}{K_O + O_L} V_L \quad (\text{Eq 10})$$

in which $S_{1,T}$ is the concentration of toluene in the liquid, X_a is the concentration of active biomass, O_L is the concentration of dissolved oxygen, V_L is the volume of the liquid, and K_O is the half-maximum-rate concentration for oxygen in oxygenation. A dual-limitation term for oxygen was used to include the effects of oxygen. The oxygen consumption in the bulk liquid includes utilization associated with the degradation of toluene and its intermediate, and the decay of suspended biomass:

$$R_{O,L} = \alpha_{10,T} R_{1,T,L} + \alpha_{20,T} R_{2,T,L} + \alpha_{0,X} b X_a V_L \frac{O_L}{K_{O,r} + O_L} \quad (\text{Eq 11})$$

in which $K_{O,r}$ is the half-maximum-rate concentration for oxygen during respiration. In Equation 11, $\alpha_{0,X}$ is the oxygen stoichiometric coefficient for complete oxidation of biomass and equals $1.42 \text{ g-O}_2/\text{g-X}_a$ based on the molecular formula of biomass, $C_3H_7O_2N$. The stoichiometric coefficient of oxygen is $1_{0,T}$ in the first-step of toluene degradation. Based on the toluene degradation pathway, one mole of oxygen reacts with one mole of toluene to form one mole of 3-methylcatechol in the first-step reaction. Thus, $\alpha_{10,T}$ equals $0.348 \text{ g-O}_2/\text{g-toluene}$. In the second-step reaction, one mole of oxygen is used as a cosubstrate for every mole of 3-methylcatechol utilized. In addition, oxygen is used during respiration as the

electron acceptor. Thus, $\alpha_{2O,T}$ in Equation 11 is the amount of oxygen consumed per unit of 3-methylcatechol oxidized, which can be calculated based on the biomass true yield of 3-methylcatechol ($S_{2,T}$) (0.38 mg- X_a /mgCOD):

$$\begin{aligned} & \alpha_{2O,T} \left(\frac{g-O_2}{gCOD-S_{2,T}} \right) \\ &= 1 \frac{g-O_2}{gCOD-S_{2,T}} - 0.38 \frac{g-X_a}{g-COD} \frac{20 \text{mole-}e^- \text{eq}}{113g-X_a} \frac{8g-O_2}{\text{mole-}e^- \text{eq}} \\ &= 0.46 \frac{g-O_2}{gCOD-S_{2,T}} \end{aligned}$$

In Equation 11, the value of K_o equals 2.0 mg/L (Malmstead et al. 1995). The value of $K_{o,r}$ for oxygen used as the terminal electron acceptor was reported by Bae (1992) and Malmstead et al. (1995) and equals 0.02 mg/L.

Toluene and benzene as dual substrates.

The rates of removals for toluene/benzene in the liquid phase are similar to Equation 9, except that K_1 is modified by the competitive inhibition constant from the other substrate. For example, the rate of removal for toluene is:

$$R_{1,T,L,BT} = \frac{q_{1,\max,T} S_{1,T,L}}{K_{1,T} \left(1 + \frac{S_{1,B,L}}{K_{BT}} \right) + S_{1,T,L}} X_a \frac{O_L}{K_o + O_L} V_L \quad (\text{Eq 12})$$

The rates of removals for the intermediates of toluene ($R_{2,T,L,BT}$) and benzene ($R_{2,B,L,BT}$) are the same as Equation 10.

The rate of oxygen consumption is similar to Equation 11, except that degradation of toluene and benzene contribute to oxygen consumption:

$$\begin{aligned} R_{O,L,BT} &= \alpha_{1O,T} R_{1,T,L,BT} + \alpha_{2O,T} R_{2,T,L,BT} + \alpha_{1O,B} R_{1,B,L,BT} + \\ & \alpha_{2O,B} R_{2,B,L,BT} + \alpha_{O,X} b X_a V_L \frac{O_L}{K_{O,r} + O_L} \end{aligned} \quad (\text{Eq 13})$$

in which $\alpha_{1O,B}$ and $\alpha_{2O,B}$ equal 0.41 g- O_2 /g-benzene and 0.55 g- O_2 /gCOD- $S_{2,B}$, respectively.

Toluene and *p*-Xylene as dual substrates.

When toluene and *p*-xylene were fed simultaneously into the reactor, toluene was degraded as the primary substrate, and *p*-xylene was degraded as a cometabolic compound. The rates of removals for toluene ($R_{1,T,L,PT}$) and its intermediate ($R_{2,T,L,PT}$) in the liquid phase are similar to Equations 12 and 10, except that the second substrate is *p*-xylene.

The removal rate of *p*-xylene by the suspended biomass, $R_{1,P,L,PT}$ ($M_{\text{xyl}}T^{-1}$), can be expressed as (Yu 1998):

$$R_{1,P,L,PT} = (\beta_{1,T}R_{2,T,L,PT} + \beta_{2,T}bX_aV_L \frac{O_L}{K_O + O_L})^* \quad (\text{Eq 14})$$

$$\frac{S_p}{K_p(1 + \frac{S_{1,T}}{K_{TP}}) + S_p}$$

The rate of oxygen consumption is modified from Equation 12:

$$R_{O,L,PT} = \alpha_{1O,P}R_{1,P,L,PT} + \alpha_{1O,T}R_{1,T,L,PT} + \alpha_{2O,T}R_{2,T,L,PT} + \quad (\text{Eq 15})$$

$$\alpha_{O,X}bX_aV_L \frac{O_L}{K_{O,r} + O_L}$$

in which $\alpha_{1O,P}$ equals 0.30 g-O₂/g-xylene.

Removals by the Biofilm

At steady state, there is no net accumulation of any substrate in the biofilm. Therefore, the rate of utilization or production of a compound by the biofilm, which sometimes was called the rate of surface removal (Pedersen and Arvin 1995) or production, equals its mass flux into the biofilm.

Toluene as a single substrate.

At steady states, the mass flux of toluene into the biofilm, $J_{1,T}$ ($M_{\text{tol}}L^{-2}T^{-1}$), can be obtained from the mass balance of toluene in the reactor:

$$J_{1,T} = \frac{M_{GL,T} - R_{1,T,L} - Q_L S_{1,T,L}}{A} \quad (\text{Eq 16})$$

where $M_{GL,T}$, $R_{1,TL}$ are defined in Equations 6 and 8, respectively, and $S_{1,TL}$ is the toluene concentration in the liquid effluent ($M_{tol}L^{-3}$), and Q_L is the volumetric liquid flowrate of the effluent (L^3T^{-1}).

The toluene intermediate in the bulk liquid, $S_{2,TL}$, is generated either from the reaction of toluene in the liquid phase or outward diffusion from the biofilm, where the majority of the toluene is degraded. The mass flux of toluene intermediate into the biofilm, $J_{2,T}$ ($M_{meat}L^{-2}T^{-1}$), is then:

$$J_{2,T} = \frac{\alpha_{12,T}R_{1,T,L} - R_{2,T,L} - Q_L S_{2,T,L}}{A} \quad (\text{Eq 17})$$

The sign of $J_{2,T}$ could be negative in Equation 17, which indicates the flux of toluene intermediate is from the biofilm to the liquid, or it could be positive, which means that the intermediate's flux is into the biofilm.

The oxygen transferred from the gas phase into the liquid phase was used in the first- and second-step reactions, used in biomass decay, diffused into the biofilm, or advected out in the effluent. The mass flux of oxygen into the biofilm, J_o ($M_{oxy}L^{-2}T^{-1}$), is:

$$J_o = \frac{M_{GL,O} - R_{O,L} - Q_L O_L}{A} \quad (\text{Eq 18})$$

in which $M_{GL,O}$ and $R_{O,L}$ are defined in Equations 8 and 11, respectively.

To access the significance of mass-transfer limitation through the liquid-biofilm layer and the biofilm, the total effectiveness factor, η_T , is calculated for toluene:

$$\eta_T = \frac{r_{obs}}{r_{S_L}^*} \quad (\text{Eq 19})$$

where r_{obs} is the observed removal rate of toluene ($M_{tol}T^{-1}$), and r_{SL}^* is the rate that would occur if the toluene concentration equals its value in the bulk liquid everywhere in the carrier ($M_{tol}T^{-1}$). With the assumption that no removal occurs in the liquid film at the liquid-biofilm interface (Figure 15), $r_{obs} = J_{1,TA}$. The value for r_{SL}^* can be computed from the rate of toluene removal by the suspended biomass:

$$r_{S_{1,T,L}}^* = \frac{R_{1,T,L}TX_f}{X_a V_L} \quad (\text{Eq 20})$$

where $R_{1,TL}$ is defined in Equation 9, and TX_f is the total amount of biomass in the carriers (M_x), which equals the product of number of carriers loaded and the average biomass weight per carrier. In this study, the effectiveness factors for

toluene intermediate were not computed, because it also was produced inside the biofilm.

The total effectiveness factor includes the mass-transfer resistance in the biofilm and the liquid film. In this study, it is assumed that the resistance in the liquid film is negligible compared to the resistance in the biofilm because of the following two facts: (1) the flow regime in the reactor was turbulent due to its three-phase nature, and (2) the microstructure of the carrier surface is rough and highly irregular. The assumption implies that the total effectiveness factor is an indicator of the mass-transfer resistance in the biofilm. A low value of η_T means high mass-transfer resistance in the biofilm, and that the depth of penetration in the biofilm for toluene is small.

Toluene and benzene as dual substrates.

When toluene and benzene are degraded simultaneously, the mass fluxes of toluene/benzene and their intermediates are similar to Equations 16 and 17. For example, the mass fluxes for toluene and its intermediate are:

$$J_{1,T,BT} = \frac{M_{GL,T} - R_{1,T,L,BT} - Q_L S_{1,T,L}}{A} \quad (\text{Eq 21})$$

$$J_{2,T,BT} = \frac{\alpha_{12,T} R_{1,T,L,BT} - R_{2,T,L,BT} - Q_L S_{2,T,L}}{A} \quad (\text{Eq 22})$$

The mass-flux equation for oxygen is similar to Equation 18:

$$J_{O,BT} = \frac{M_{GL,O} - R_{O,L,BT} - Q_L O_L}{A} \quad (\text{Eq 23})$$

Toluene and *p*-xylene as dual substrates.

The mass-flux equations for toluene/*p*-xylene, toluene intermediate, and oxygen are the same as Equations 21-23, except that $R_{1,T,L,BT}$, $R_{2,T,L,BT}$, and $R_{O,L,BT}$ are replaced by $R_{1,T,L,PT}$ ($R_{1,P,L,PT}$ for *p*-xylene), $R_{2,T,L,PT}$, and $R_{O,L,PT}$, respectively. Since the *p*-xylene intermediate is not degraded by the biofilm, its mass flux is:

$$J_{2,P,PT} = \frac{\alpha_{12,P} R_{1,P,L,PT} - Q_L S_{2,P,L}}{A} \quad (\text{Eq 24})$$

Because the *p*-xylene intermediate did not accumulate inside the carriers, it can only take a negative value.

5 Results

Gas-Liquid Mass Transfer

The relationship between the concentrations of toluene in the gas and liquid phases during all the experiments (Ss1-Ss8) are shown in Figure 16. Also shown in Figure 16 are the conditions when the toluene in the two phases is at equilibrium (solid line). Clearly, the toluene in the gas and liquid phases was near equilibrium during this study. The same is true for benzene and *p*-xylene (Figure 17). Because biodegradation of BTX drives their transfer from the gas into the liquid phase, gas-liquid mass transfer of BTX was fast comparing to their biodegradation in the reactor and, consequently, did not limit the removal of BTX in this study.

If gas-liquid equilibrium existed for oxygen, the liquid concentrations of oxygen should equal their O^* values shown in Tables 9-11. As documented later in this chapter, the oxygen concentrations in the gas and liquid phases were not at equilibrium. Equation 8 shows that the difference between the O^* and liquid oxygen concentration drives the gas-liquid mass transfer of oxygen. Therefore, in this study, the total oxygen surface loading rates were calculated as $M_{GL,O}/A$, where $M_{GL,O}$ was defined in Equation 8.

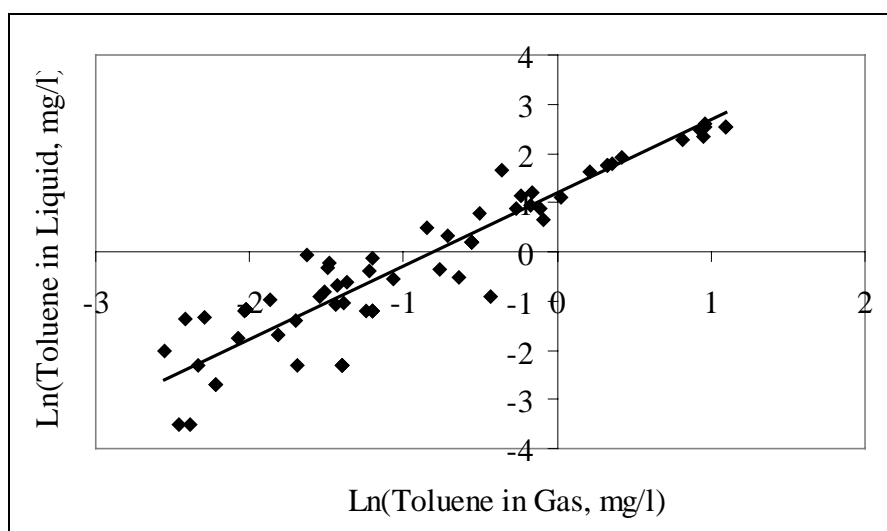


Figure 16. Relationship between toluene concentrations in the gas and liquid phases. The symbols are experimental data. The solid line is the gas-liquid equilibrium.

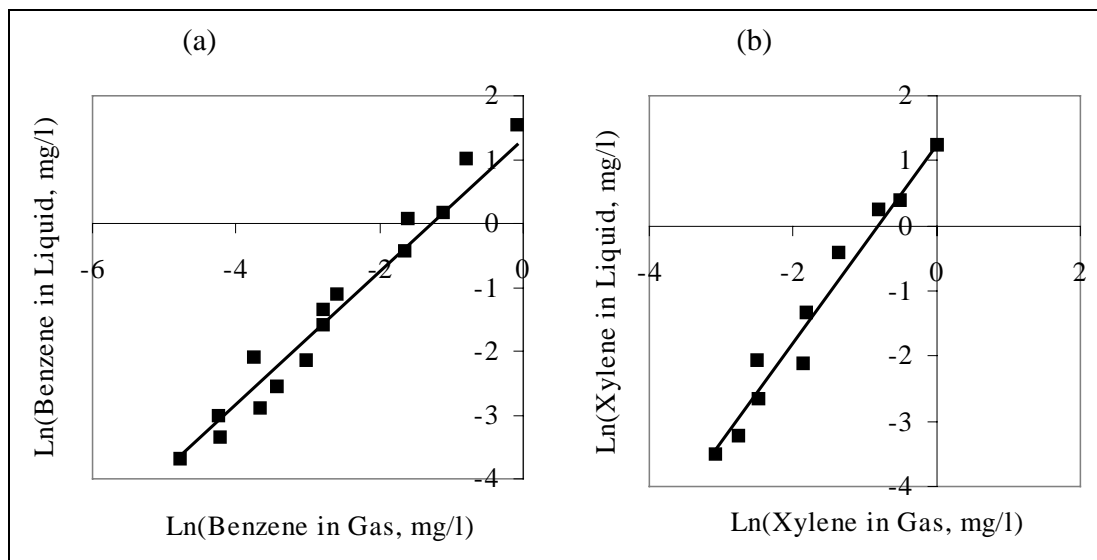


Figure 17. Relationship between (a) benzene and (b) *p*-xylene concentrations in the gas and liquid phases. The symbols are experimental data. The solid line is the gas-liquid equilibrium.

Biomass in the Circulating-Bed Biofilm Reactor

Biomass Fixed in the Porous Carriers

For every steady state, 20 to 30 carriers were removed from the reactor and measured for biomass attached to the carriers. Figure 18 shows the average biomass (dry weight) per carrier for the seven steady states described in Tables 9-11 and for Ss0. The datum Ss0 was taken 2 wk prior to SS1, and it indicates that the biomass accumulation in the carriers had reached a constant value. Figure 18 also shows that, as the toluene loading increased from 0.030 mol/m²-day to 0.059 mol/m²-day (Ss1 to Ss3), the biomass accumulated in the carriers also increased. Two samples were taken at the second steady state, Ss2. The first one was before any short-term experiments for Ss2 were started, and the second one was taken after Run Ss2-4 was completed and before Run Ss2-5 was started. The biomass dry weights in the carriers between the two measurements were almost identical, 1.4 mg/carrier. From Ss3 to Ss8, the biomass accumulated in the carriers did not change significantly due to the near-constant total COD loading rates.

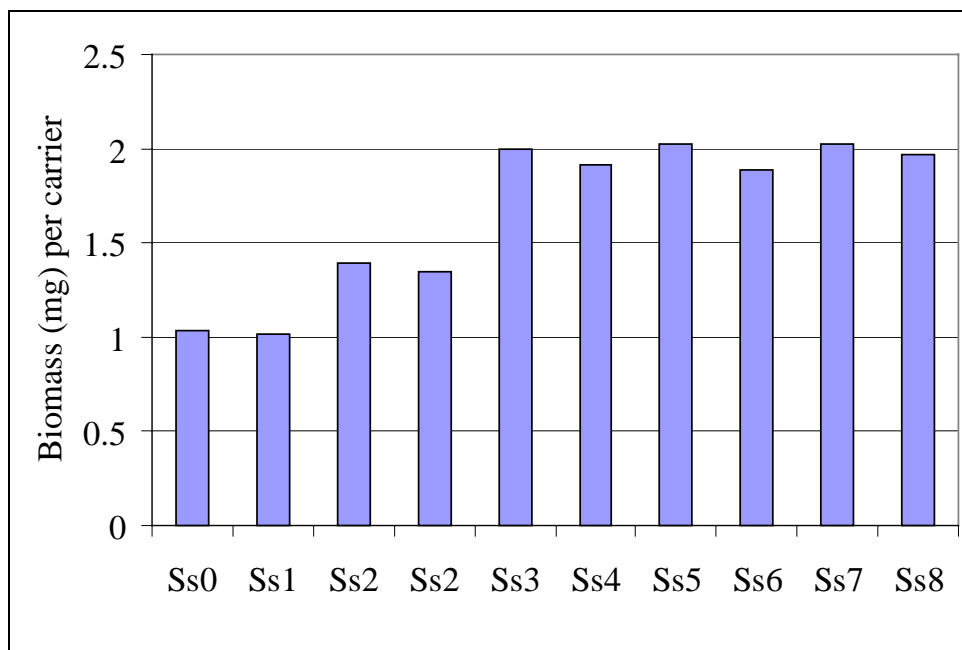


Figure 18. Average weight of biomass per porous carrier.

With the amount of carriers loaded in this study, the reactor had a specific biofilm surface area of $263 \text{ m}^2/\text{m}^3$. The biofilm concentration in the reactor, which is proportional to its weight per carrier, was $8.2 \text{ g-}X_a/\text{m}^2$ -biofilm surface or $2.2 \text{ kg-}X_a/\text{m}^3$ -reactor volume during Ss1. The biofilm accumulation inside the carriers can be calculated from the biomass dry weight and wet volume ($9.5 \times 10^{-2} \text{ cm}^3$) of each carrier based on the assumption that the pores were evenly filled with biomass after a long period of growth. During Ss1, the biofilm accumulation was $12 \text{ kg}/\text{m}^3$ -carrier.

Examining the carriers under an 80X stereoscope, it was found that most of the biomass was inside the carriers, not on the outer surface. Thus, the carriers efficiently protected the biomass from being washed out. Since the void volume inside each carrier was fixed, higher biomass accumulation suggested that the biomass accumulation was higher with higher substrate loading conditions.

Biomass in the Suspended Phase

The liquid-phase biomass concentrations during steady states Ss1-Ss3 and their short-term experiments are shown in Figure 19. In general, the values for each set of experiments for a series vary around a mean. For example, the biomass concentrations of the varied-toluene-loading experiments from Ss1 fluctuated from 7 mg/L to 15 mg/L , with a mean of nearly 11 mg/L . The mean values changed systematically, and more biofilm accumulation gave more biomass in the effluent. However, changes among the short-term experiments for a given

steady state showed no strong patterns except for Ss3, which had lower suspended biomass concentrations at high toluene loading or low oxygen loading rates. It is not clear if changes in the liquid-phase biomass were caused by changes in growth of suspended bacteria or by detachment of biofilm. However, evidence suggests that the detachment may have been more important. The suspended biomass always was less than 1 percent of the total biomass present in the reactor, and it was mostly tiny flocs, suggesting that they were detached from the biomass on the carriers.

The suspended biomass concentrations during Ss4-Ss6 and Ss7-Ss8 showed similar trends to those observed in Ss3 and varied between 30-44 $\text{mg-X}_a/\text{L}$ and 30-40 $\text{mg-X}_a/\text{L}$, respectively (data not shown).

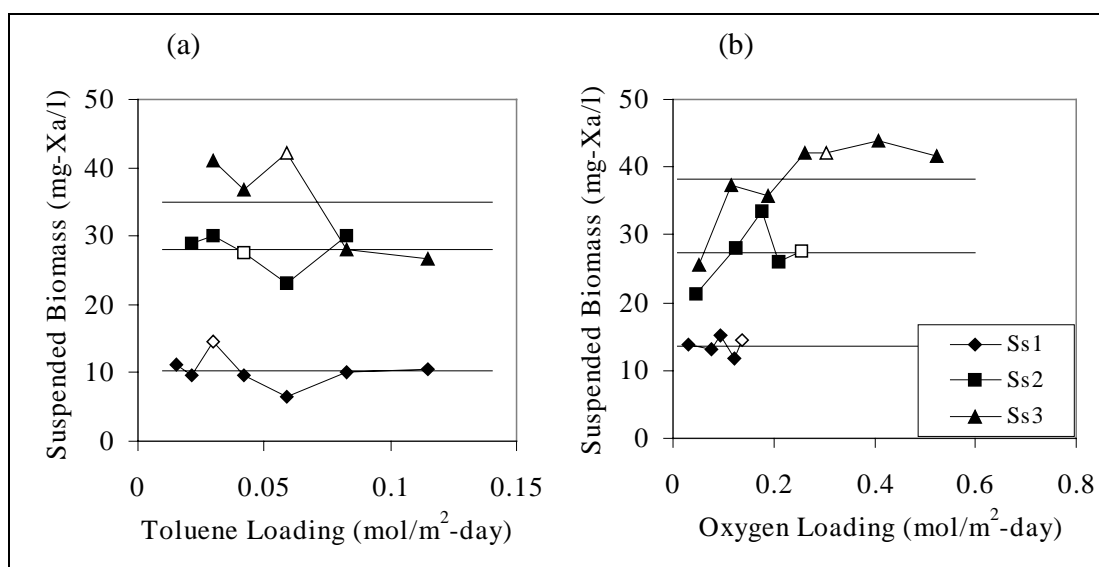


Figure 19. Measured and average biomass concentrations in the bulk liquid during steady states Ss1-Ss3 and their short-term experiments. (a) Runs with 100% air, (b) Runs with toluene loading rates at the steady-state values: 0.030, 0.042, and 0.059 $\text{mol}/\text{m}^2\text{-day}$ for Ss1, Ss2, and Ss3, respectively. The open symbols are data from the steady states. The horizontal lines are means of the data for all runs associated with a steady state.

Removals of Toluene as the Sole Substrate

Overall Responses of the Reactor

The results from the steady-state runs Ss1-Ss3 and their corresponding short-term experiments are compared in Figures 20 to 37.* In these figures, the

* Figures will be presented as they are discussed in the remainder of this chapter.

graphs labeled (a) show the results for runs of varying total toluene surface-loading rates when the gas stream was fixed as 100 percent air. The graphs labeled (b) show the results for runs of varying total oxygen surface-loading rates when the toluene loading was fixed at one of the steady state values: 0.030, 0.042, and 0.059 mol/m²-day for Ss1, Ss2, and Ss3, respectively. In these figures, the open symbols are for the steady states, and the closed symbols are for the short-term experiments.

Figure 20 shows the DO concentrations in the liquid phase at the three steady states and their short-term experiments. Figure 20(a) shows that, as the toluene loading increased, the DO concentration decreased steadily and then leveled off. The leveling implies that the reactor had reached its capacity for oxidizing the toluene. Figure 20(a) also shows that, at equal toluene-fluxes, the oxygen consumption was higher when more biofilm was available for biodegradation (i.e., Ss3>Ss2>Ss1). In Figure 20(b), the dissolved oxygen concentration increased with the oxygen flux. Figure 20(b) also shows that, at equal oxygen fluxes, the oxygen consumption was higher when more biofilm was available for biodegradation.

Although the liquid-phase oxygen concentration was at least 3 mg/L when gas stream was 100 percent air, oxygen limitation probably occurred inside the carrier due to diffusion limitation. The leveling off to maximum capacity (Figure 20(a)) was possibly controlled by oxygen limitation inside the carriers.

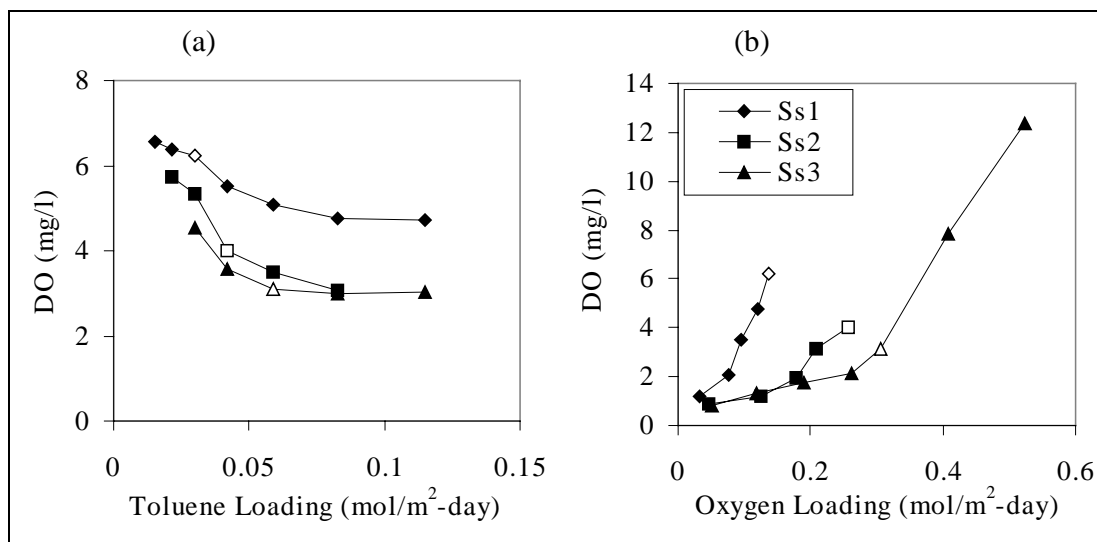


Figure 20. DO concentrations in the bulk liquid during Ss1-Ss3.

Figures 21-23 show the concentrations of toluene in the gas effluent, toluene in the liquid effluent, and the COD in the liquid effluent during steady states Ss1-Ss3 and their short-term experiments. As toluene loading increased or oxygen loading decreased, all three concentrations increased dramatically.

Comparing the (a) graphs of Figures 21-23 with the (a) graph of Figure 20 suggests that oxygen limitation was the most significant factor controlling toluene removal for high toluene loading. On the other hand, the last three data points for Ss2 and Ss3 and the last four points for Ss1 did not show significantly improved toluene and COD removal with increasing oxygen fluxes (presented in Figure 20(b)). Therefore, oxygen was not rate limiting when the liquid-phase oxygen concentration was greater than 2-3 mg/L for the steady state toluene loading rates used.

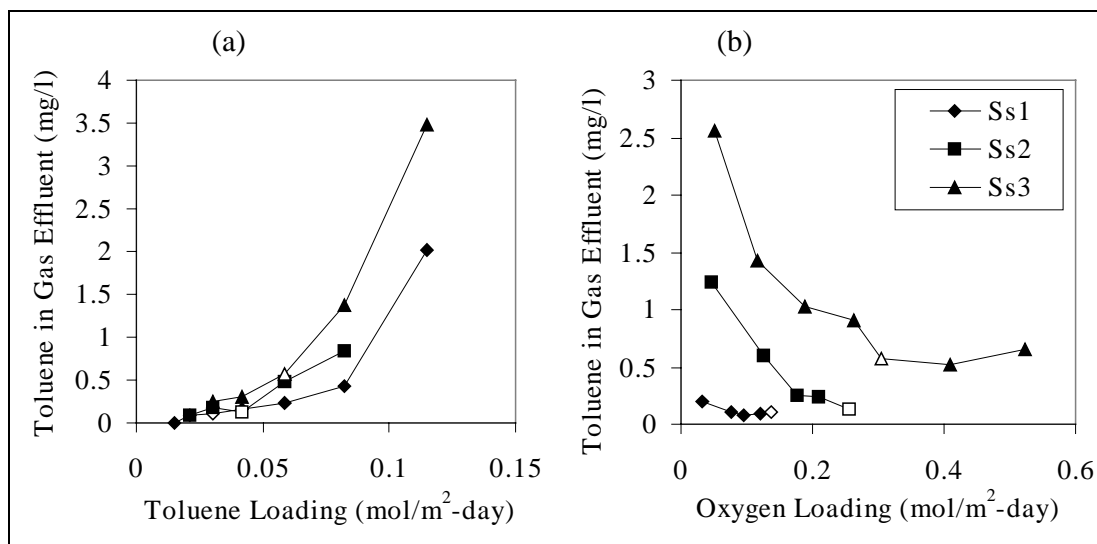


Figure 21. Toluene concentrations in the gas effluent during Ss1-Ss3.

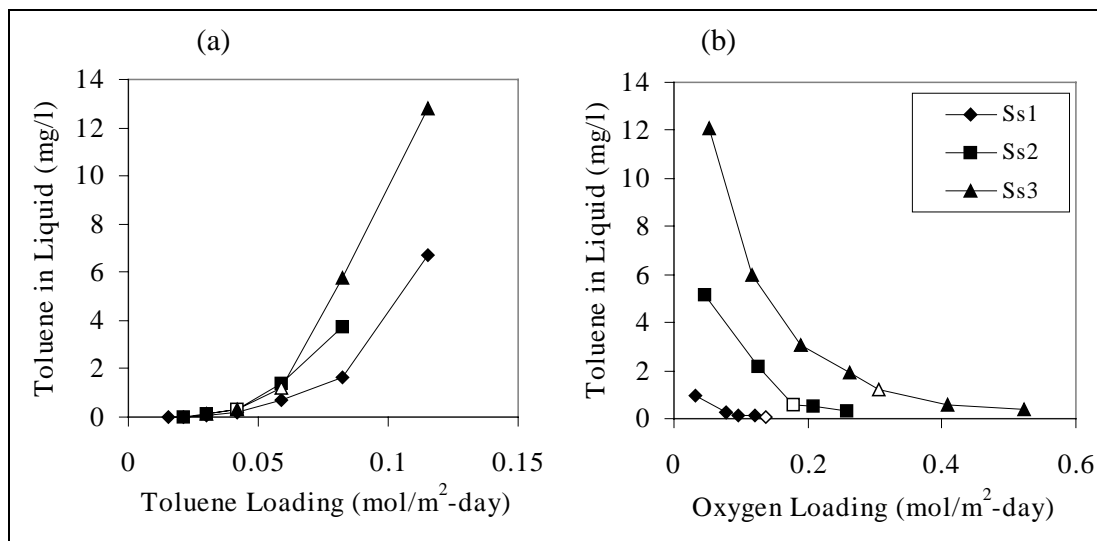


Figure 22. COD concentrations in the bulk liquid during Ss1-Ss3.

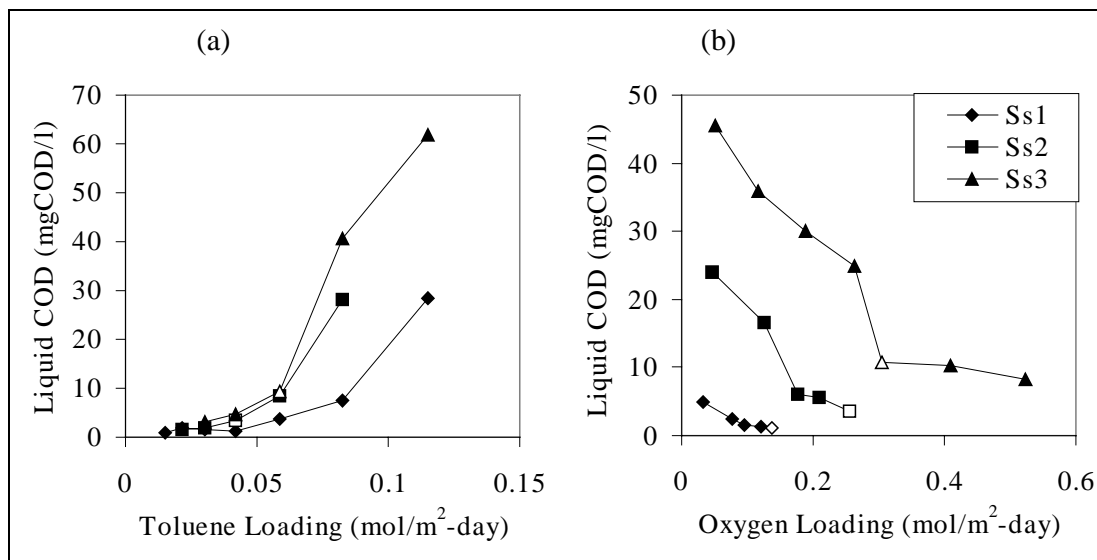


Figure 23. COD concentrations in the bulk liquid during Ss1-Ss3.

The COD in the liquid measures the total oxygen demand by toluene, its intermediate, and soluble microbial products. Figure 24 shows the fractions of the liquid COD attributed to toluene during Ss1-Ss3 and their short-term experiments. When the gas stream was 100 percent air, the fractions of toluene/total COD were higher with increased toluene loading (Figure 24(a)). When the total toluene loading was fixed, the fractions of toluene/total COD increased when oxygen flux decreased (Figure 24(b)). These trends support that the first step — toluene oxygenation — was rate limiting when the toluene loading was high and/or the oxygen loading was low.

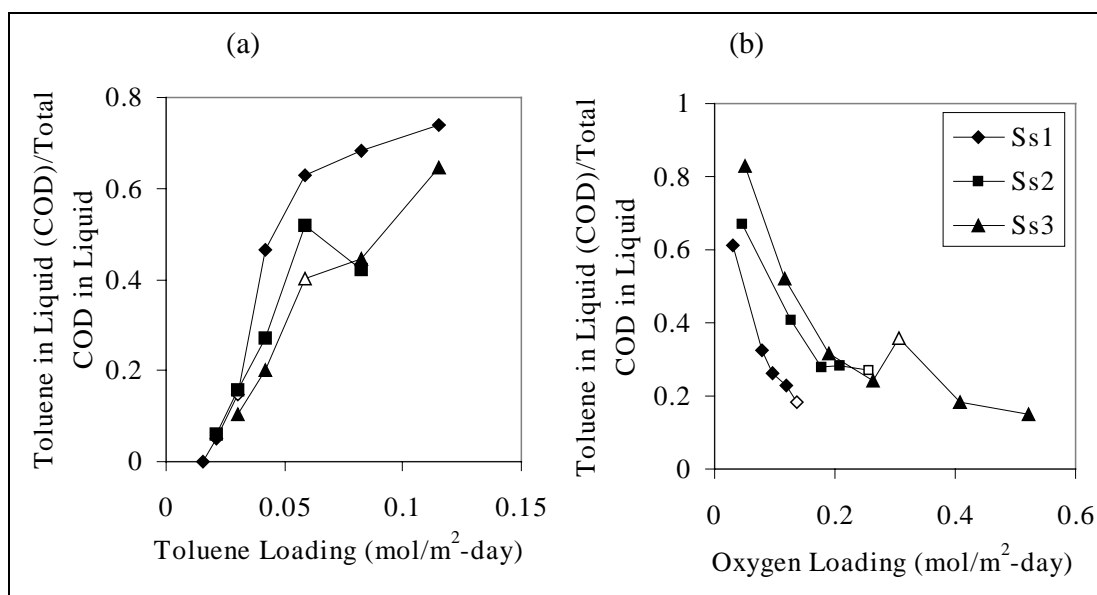


Figure 24. The fraction of COD in the liquid that was toluene during Ss1-Ss3.

Two removal efficiencies by the circulating-bed biofilm reactor are calculated. The first is the removal efficiency of toluene, calculated based on the amount of toluene entering (gas phase) and leaving (gas and liquid phases) the reactor. The second is the removal efficiency of total COD, calculated based on the amount of COD entering (toluene in the gas phase) and leaving (toluene in the gas and liquid phases plus intermediate COD in the liquid phase) the reactor. Figures 25 and 26 show the percentage removals of toluene and COD, respectively. In general, the efficiencies decreased with increases in toluene loading or decreases in oxygen loading. Dramatic decreases are observed for the highest one or two toluene-loading rates and for the 1 to 4 lowest oxygen-fluxes, which also were when cresols were detected in the liquid effluent. For example, the efficiencies for Ss1 and its short-term runs were higher than 92 percent for all but the highest toluene or the lowest oxygen loading. For the lowest toluene loading ($0.015 \text{ mol/m}^2\text{-day}$), the toluene removal was almost 100 percent, and a very small amount of COD (0.93 mgCOD/L) was in the liquid effluent. Except for the highest toluene loading, the COD removal was only slightly less than the toluene removal, and effluent COD was 0.93 to 7.6 mgCOD/L . At the highest toluene loading, the intermediates in the liquid phase were high (16 mgCOD/L), and the COD removal was 3 percent lower than toluene (77 percent vs. 80 percent). Thus, in cases for which intermediates persist, the removal of COD may be the more stringent criterion for assessing reactor performance.

The discrepancies between the removal efficiencies of toluene and COD also were significant at very low oxygen-loading rates. For example, at the lowest oxygen loading rate ($0.025 \text{ mol/m}^2\text{-day}$), the efficiencies for toluene and COD removal of Run Ss2-8 were 55 percent and 49 percent, respectively (Figures 25(b) and 26(b)). Figures 25 and 26 also show that, when oxygen-loading rates were above certain values, the removals of toluene and COD did not increase further because oxygen was not limiting the reaction anymore.

Figures 25 and 26 show that the toluene removal in the Ss3 experiments was less than in the Ss1 experiments, although Ss3 had more biomass in the carriers. This result is probably caused by greater oxygen limitation in the biofilm in Ss3. Oxygen availability might be more severely restricted during Ss3 than Ss1 for several reasons. First, the higher biomass accumulation in the carriers during Ss3 increased the mass-transfer resistance in the biofilm significantly. Second, the larger amount of biomass in the carriers consumed more oxygen for respiration (Figure 20). Consequently, the penetration depth of oxygen in the biofilm decreased significantly. Although more biomass accumulated in the carriers during Ss3, less biomass was available to degrade toluene and its intermediate.

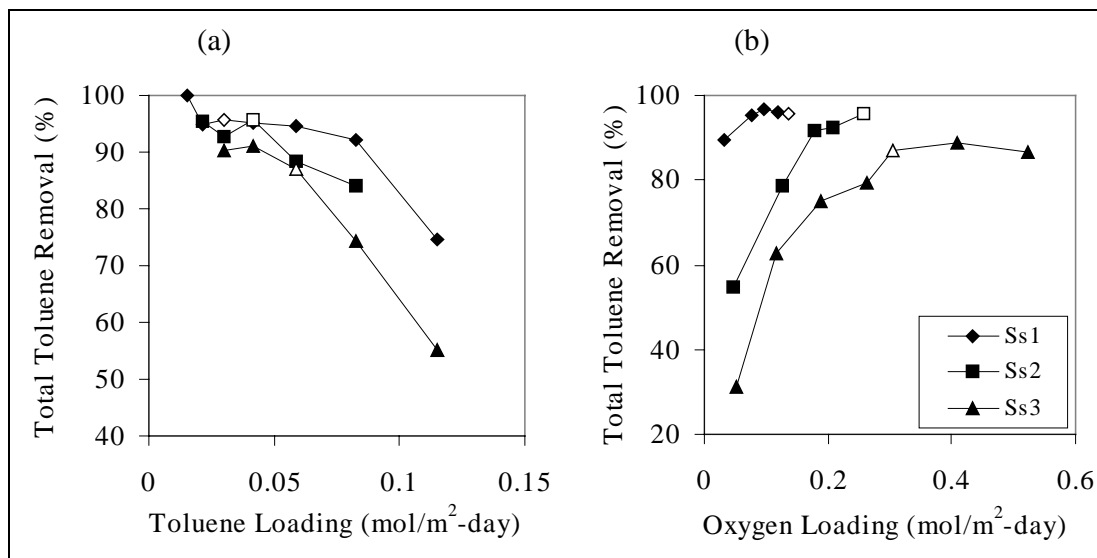


Figure 25. Toluene removal from the circulating bed during Ss1-Ss3.

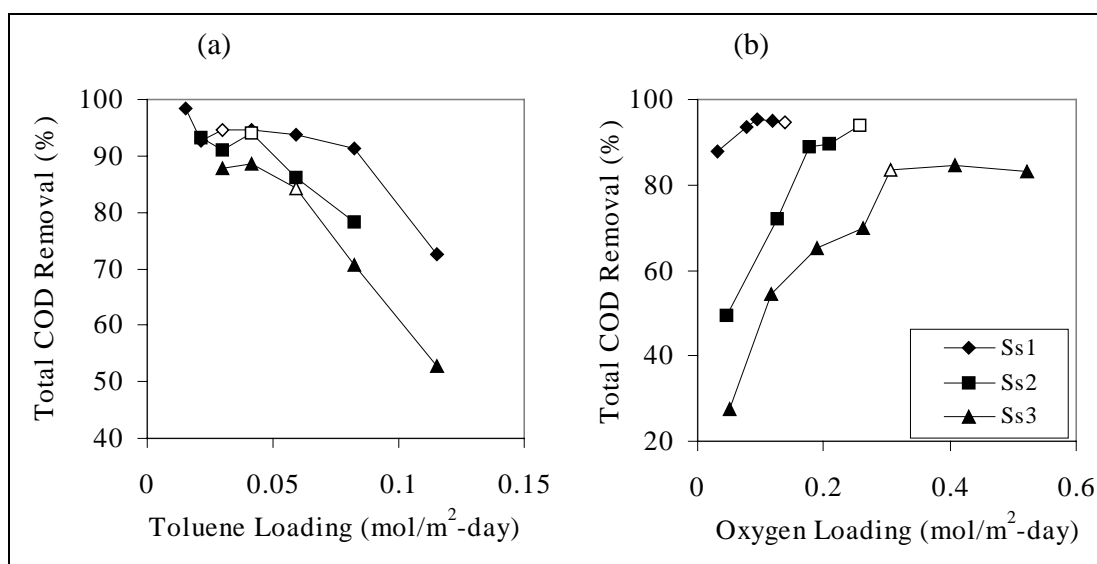


Figure 26. COD removal from the circulating bed during Ss1-Ss3.

Figure 27 shows the percentages of COD removals vs. directly measured variables such as toluene and DO concentration in the bulk liquid. When the gas stream was 100 percent air, total COD removal decreased linearly with the liquid toluene concentration, and the percentage of removal was lower when the biofilm accumulation was greater. When toluene-loading rates were fixed, low DO concentration dramatically decreased the percentages of COD removed. The DO concentration, above which the maximum rate occurred, depended on biofilm accumulation. A higher DO was needed with larger biofilm accumulation. For all the runs in this study, a DO concentration above 3 mg/L did not improve the COD removal significantly.

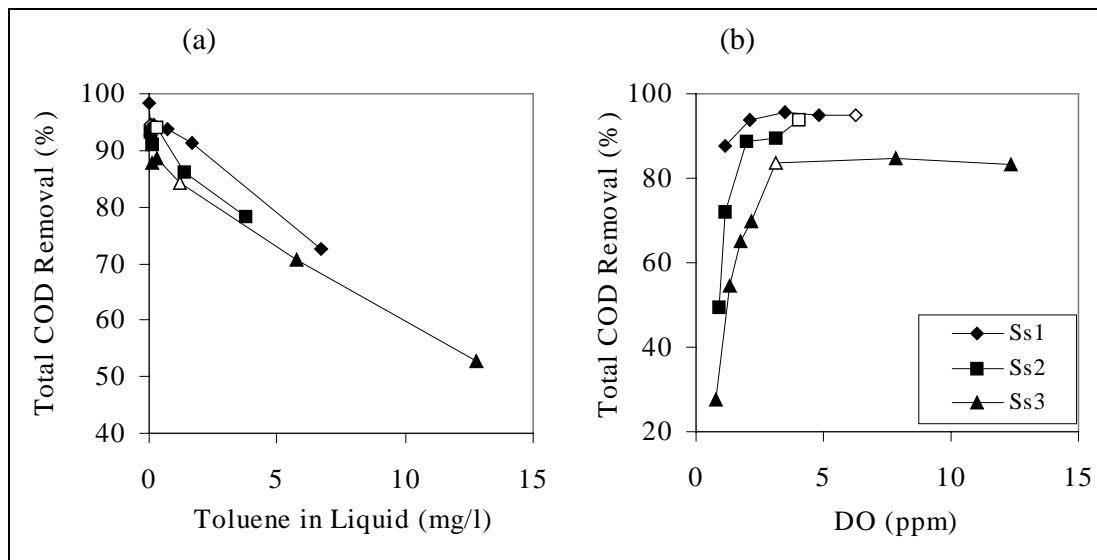


Figure 27. COD removals at various concentrations of toluene and DO from the circulating bed during Ss1-Ss3.

Removals by the Suspended Biomass

Figure 28 shows what percentages of the total removal of toluene were attributed to the suspended biomass in the circulating-bed biofilm reactor. The percentage of total toluene removal by the suspended biomass varied from zero to as high as 30 percent. When the gas stream was 100 percent air (Figure 28(a)), the percentages increased with higher toluene loading and with greater biomass accumulated in the carriers, which correlates to a higher average suspended-biomass concentration (Figure 19). When the toluene loading was fixed at the steady state values (Figure 28(b)), increased oxygen loading shifted the removal of toluene to the biofilm. Both results taken together strongly support that oxygen was limiting the toluene removal inside the biofilm. Dual limitation of toluene and oxygen occurred in the biofilm, but the biomass in the suspended phase was not subjected to the diffusion limitations in the carriers and responded to the increases of toluene concentration in the liquid phase more dramatically. Therefore, its contribution to the total toluene removal increased whenever the biofilm became more diffusion-limited for oxygen. At higher biomass concentrations in the carriers, the resistance to mass transfer was greater, making the contribution of suspended biomass greater. Likewise, a low DO concentration accelerated oxygen limitation in the biofilm.

Figure 29 shows the percentages of the toluene intermediate removed by the suspended bacteria. Although a higher percentage was removed in the liquid phase when more biomass accumulated in the carriers, the trends are opposite to those for toluene in response to toluene and oxygen loading. An increase of toluene loading or a decrease in O_2 loading shifted the intermediate removal into the

biofilm. These trends could be caused by toluene inhibition, which was relieved by the low toluene concentrations inside the biofilm. Toluene concentrations were higher in the bulk liquid for high toluene loading and low oxygen loading (Figure 20). Thus, the impact of diffusion resistance in the biofilm would be greatest in these cases and would have the positive effect of reducing inhibition.

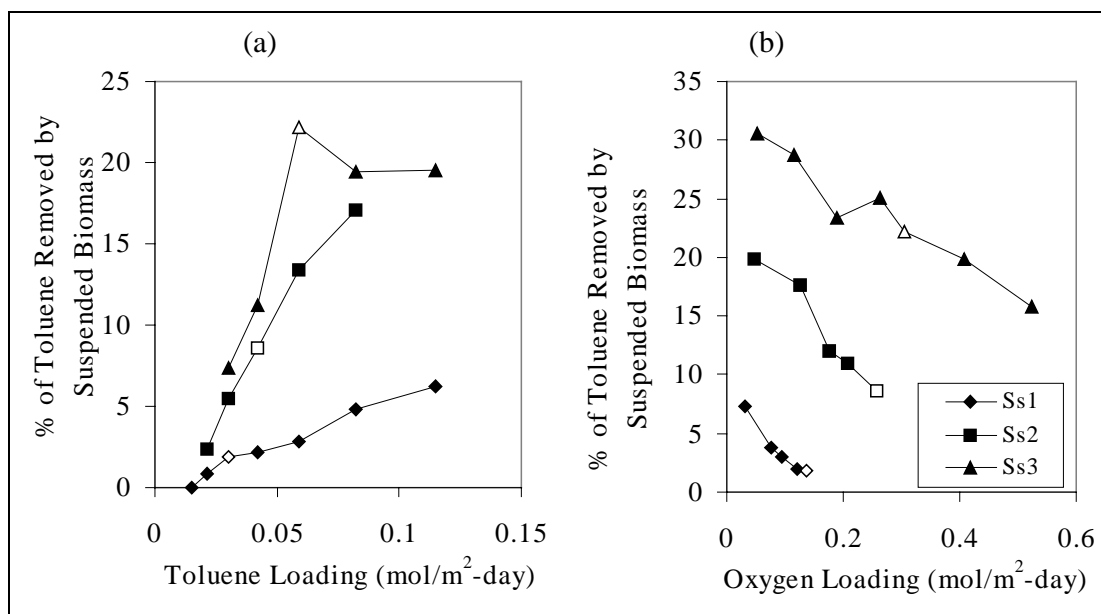


Figure 28. Percentages of toluene removal by the suspended biomass to the total toluene removal during steady states Ss1-Ss3 and their short-term experiments.

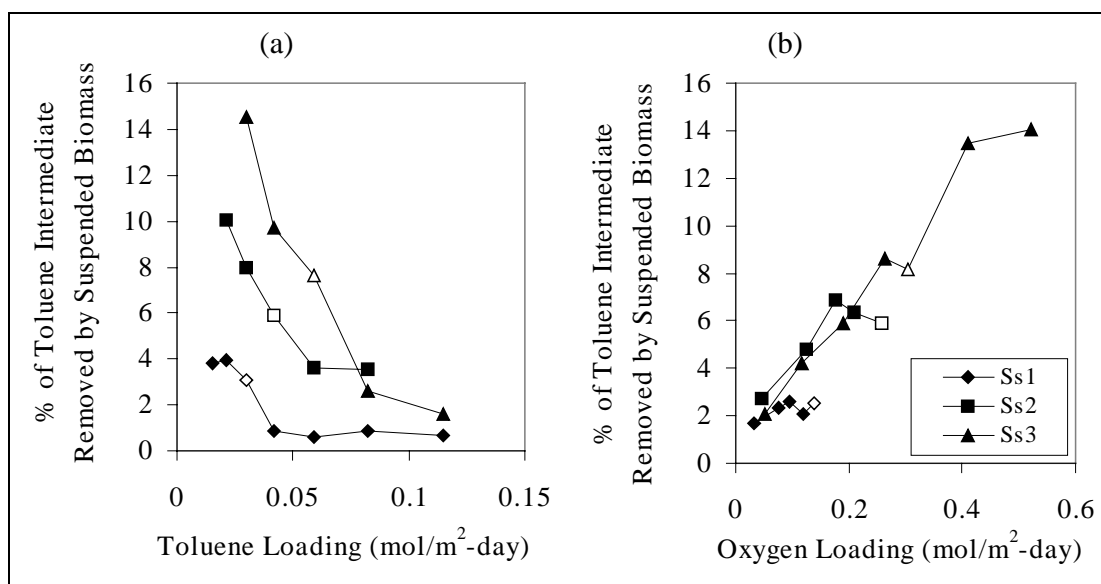


Figure 29. Percentages of toluene intermediate removal by the suspended biomass to its total removal during steady states Ss1-Ss3 and their short-term experiments.

The percentages of oxygen consumed in the liquid, shown in Figure 30, do not show a clear trend for toluene, but decrease with increasing oxygen fluxes. This result can be explained by the stoichiometry and kinetics of oxygen consumption during the two steps of toluene degradation. In the first reaction, 1 mole of oxygen reacts with 1 mole of toluene to produce one mole of its intermediate. Based on the value of $\alpha_{2,O,T}$, each mole of toluene intermediate consumes 3.68 moles of oxygen during its complete oxidation. When toluene loading increases, the increase in oxygen consumption by the first-step reaction (Figure 28(a)) and the decrease in oxygen consumption by the second-step reaction (Figure 29(a)) in the liquid offset each other. Consequently, the total amount of oxygen consumed in the liquid shows no clear trends with toluene loading. On the other hand, when oxygen loading increases, the increase in oxygen consumption in the biofilm by the first-step reaction (Figure 28(b)) outweighs the increase in oxygen consumption in the liquid (Figure 29(b)). Therefore, oxygen consumption in the liquid became less important when the oxygen loading increases.

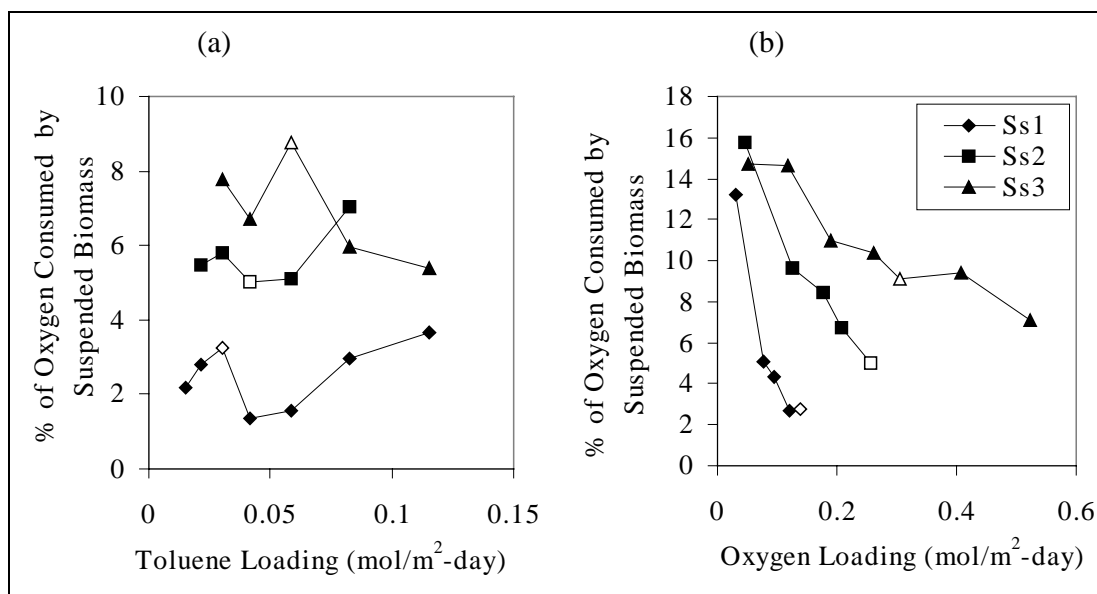


Figure 30. Percentages of oxygen consumed by the suspended biomass to its total consumption during steady states Ss1-Ss3 and their short-term experiments.

Removals by Biofilm

Figure 31 shows that, when the total surface loading of toluene and oxygen increased, their surface removals by the biofilm also increased. The slope of the relationship for toluene decreases as its loading increases, while the slope for oxygen is a constant. The trends for toluene suggest that there is a toluene removal “capacity” for the amount of biomass active under the steady state conditions; above that capacity increased toluene loading does not increase its removal

in the biofilm, even when oxygen does not appear limiting in the biofilm. The overall effective factor for toluene, calculated using the concentrations of toluene and oxygen in the bulk liquid, at the highest toluene-loading rate during Ss3 was less than 0.03. Therefore, only a small fraction of biomass in the carriers, at the outer surface, was active in degrading toluene.

Figure 32 shows the effectiveness factors of biofilm for toluene during Ss1-Ss3 and their short-term experiments. When the gas stream was 100 percent air (Figure 32(a)), the effectiveness factors were higher when biofilm accumulation was lower, possibly due to the less mass-transfer resistance associated with lower biofilm accumulation. For the same biofilm accumulation in each steady

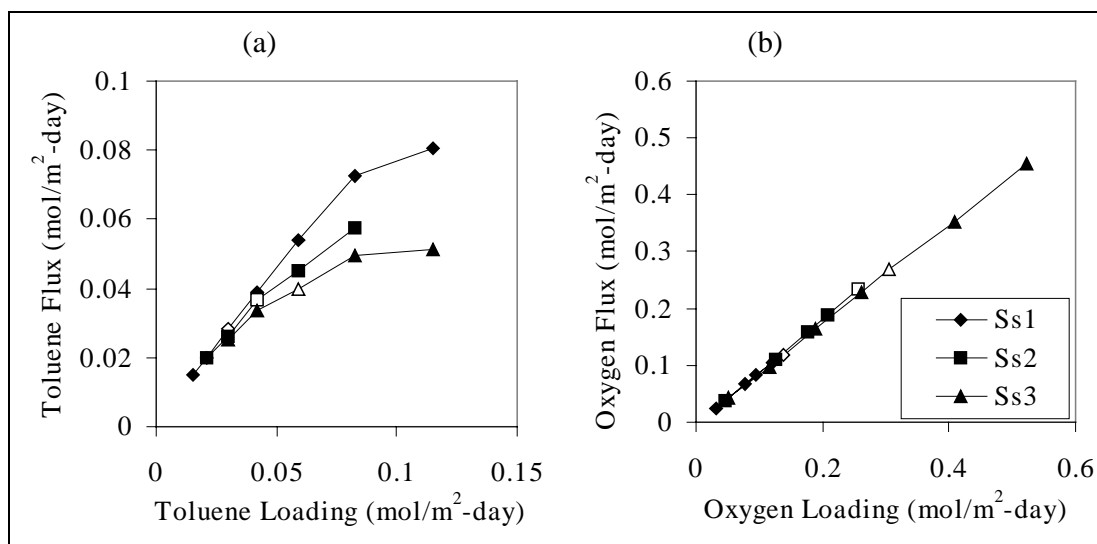


Figure 31. Relationship between total toluene/oxygen loading rates and their biofilm removals during steady states Ss1-Ss3 and their short-term experiments.

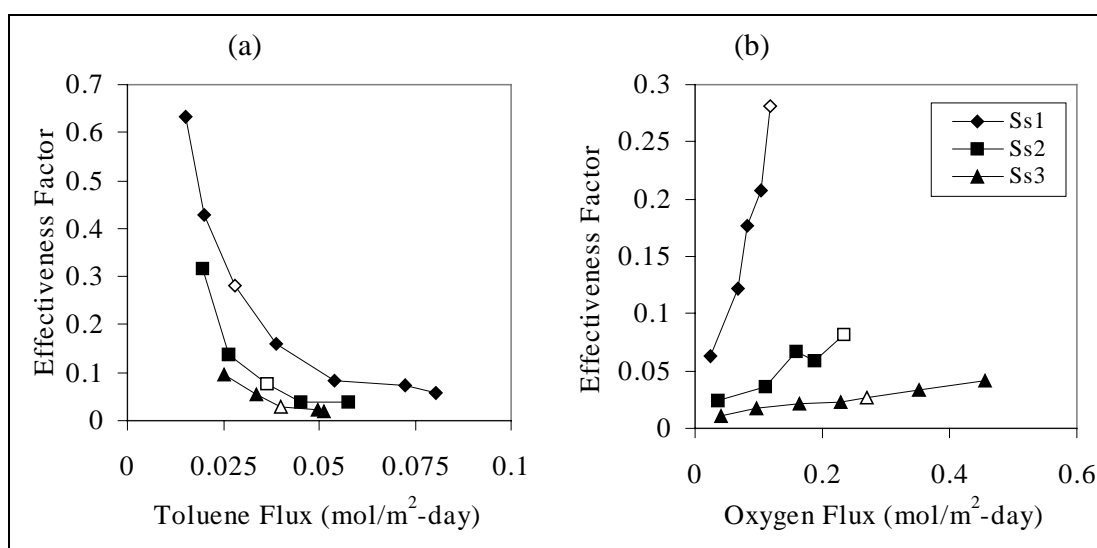


Figure 32. Relationship between toluene/oxygen fluxes and the total effectiveness factors for toluene during steady states Ss1-Ss3 and their short-term experiments.

state, increased toluene-loading rates caused the effectiveness factors to decrease and eventually level off. This result supports that oxygen was depleted in a shallower depth from the biofilm surface at higher toluene fluxes and limited the toluene degradation reaction. The effects of oxygen on toluene degradation are further demonstrated in Figure 32(b). When the toluene loading was fixed during each steady state, decreased oxygen loading caused the effectiveness factors for toluene to decrease continuously. In other words, the portion of the biofilm active in substrate oxidation became smaller as the DO concentration declined.

Figure 33 shows the fluxes of the toluene intermediate into (or out of) the biofilm at various toluene or oxygen loading rates. At low toluene loading, the intermediate diffused from biofilm into the liquid, as indicated by the negative signs for its fluxes. As toluene loading increased, the intermediate fluxes from the biofilm decreased, reached zero at about $0.32 \text{ mol/m}^2\text{-day}$, and then increased in the reverse direction. Since the fluxes were positive, the intermediate diffused into the biofilm at high toluene loading rates. The changes happened at about the same toluene-loading rate, but were more dramatic for carriers with higher biomass accumulation. The intermediate flux leveled off at higher toluene loading, while for Ss3, the flux into the biofilm started to decrease even at very high toluene loading. The change of flux direction was caused by two related phenomena. First, a larger percentage of toluene was removed in the liquid at high toluene loading (Figure 28(a)), which caused the intermediate to accumulate in the liquid. Second, intermediate removal was less inhibited by toluene in the biofilm, where the toluene concentrations were lower than that in the liquid. Perhaps at the very high toluene loading (the highest one for Ss3), the toluene in the biofilm began inhibiting the intermediate degradation.

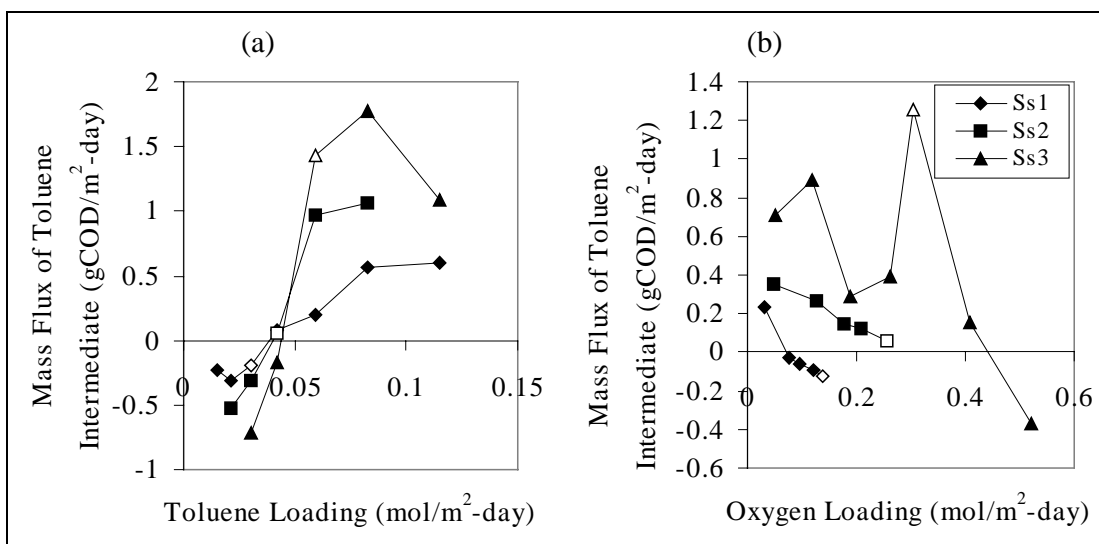


Figure 33. Relationship between total toluene/oxygen loading and the mass fluxes of toluene intermediate into the biofilm during steady states Ss1-Ss3 and their short-term experiments.

The fluxes of intermediate in response to the oxygen loading, on the other hand, showed the opposite trends, except for one outlier at Ss3. At higher oxygen loading rates, more toluene was converted to its intermediate in the biofilm (Figure 28(b)). Therefore, the intermediate fluxes were negative as oxygen limitation on toluene degradation was relieved. The oxygen fluxes at which the intermediate flux changed its direction were much lower for carriers with lower biomass accumulations, likely due to their lower O_2 consumption by respiration or mass-transfer resistance. The change in direction of the toluene intermediate is an important finding in this study because it supports the ideas that (1) toluene degradation is limited strongly by oxygen, and (2) the intermediate degradation is limited strongly by toluene inhibition.

Figure 34 shows the fluxes of the toluene intermediate at various ratios of the toluene and oxygen fluxes. Both types of experiments with varying toluene and oxygen loading rates showed the same trends. When the gas stream was 100 percent air (graph (a)), the flux of intermediate for Ss1 was zero when the ratio was near the stoichiometric ratio for complete oxidation of toluene (0.21 mol-toluene/mol- O_2). With higher toluene/oxygen flux ratios, the flux of intermediate was positive, but much more dramatic for carriers with higher biomass accumulations. When more biomass accumulated in the carriers, the toluene/oxygen flux ratios at which the intermediate flux was zero were lower than the stoichiometric ratio for complete oxidation of toluene. This result supports that oxygen consumed in the carriers for biomass respiration was important in relation to the consumption by toluene degradation reactions.

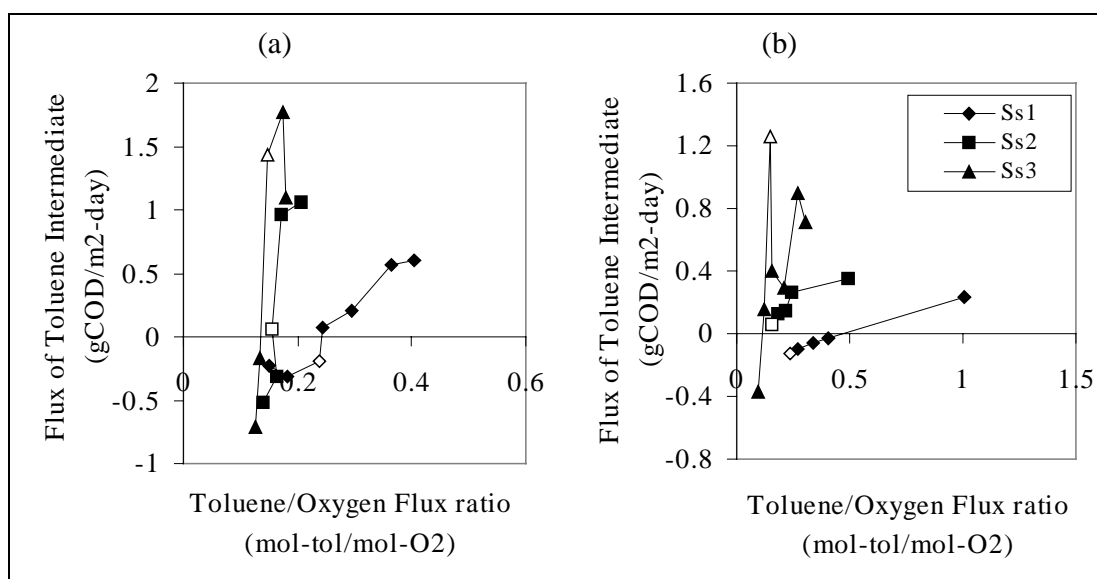


Figure 34. Mass fluxes of toluene intermediate into the biofilm at various ratios of toluene and oxygen fluxes.

Figures 35 and 36 show the dependencies of mass fluxes of toluene, its intermediate, and oxygen into the biofilm on the concentrations of toluene and oxygen in the liquid, respectively. Figure 36 shows that the toluene flux (i.e., biofilm surface removal rate) follows a relationship similar to the Monod-type with toluene and oxygen concentrations. At low concentrations of toluene or oxygen in the liquid, the flux increases linearly (first order) with the concentrations of toluene or oxygen. At higher concentrations, the reaction order decreases to zero, indicating that the other substrate is rate limiting. The apparent “half-maximum-rate” concentrations for oxygen, $K_{o,p}$ depend on biomass accumulation in the carriers and equal 0.65, 0.85, and 1.2 mg- O_2 /L for biomass densities of 12, 16, and 23 kg/ m^3 (Ss1-Ss3), respectively.

The trends of intermediate flux into the biofilm in response to the concentrations of toluene and oxygen, presented in Figure 36, are similar to those shown in Figure 33. With increased toluene concentration or decreased oxygen concentration, the direction of mass flux of intermediate shifts from outward to inward as a result of stronger inhibition by the toluene in the liquid phase. The inhibition effect caused by high concentration of toluene in the liquid is also shown for Ss3 (graph (a)).

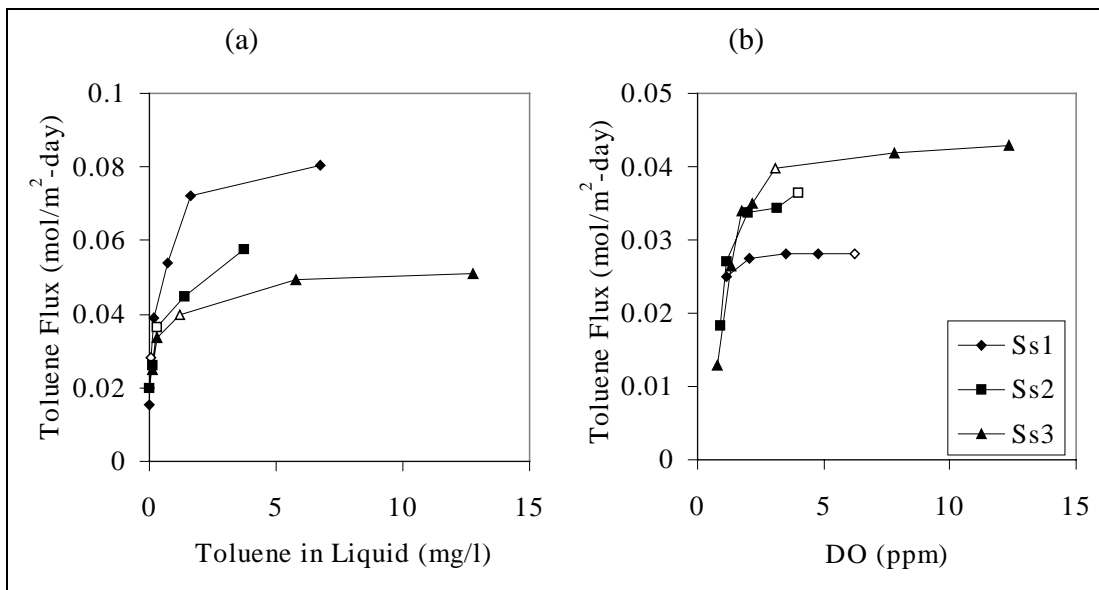


Figure 35. Dependency of toluene fluxes into the biofilm on the concentrations of toluene and oxygen in the liquid.

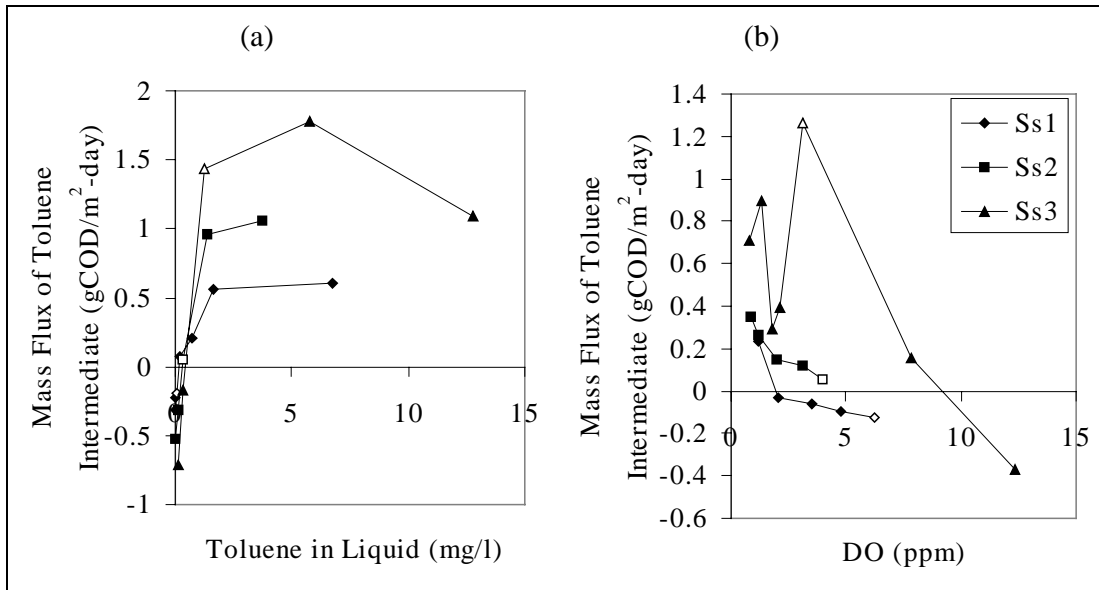


Figure 36. Dependency of intermediate fluxes into the biofilm on the concentrations of toluene and oxygen in the liquid.

The dependency of oxygen flux on the toluene and oxygen concentrations in the liquid is shown in Figure 37. When the gas stream was 100 percent air (graph (a)), the oxygen flux into the biofilm increased quickly with toluene concentration and reached a plateau, after which further increase of toluene concentration had no effect on oxygen consumption in the biofilm. On the other hand, when toluene loading was kept the same (graph (b)), oxygen flux continued to increase with DO concentration. This result supports the observation of Figure 34 that oxygen consumed in the carriers by biomass respiration was important for establishing the active depth of the biofilm.

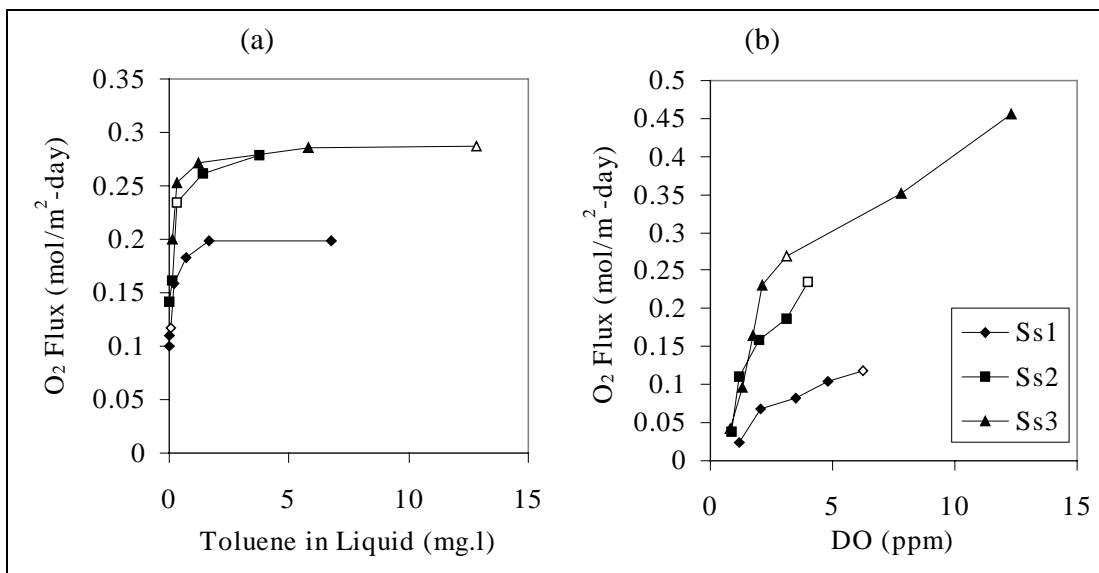


Figure 37. Dependency of oxygen fluxes into the biofilm on the concentrations of toluene and oxygen in the liquid.

Summary

The experiments using toluene as the sole substrate systematically studied the reactor performance under either toluene- or oxygen-varying conditions at three different biofilm accumulations. The most significant findings of these experiments are that toluene removal is most strongly limited by the availability of oxygen, and that toluene intermediate removal is most strongly limited by inhibition from toluene.

The first conclusion is demonstrated by these observations. When the oxygen loading decreased, the fraction of effluent COD that was toluene increased significantly, and the toluene removal efficiencies were much lower. The rate of toluene surface removal by the biofilm also decreased as the DO concentration in the bulk liquid decreased, causing a shift of zero-order kinetics for DO at high DO concentrations to first-order at low DO concentrations. One interesting behavior of the reactor was that the toluene removals decreased at higher biofilm accumulation in the carriers. Since the reaction kinetics were the same at these different biofilm accumulations, the decrease in toluene/COD removals is most likely due to more severely limited oxygen availability inside the carriers at higher biomass accumulation, when endogenous respiration was greater.

The second conclusion is demonstrated by these observations. Increased toluene loading caused more toluene intermediate to be removed inside the biofilm. When toluene loading was low, intermediate produced from toluene degradation inside the biofilm diffused out of the biofilm, while at high toluene loading the intermediate diffused into the biofilm, where the concentration of toluene was lowered by diffusion limitation. Similarly, when oxygen loading decreased in the reactor, the resulting higher concentrations of toluene in the liquid caused the toluene intermediate to diffuse into the biofilm.

Another important finding is that the suspended biomass played a key role even though it was only about 1 percent or less of the total biomass. Since biomass grows when degrading toluene, the suspended biomass is always present in this type of reactor, either from growth of the suspended biomass itself or detachment from the carriers. The change in the direction of the mass flux of toluene intermediate is a key sign of the role of the suspended biomass in toluene degradation. For example, when toluene loading was high (high toluene concentration in liquid) or the DO low, the suspended biomass quickly transformed a large quantity of toluene into its intermediates, which then diffused into the biofilm and was removed there. The suspended biomass could become more important in these settings because it was less diffusion limited, particularly for oxygen. On the other hand, the intermediate generated by the suspended biomass had to be degraded in the biofilm, where toluene inhibition was relieved by diffusion resistance.

These results have significant implications in optimizing the reactor performance. For example, they suggest that a large accumulation of biofilm should be avoided in order to maximize the toluene removal efficiency and oxygen utilization efficiency. In this study, the only factor that affected the biofilm accumulation was the COD loading. Other factors that could affect the biofilm accumulation inside the carriers are most possibly related to the physical/chemical characteristics of the carriers, such as porosity, pore size, and the surface properties of the pores.

Removals of Toluene and Benzene as Dual Substrates

Overall Responses of the Reactor

Steady states 4 to 6 (Ss4-Ss6) studied the removals of toluene and benzene as dual substrates. To avoid complications caused by variation in biomass accumulation in the carriers, the total surface loading of COD was maintained the same as Ss3, while toluene was replaced by benzene from Ss4 to Ss6 (Table 10). Figure 18 showed that the weight of biomass per carrier only varied slightly from Ss4 to Ss6. Figures 38 and 39 show the concentrations of toluene and benzene in the gas and liquid effluents during Ss4-Ss6, respectively. The general trends shown in Figures 38 and 39 are similar to those for toluene during Ss1-Ss3 (Figures 21(a) and 22(a)). Toluene and benzene concentrations increased steadily with their total surface loading rates. Since more toluene was replaced by benzene in the toluene/benzene mixture from Ss4 to Ss6, the concentrations of toluene at the same COD loading rates were from Ss4 to Ss6, while the trends for benzene were the opposite.

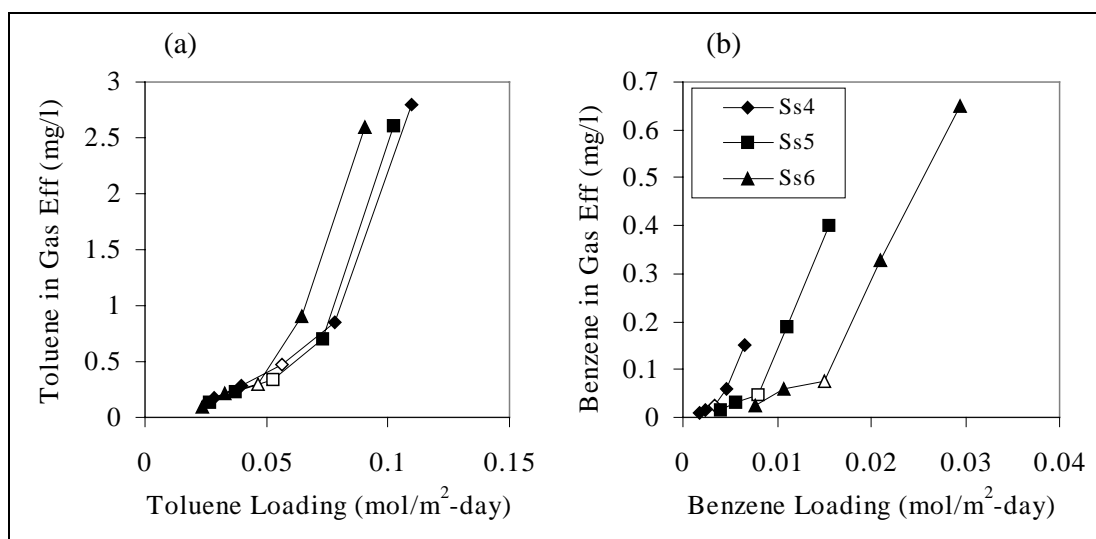


Figure 38. Concentrations of toluene and benzene in the gas effluent during Ss4-Ss6.

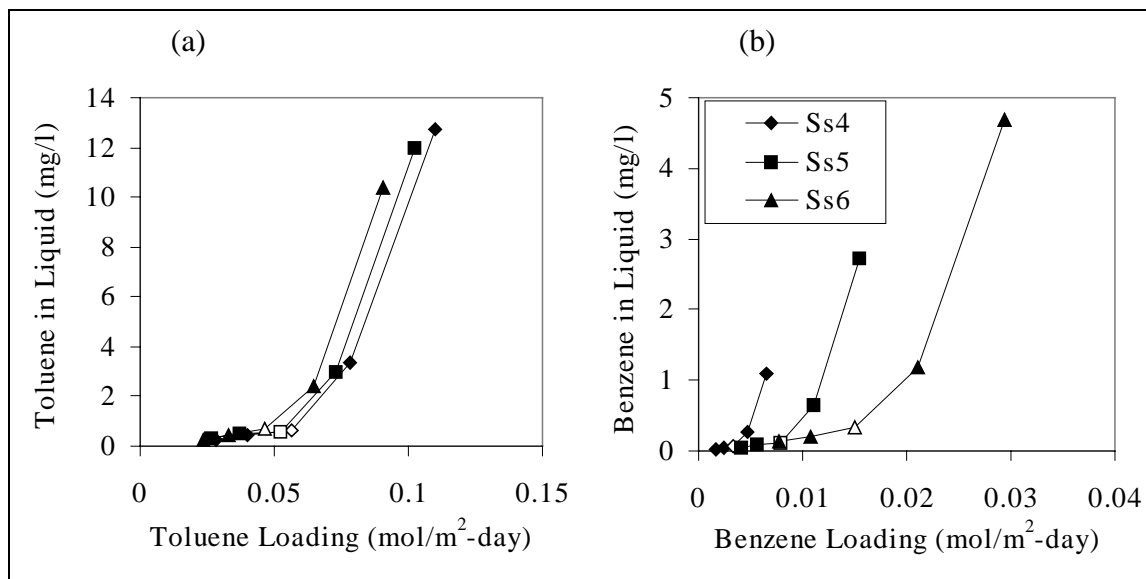


Figure 39. Concentrations of toluene and benzene in the liquid effluent during Ss4-Ss6.

For toluene, its concentrations in the liquid were less than 1.0 mg/L for all the runs except the two highest COD loading rates. For benzene, its concentrations in the liquid were less than 0.5 mg/L for all the runs except the highest COD loading of Ss4 and the two highest COD loading rates of Ss5-Ss6.

Figure 40 shows the concentrations of DO and COD in the bulk liquid during Ss4-Ss6. The values of DO and COD were very close to each other during the steady states and short-term experiments. They also were close to those for Ss3 (Figures 20(a) and 23(a)). In general, the DO values decreased initially and then leveled off as the total COD loading increased. The COD concentrations in the bulk liquid increased steadily with the total COD loading. Runs Ss3 to Ss6 spanned more than 1 month over time. The DO and COD removal results indicate that stable biofilm activity in the circulating bed was maintained in this study even after many short periods of overloading and underloading during the short-term experiments.

The similarities in reactor performance among Ss4-Ss6 also can be found in Figures 41 and 42, which show the percentages for toluene, benzene, and total COD removal. Similar to the runs with toluene as the sole substrate, the removal efficiencies of toluene and benzene differed from those of COD. At low loading rates, more than 90 percent of toluene and benzene were removed, while only 85 to 90 percent of the COD was removed. At the highest loading rate, however, the removals of toluene, benzene, and COD were between 57 and 60 percent, 45 and 53 percent, and 51 and 55 percent, respectively. Thus, when more than one substrate was degraded, their removal efficiencies were all different, depending on the kinetics of their biodegradation reactions and interactions. Therefore,

removals of COD and individual substrates need to be monitored to fully characterize system performance.

Figure 42 also shows that the COD removals among Ss4-Ss6 were nearly identical when the loading was below 17 gCOD/m²-day, which was the steady state. When the loading was higher than the steady state value, the COD removal in the reactor was slightly lower when toluene was replaced by benzene. Overall, the COD removals reached a plateau for the highest two loading rates, for which percentage removals decreased from more than 85 percent to slightly over 50 percent. For the lowest three COD loading rates, the percentage removals only decreased from 90 to 85 percent.

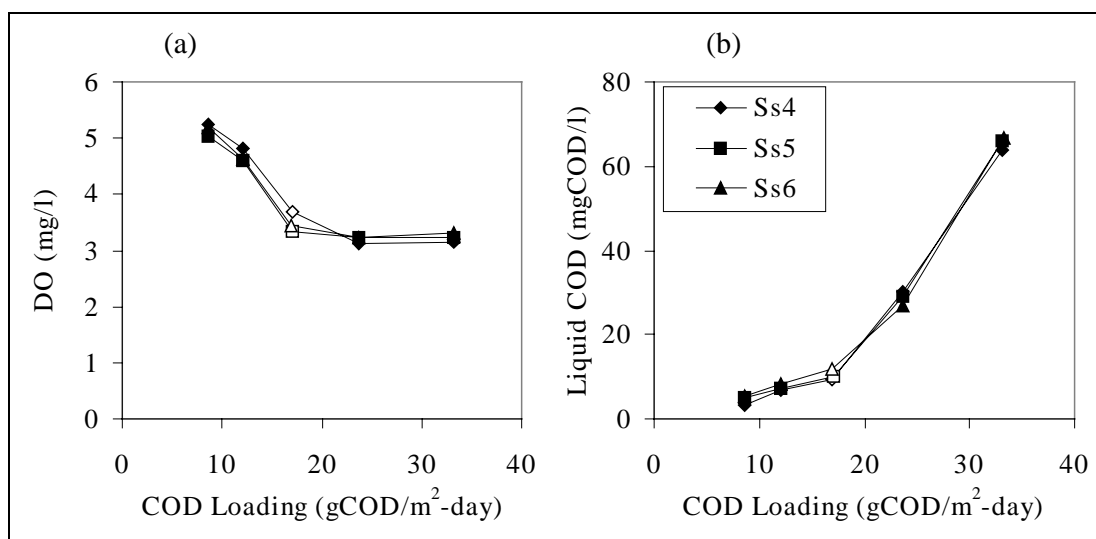


Figure 40. DO and COD concentrations in the bulk liquid during Ss4-Ss6.

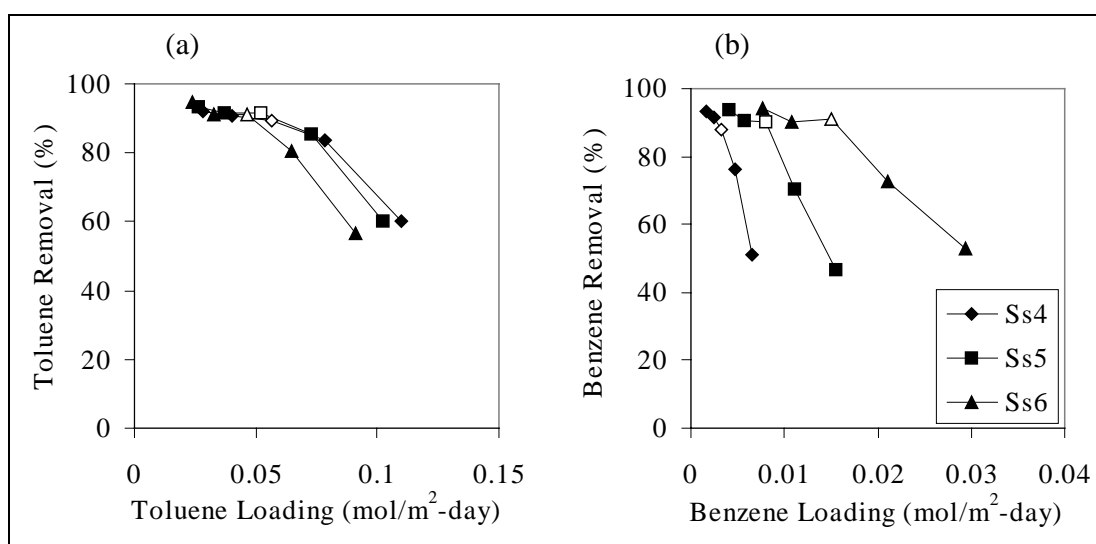


Figure 41. Toluene and benzene removals from the circulating bed during Ss4-Ss6.

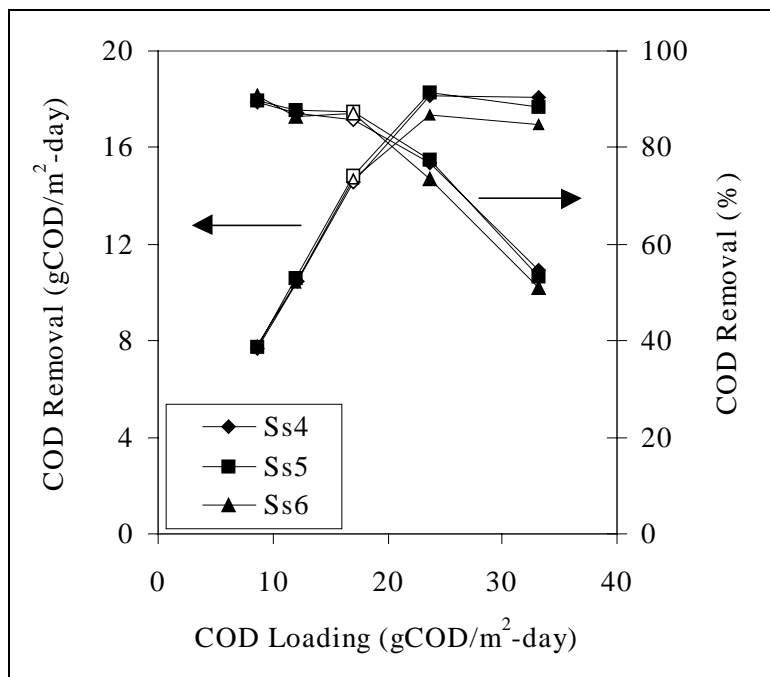


Figure 42. COD removals from the circulating bed during Ss4-Ss6.

The slightly decreased reactor performance when more toluene was replaced by benzene was most likely due to the competitive inhibition between toluene and benzene (Yu 1998). The inhibition effect is only significant when the concentration of the inhibiting compound is well above the inhibition constant. The inhibition constants for toluene and benzene, K_{TB} and K_{BT} , were similar (i.e., 0.49 mg-toluene/l and 0.51 mg-benzene/L, respectively) (Yu 1998). Figure 39 shows that the toluene and benzene concentrations were below 1.0 mg/L for all the loading rates equal and less than the steady state values. Therefore, the inhibition effects between toluene and benzene were minimal under these loading rates, as indicated by the nearly identical reactor performance among Ss4-Ss6.

At the two highest COD loading rates, the liquid concentrations of toluene were greater than 2.0 mg/L, and the liquid concentrations of benzene were greater than 0.5 mg/L, except for the second highest loading rate during Ss4. Toluene and benzene inhibit each other's first-step reactions. The inhibition between toluene and benzene was the strongest during Ss6 because both substrates were at higher concentrations. Consequently, the overall reactor performance was the worst for Ss6 during the highest two loading rates. Since the concentrations of toluene were always higher than that of benzene, the inhibition of benzene degradation from toluene was the greater. This result contributed to the observation that the percentage removals of benzene were about 10 percent lower than toluene at the highest COD loading rate, although the benzene loading was only about one-third the loading of toluene.

During Ss4-Ss6, other trends observed for toluene and benzene were similar to those for toluene during Ss1-Ss3. The effect caused by the noncompetitive inhibition from BTX to their intermediates is one example. Figure 43 shows the percentages of toluene and benzene intermediates that were removed by the suspended biomass. For both, increased loading rates during each steady state/short-term runs forced their intermediates to be removed in the biofilm, where inhibition was less severe due to the lower toluene and benzene concentrations. From Ss4-Ss6, benzene concentrations in the liquid decreased at the same benzene loading (Figure 39(b)). Consequently, the percentages of benzene intermediates removed by the suspended biomass were highest for Ss6 at the same benzene loading. In this study, only the total COD values for toluene and benzene intermediates were measured directly. The COD for each intermediate was computed from the molar ratio between the intermediates of toluene and benzene, which equaled the ratio of their peak areas on the HPLC spectrum.

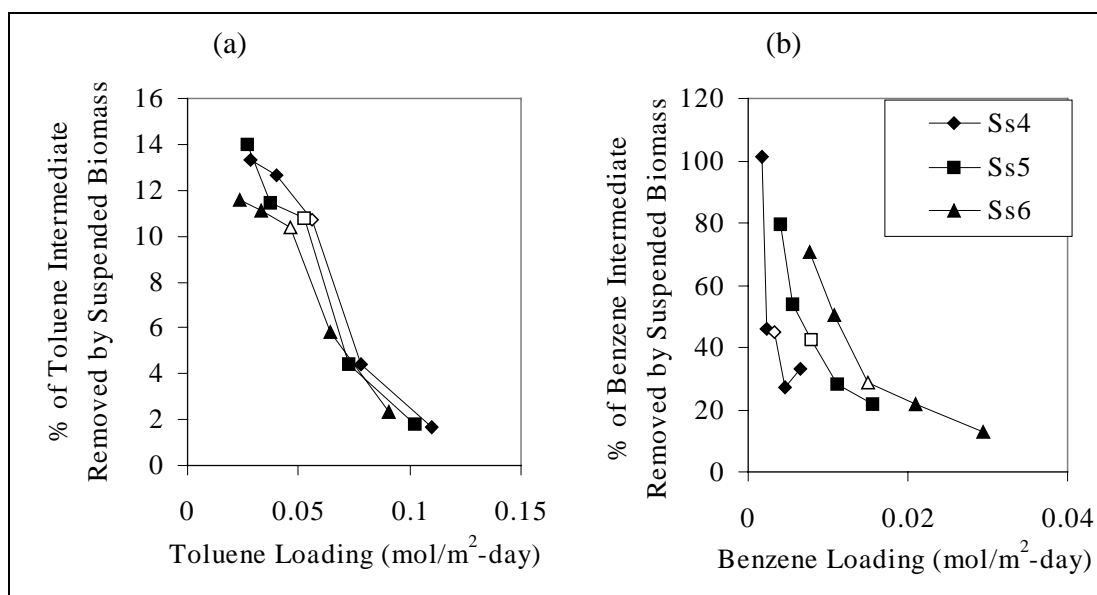


Figure 43. Percentages of toluene and benzene intermediates removed by suspended biomass during Ss4-Ss6.

Competitive Inhibition between Toluene and Benzene

Figure 42 shows that competitive inhibition between toluene and benzene caused the reactor performance to decrease slightly when toluene was replaced by benzene in the mixture. The mole fractions of benzene in the toluene/benzene mixture were 0.056, 0.13, and 0.26 in Ss4-Ss6, respectively. Since the total COD loading rates were the same during the three steady states and their short-term experiments among Ss4-Ss6 (Table 10), the steady state and short-term runs were regrouped based on their COD loading rates. This rearrangement facilitated the comparison among runs with similar toluene, but dramatically

different benzene loading rates. Table 13 lists the five new groups, their original run names, and their loading conditions. Only Groups 4 and 5 showed notable effects of inhibition between toluene and benzene, while Groups 1-3 showed little or no effects of inhibition between toluene and benzene.

The removal efficiencies for toluene and benzene in the reactor are shown in Figure 44 according to the five groups. The removal efficiencies and benzene loading rates within a group show little correlation. However, the efficiencies decrease sharply as the COD loading rates increase (Groups 4 and 5).

Table 13. New groups of the runs of Ss4-Ss6.

Group Name	Run Name in Table 10	Total COD Loading (gCOD/m ² day)	Toluene (mol/m ² day)	Benzene (mol/m ² day)
Group 1	Ss4-1	8.6	0.029	0.0017
	Ss5-1		0.027	0.0041
	Ss6-1		0.024	0.0077
Group 2	Ss4-2	12.1	0.040	0.0024
	Ss5-2		0.037	0.0057
	Ss6-2		0.033	0.011
Group 3	Ss4	17.0	0.056	0.0034
	Ss5		0.052	0.0080
	Ss6		0.046	0.015
Group 4	Ss4-3	23.7	0.078	0.0047
	Ss5-3		0.073	0.011
	Ss6-3		0.065	0.021
Group 5	Ss4-4	33.2	0.11	0.0066
	Ss5-4		0.10	0.016
	Ss6-4		0.091	0.030

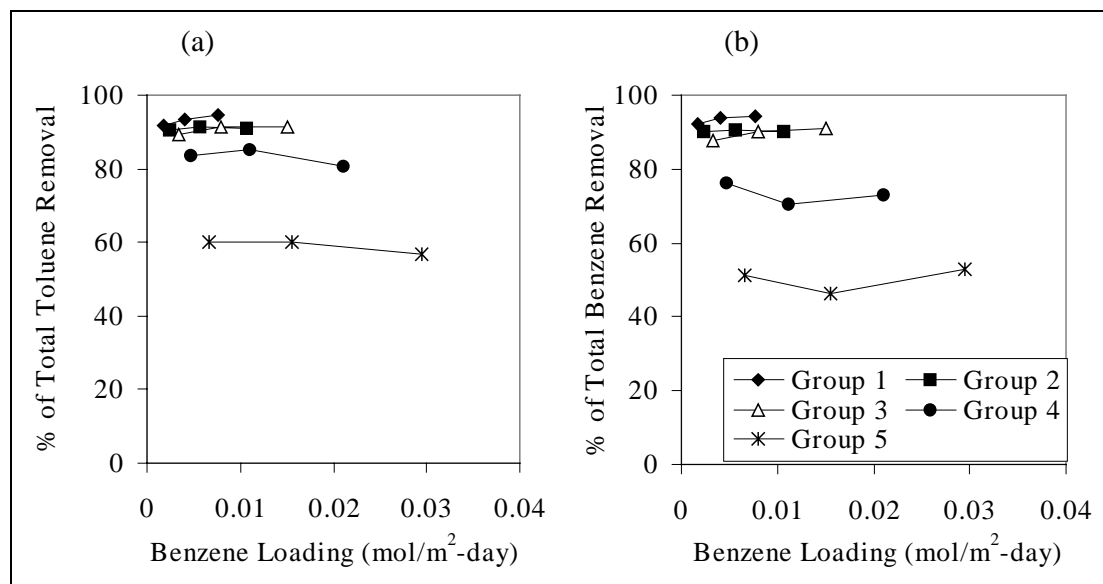


Figure 44. Effect of benzene loading on toluene and benzene removal during Ss4-Ss6.

Figure 45 shows the removal efficiencies of COD and the COD quality of effluents during Ss4-Ss6, again according to the five groups. The results show that, when toluene was replaced by benzene, the overall COD removals changed only slightly, but the fraction of COD in the effluent attributed to benzene and toluene increased slightly, as the benzene loading increased. In general, because the degradation kinetics of toluene and benzene are similar, their coexistence did not cause the reactor performance to change dramatically from treating one of them as the sole substrate.

The percentages of total toluene and benzene removals by the suspended biomass during Ss4-Ss6 are shown in Figure 46. For toluene, increases in benzene loading decreased the fraction of toluene removed in the bulk liquid. The decreases in percentages were especially significant for Groups 4 and 5, both of which dropped 27 percent. On the other hand, the percentages of benzene removed in the bulk liquid were always much lower than those of toluene and remained relatively constant (mean 5.1 percent).

The differences in the trends for toluene and benzene are most likely due to the inhibition effects between them. In any run, the concentration of toluene was always at least two times higher than that of benzene. Therefore, the stronger inhibition from toluene to benzene caused most of the benzene degradation to occur inside the biofilm.

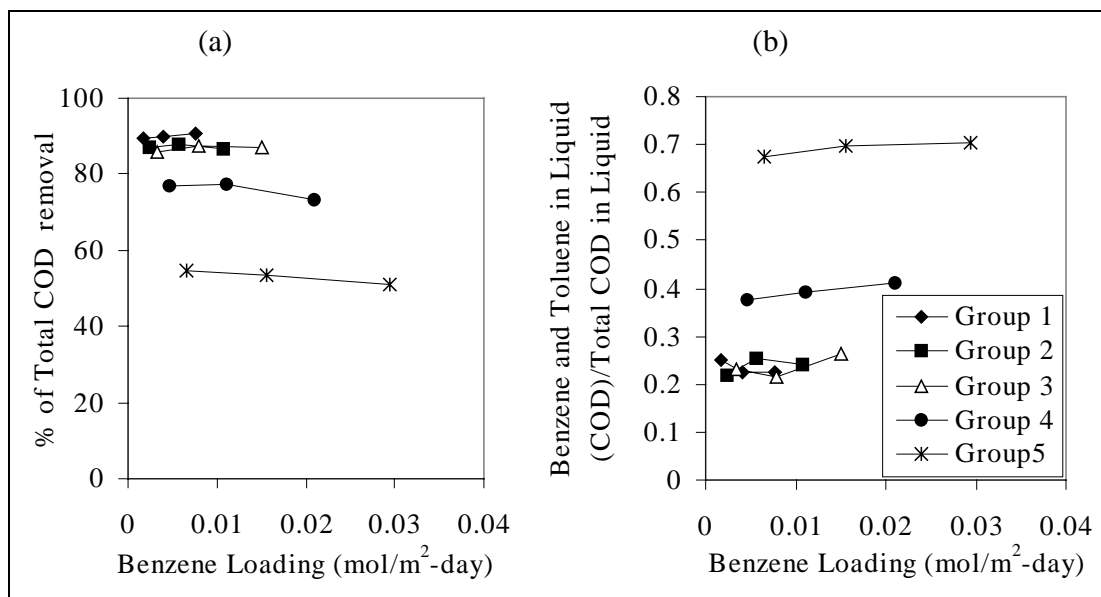


Figure 45. Effect of benzene loading on COD removals during Ss4-Ss6.

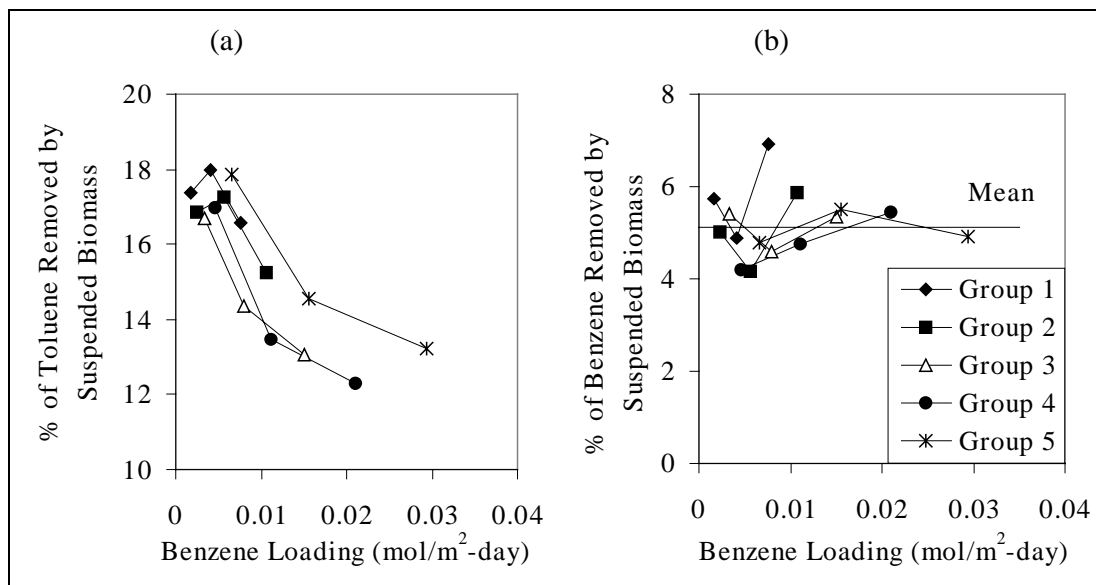


Figure 46. Percentages of toluene and benzene removals caused by suspended biomass during Ss4-Ss6.

Figure 47 compares the percentages of toluene and benzene intermediates that were removed in the bulk liquid. Except for Groups 1 and 2, whose data were more scattered due to their low substrate loading rates, benzene loading had little effect on toluene intermediate removal in the liquid when the total COD loading rate was fixed. The percentage removals of benzene intermediate in the liquid decreased in response to increased benzene loading due to the inhibition for benzene to its intermediate. At higher COD loading rates, higher portions of toluene and benzene intermediates were removed in the biofilm because of the overall higher concentrations of toluene and benzene in the liquid. This result supports the concept that more removal occurred inside the biofilm when inhibition was most important in the bulk liquid.

Figures 45-47 show that increases in benzene loading caused more toluene and the intermediates of toluene and benzene to be removed inside the biofilm, but did not change the overall reactor performance significantly. The relationships among toluene and benzene loading and their mass fluxes into the biofilm are shown in Figure 48. In both cases, the fluxes into the biofilm increased with the total surface loading rates. These trends are similar to runs with toluene as the sole substrate, which were shown in Figure 31.

The effect of toluene loading on the mass fluxes of its intermediate is similar to the results from Ss1-Ss3 (Figure 49(a)). Except for the lowest two COD loading groups, for which data did not show clear trends due to small values, the intermediate flux into the biofilm increased with toluene loading. Within each group, higher toluene loading was associated with lower benzene loading. Therefore,

higher benzene loading in a group was related to lower mass flux of toluene intermediate into the biofilm or fluxes out of the biofilm. This result occurred because, at higher benzene loading rates, the higher liquid benzene concentrations caused more toluene to be converted to its intermediate inside the biofilm, where inhibition was reduced. The same reasoning explains Figure 49(b). When the COD loading was fixed in one group, more benzene intermediate diffused out of the biofilm at higher benzene loading rates because about 95 percent of the benzene were removed inside the biofilm, where inhibition was relieved.

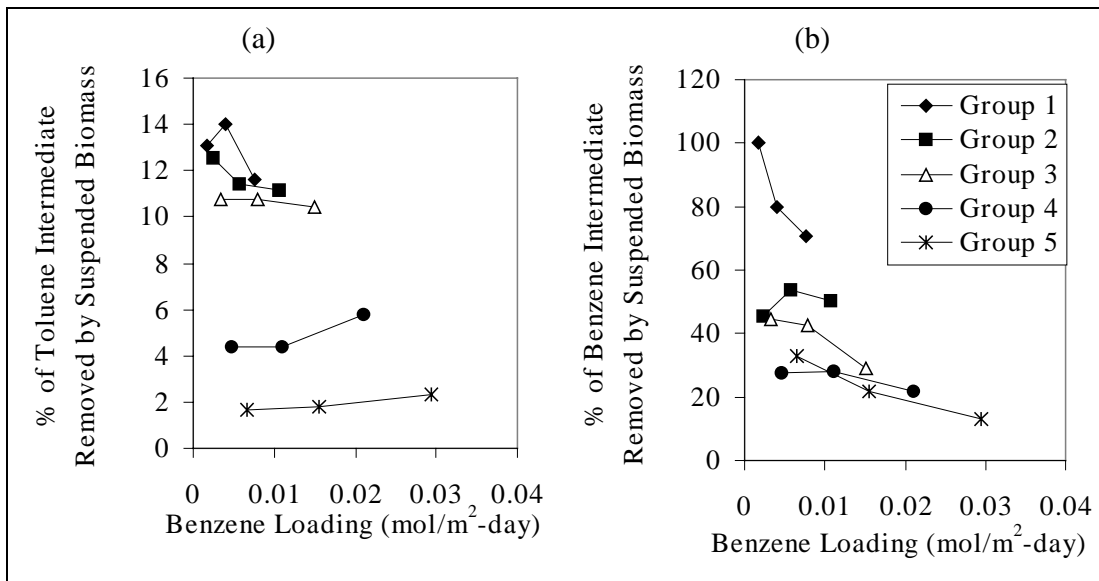


Figure 47. Percentages of toluene and benzene intermediate removals caused by suspended biomass during Ss4-Ss6.

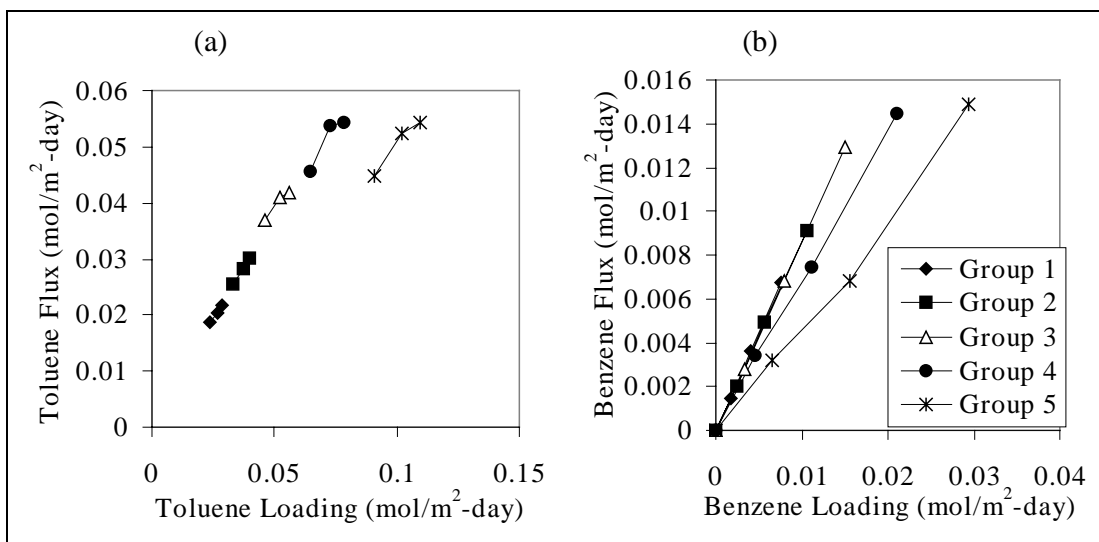


Figure 48. Relationship between toluene/benzene loading rates and their mass fluxes into the biofilm during Ss4-Ss6.

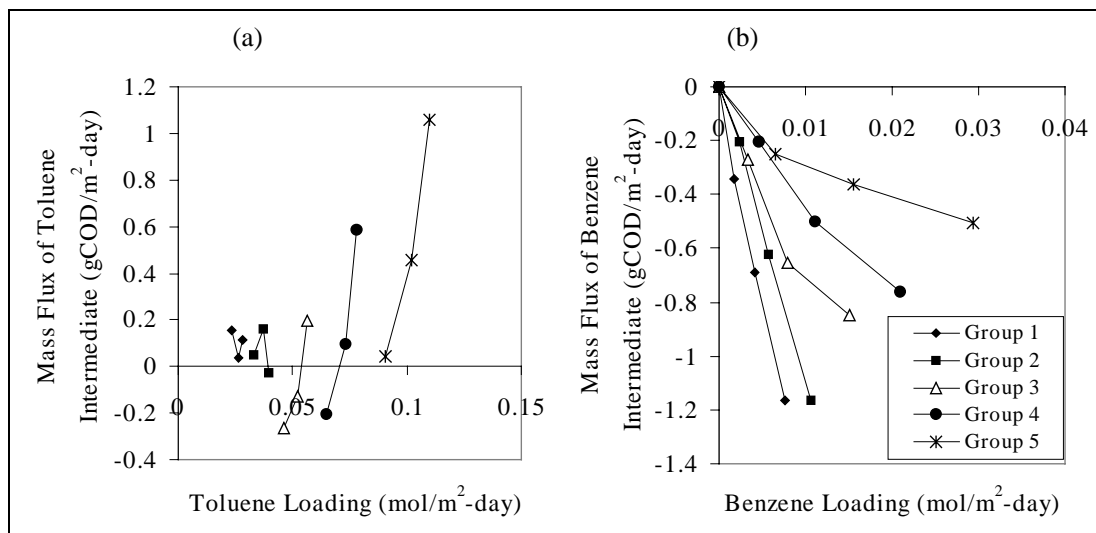


Figure 49. Relationship between total toluene/benzene loading and the mass fluxes of their intermediates into the biofilm during Ss4-Ss6.

Summary

The experiments using toluene and benzene as dual substrates focused on studying how the interactions between competing substrates affect reactor performance. It is known that *P. putida* F1 degrades toluene and benzene via similar pathways, and they competitively inhibit each other's first-step reaction. Therefore, the COD loading was maintained at a nearly constant level while the benzene mole fractions changed from 0.056 to 0.26, a 360 percent increase.

The results showed that the overall COD removal efficiencies changed little from the same COD loading with toluene as the sole substrate. The noncompetitive inhibition from toluene and benzene to their intermediates forced more intermediates to be removed in the biofilm. In addition, the benzene-loading rate had no effect on the removal efficiencies for toluene and benzene for the range of loading rates used. At higher benzene loading rates, however, more toluene was removed in the biofilm, where the competitive inhibition effect from benzene was smaller. Because toluene was always present in a much higher concentration than benzene, its inhibition effect on benzene degradation was much greater than was benzene's effect on toluene degradation. For the toluene and benzene mixtures used, only 5 percent of benzene was removed in the bulk liquid, while the percentages for toluene were always greater than 12 percent (12 to 18 percent). As a result, toluene intermediate diffused into the biofilm at higher toluene loading rates, while benzene intermediate always diffused out of the biofilm. Overall, the competitive inhibition between toluene and benzene caused more substrates to be removed in the biofilm, where inhibition was relieved.

Removals of Toluene and *p*-Xylene as Dual Substrates

The experiments with toluene and *p*-xylene as dual substrates, Ss7-Ss8, were designed similarly to those with toluene and benzene as dual substrates, Ss4-Ss6. The mole fractions of *p*-xylene in the toluene/xylene mixtures were 0.056 and 0.13 for Ss7 and Ss8, respectively. These mole fraction values were the same as those for Ss4 and Ss5. The total COD loading rates of Ss7-Ss8 were also kept close to the values of Ss4-Ss5. Comparing to the runs using toluene and benzene as dual substrates, the only difference in Ss7-Ss8 is that *p*-xylene was degraded as a cometabolic compound — degradation of *p*-xylene requires electrons and energy released by the degradation of toluene intermediate. In addition, the intermediate of *p*-xylene is not degradable by *P. putida* F1.

The concentrations of toluene and *p*-xylene in the gas and liquid effluents during Ss7-Ss8 are shown in Figures 50 and 51, respectively. Because the interaction between the first-step reactions of toluene and *p*-xylene is similar to that of toluene and benzene, the general trends observed during Ss4-Ss6 (Figures 38 and 39) also were found during Ss7 and Ss8. All concentrations increased dramatically at higher loading.

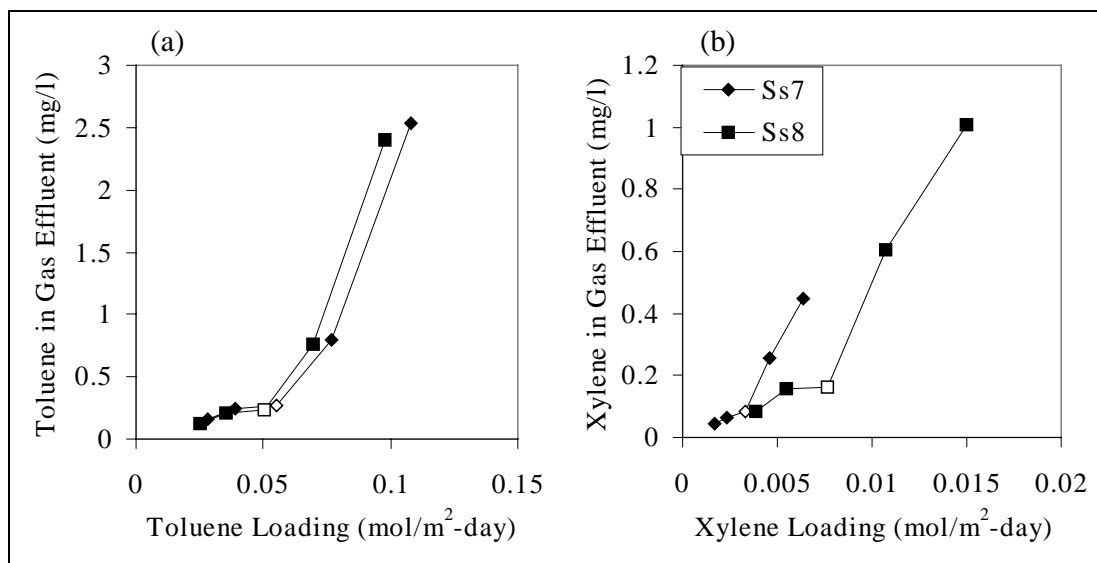


Figure 50. Toluene and *p*-xylene concentrations in the gas effluent during Ss7-Ss8.

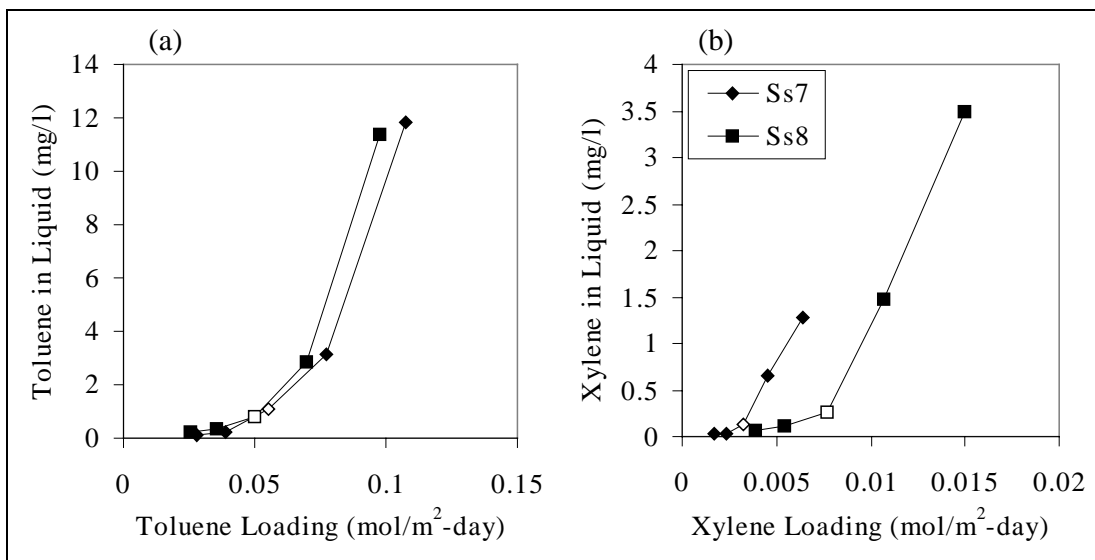


Figure 51. Toluene and *p*-xylene concentrations in the liquid effluent during Ss7-Ss8.

Figure 52 shows the DO and COD concentrations in the bulk liquid. The DO concentrations were very close for Ss7 and Ss8; the curves are similar, but slightly higher than those for Ss4-Ss5, which had the same total COD loading as Ss7-Ss8. Figure 52 also shows that the COD concentrations for Ss8 were always higher than those for Ss7. This observation is different from the runs with different toluene/benzene compositions (Figure 40) and comes about because the intermediate of *p*-xylene was not further degraded by *P. putida* F1, while toluene and benzene intermediates can be degraded completely. Therefore, the intermediate from *p*-xylene accumulated in the reactor and washed out the reactor in the effluent.

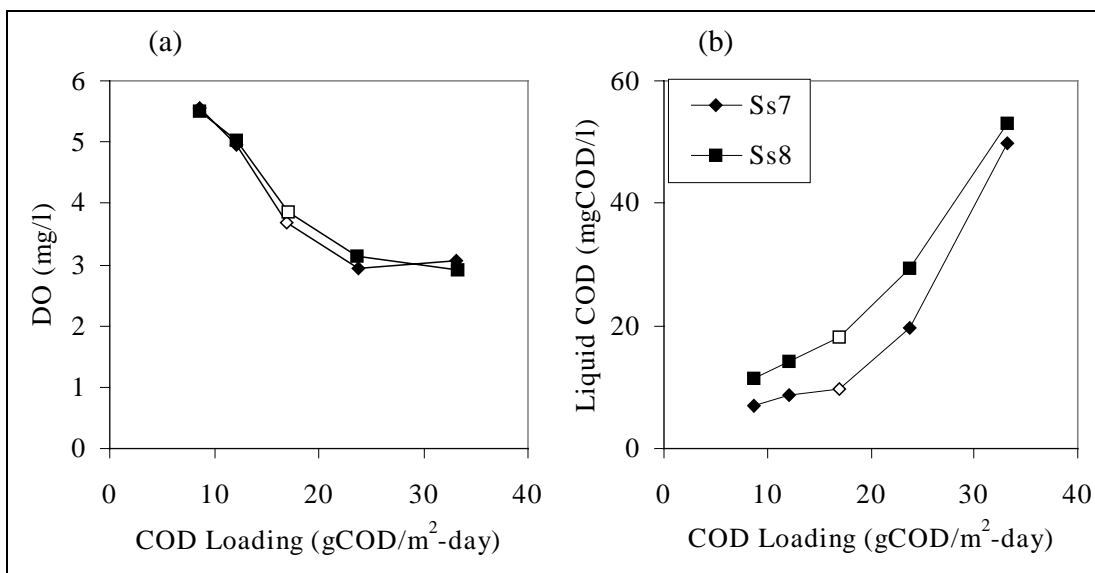


Figure 52. DO and COD concentrations in the bulk liquid during Ss7-Ss8.

The removal efficiencies of toluene and *p*-xylene during Ss7-Ss8 are shown in Figure 53. Comparing with Figure 41(a), the reactor behaved similarly in removing toluene when benzene or *p*-xylene was the second substrate, as shown by the removal efficiencies. This result can be explained from the interactions between toluene and benzene and between toluene and *p*-xylene during degradation. The values of competitive inhibition constants for benzene to toluene, K_{BT} , and for *p*-xylene to toluene, K_{pT} , are similar (0.51 mg-benzene/l and 0.87 mg-xylene/l) (Yu 1998). Therefore, the inhibition effects from benzene and *p*-xylene to toluene were similar.

However, the highest removal efficiency for *p*-xylene (Figure 53(b)) was only about 70 percent, compared to greater than 90 percent for benzene. The removals of *p*-xylene decreased dramatically as its loading increased. At the highest loading rates, only 14 and 15 percent of the *p*-xylene were removed during Ss7 and Ss8, respectively. Since the degradation of *p*-xylene was by cometabolism, it yielded no electrons for its own oxygenation. In addition, at high loading rates, the concentration of toluene was high. The inhibition caused the removal of *p*-xylene to decrease.

Since the *p*-xylene intermediates were not degraded in the reactor, the COD removal efficiencies for Ss8 (Figure 54) were always lower than for Ss7. Similar to Figure 42, the COD removal efficiency increased with COD loading initially and leveled off at the highest COD loading rate. For dual-substrate studies of toluene/benzene and toluene/xylene, the COD removal efficiencies reached their maximum values at the loading rate of 23 gCOD/m²-day and did not change between 23 and 32 gCOD/m²-day.

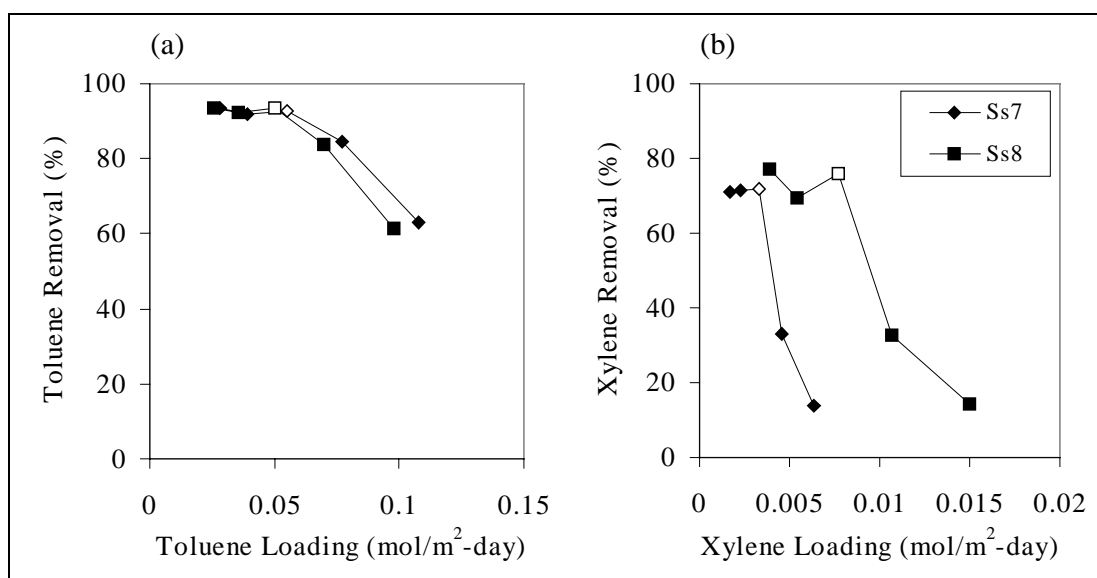


Figure 53. Toluene and *p*-xylene removal from the circulating bed during Ss7-Ss8.

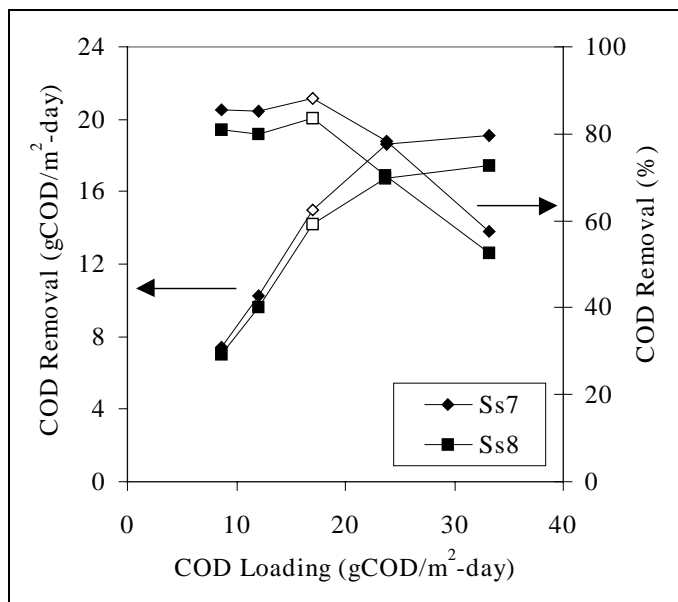


Figure 54. COD Removals from the circulating bed during Ss7-Ss8.

The runs with toluene and *p*-xylene were also regrouped as dual substrates into five groups, similar to those shown in Table 13. The average COD loading rates for Groups 6 to 10 are 8.4, 11.7, 16.5, 23.0, and 32.2 gCOD/m²-day, respectively. The same trends shown for toluene and benzene as dual substrates, presented in Figures 44 to 49, are observed for toluene and *p*-xylene as dual substrates. For example, Figure 55 shows the relationship between toluene and *p*-xylene loading rates and their mass fluxes into the biofilm during Ss7-Ss8, which was similar to that shown in Figure 48 for toluene and benzene — the fluxes of toluene and benzene increased with increased loading rates.

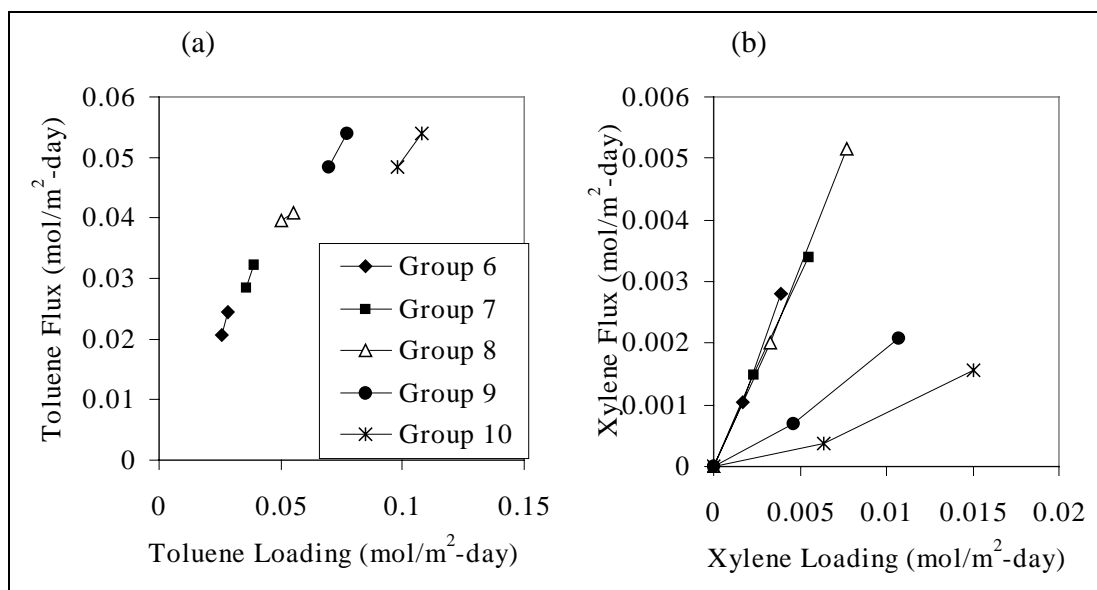


Figure 55. Relationship between toluene/benzene loading and their mass fluxes into the biofilm during Ss4-Ss6.

Summary

The experiments using toluene and *p*-xylene as dual substrates focused on studying how the interactions between a primary substrate and a cometabolite affect reactor performance. *P. putida* F1 degrades *p*-xylene cometabolically using the same enzyme that degrades toluene. Therefore, the inhibition effect between toluene and *p*-xylene was similar to that between toluene and benzene. The COD loading during the experiments was maintained at a constant level, while the benzene mole fractions changed from 0.056 to 0.13, a 130 percent increase.

Many trends for toluene/benzene degradation as dual substrates also were observed for toluene/xylene experiments. The biggest difference between the studies was that the removal efficiencies for *p*-xylene were much lower than for benzene. At the highest COD loading rates, only slightly greater than 10 percent of the xylene was removed. The degradation of *p*-xylene uses electrons released by the degradation of toluene intermediate or biomass respiration, which was controlled by toluene inhibition and oxygen availability, respectively. Therefore, higher toluene concentration lowers the rate of *p*-xylene removal by direct inhibition to *p*-xylene, indirect inhibition to its electron source, and low oxygen concentration associated with the high toluene concentrations. Consequently, a higher loading of the primary substrate toluene actually lowered the removal of the cometabolite *p*-xylene (Figure 55(b)). The trends suggest that, if the total COD loading was higher, the removal of *p*-xylene could drop to near zero.

6 Nitroglycerin Removal

Introduction

So far in this study, it has been demonstrated that a three-phase circulating-bed biofilm reactor inoculated by *P. putida* F1 is effective for removing BTX-related aromatic hydrocarbons present in gas streams. This chapter describes the ability of the same system to remove NG from the liquid phase. NG, also called glycerol trinitrate (GTN), contains three nitrate ester groups on a glycerol skeleton. Since naturally occurring nitrate esters have not been found (White and Snape 1993), NG is a xenobiotic compound. It has been widely used in the production of explosives and propellants and as a vasodilator in pharmaceuticals. During its production and usage, NG often contaminates wastewaters (Pesari and Grasso 1993). NG, as well as its incompletely nitrated byproducts such as glycerol dinitrate (GDN) and glycerol mononitrate isomers (GMN), is toxic to a number of mammalian species and microorganisms. For example, NG is toxic to mammalian species in concentrations of 30-1300 mg/kg (Wendt, Cornell, and Kaplan 1978).

Traditionally, NG has been removed from wastewater using physical and chemical methods. The physical process usually uses activated carbon to absorb the NG in wastewater and requires further treatment before final disposal. The chemical treatment methods are usually limited to hydrolysis with strong caustic solutions or denitration with alkaline sodium sulfide. While effective in treating the NG, the chemical reactions are exothermic, which can present a safety hazard due to the explosive nature of NG. In addition, a large quantity of chemicals is needed, and the excess reactants have to be further treated before being released into the environment.

In recent years, microbial degradation of NG has been studied by a number of researchers. Key information on the studies of bacterial degradation of NG is listed in Table 14. Although NG is a true xenobiotic compound, it is degradable by fungi (Ducrocq, Servy, and Lenfant 1989, 1990; Servent et al. 1991, 1992; and Zhang et al. 1997) and bacteria (Wendt, Cornell, and Kaplan 1978; Pesari and Grasso 1993; Meng et al. 1995; White, Snape, and Nicklin 1996; Blehert et al. 1997; Christodoulatos, Bhaumik, and Brodman 1997; and Bhaumik et al. 1997, 1998). The consensus is that NG is reductively denitrated stepwise to GDN,

Table 14. Studies of bacterial biodegradation of nitroglycerin.

Authors	Source of Bacteria	Bacterial Culture	C-source	Intermediate	C-end products	N-end products	Toxicity	Other
Wendt, Cornell, and Kaplan (1978)	activated sludge	8 gram-negative strains	glucose	1,3-GDN 1,2-GDN GMNs	glycerol (assumed)	nitrite	none (NG < 150 mg/L)	stepwise reaction, last step slowest
Pesari and Grasso (1993)	activated sludge	mixed	ethyl acetate	not measured	n/a	nitrate	none (NG < 200 mg/L)	aerobic & anoxic (SBR)
Meng et al. (1995)	soil/sediment pre-exposed to nitrate esters	<i>Bacillus thuringiensis/cereus</i> and <i>Enterobacter agglomerans</i>	meat/yeast extract and other nutrients	1,3-GDN 1,2-GDN 1-GMN 2-GMN	glycerol	nitrite, then converted to nitrite	when > 340 mg/L	constitutive activity, cofactors (NADH) not needed
White, Snape, and Nicklin (1996)	soil, river water, and activated sewage sludge	<i>Pseudomonas</i> sp. and <i>Agrobacterium radiobacter</i>	glycerol	1,3-GDN 1,2-GDN 1-GMN 2-GMN	GMNs	nitrite		NG as sole N-source NADH accelerates denitration
Blehert et al. (1997)	NG-contaminated soil	<i>Pseudomonas putida</i> II-B and <i>Pseudomonas fluorescens</i> I-C	glucose	I-B: 1,3-GDN, 1-GMN II-B: mixed	GMNs	nitrite		enzymes are NADPH-dependent; NG as sole N-source
Bhaumik et al. (1997, 1998), Christodoulatos, Bhamik, and Brodman (1997)	activated sludge; anaerobic digester sludge	mixed	glucose	1,3-GDN 1,2-GDN 1-GMN 2-GMN	glycerol (assumed)	nitrate and nitrite	self-inhibitory, but reversible between 50-200 mg/l	anaerobic system more efficient than aerobic ones

GMN, and eventually glycerol. Figure 56 shows these steps, which seem to occur aerobically or anaerobically. Although the pathway for NG biotransformation is known, the kinetic details of NG degradation are still an active topic of study.

Table 14 shows that a number of mixed cultures and bacterial strains are capable of degrading NG under aerobic or anaerobic conditions. While some studies isolated the NG-degraders from sources that had been exposed to NG or other nitrate esters, others showed that many bacterial strains from activated sludge also could degrade NG. This latter finding suggests that the enzymes involved in NG degradation probably are nonspecific to NG. This hypothesis is supported by the following studies. Blehert et al. (1997) tested 16 bacterial strains that had not been previously exposed to NG and found that 9 strains were able to degrade more than 90 percent of the NG at low concentrations (0.44 mM). The bacterial strains tested NG-degradable included two *E. coli* strains, several *Pseudomonas* strains, and several *Klebsiella* strains. Meng et al. (1995) studied NG degradation using bacteria isolated from sites exposed to nitrate esters. They reported that the NG-degrading enzymes were expressed constitutively (i.e., NG was not needed for the induction of the enzymes). Based on thermodynamic principles and the NG degradation pathway (Figure 56), Smet, VanLangehove, and Verstraete (1996) also concluded that complete degradation of NG under aerobic or anaerobic conditions was theoretically feasible without using additional carbon or nitrogen sources.

Even though a wide range of bacterial cultures can degrade NG, most of the them cannot use NG as a sole carbon source (Wendt, Cornell, and Kaplan 1978; Pesari and Grasso 1993; White, Snape, and Nicklin 1996; Blehert et al. 1997; Bhaumik et al. 1997, 1998). Christodoulatos, Bhaumik, and Brodman (1997) reported that a mixed culture from anaerobic digester sludge could use NG as a sole carbon source, but the rate of utilization was very slow; thus, long retention times were required to achieve adequate efficiency. Although, under most circumstances, NG was degraded cometabolically by bacteria grown on easily degradable carbon sources (Table 14), Bhaumik et al. (1997 and 1998) reported that the rate of NG degradation depended strongly on the concentration of the primary electron-donor substrate, glucose. Bhaumik et al. (1998) reported that aerobic denitration reaction stopped once the primary donor substrate was depleted. Some bacteria could not use NG as a nitrogen source (Wendt, Cornell, and Kaplan 1978), but others demonstrated an ability to use NG as sole N-sources (White, Snape, and Nicklin 1996; and Blehert et al. 1997).

The reason for cometabolism of NG lies in the kinetics of its degradation. Wendt, Cornell, and Kaplan (1978) reported that each reaction in the NG degradation pathway proceeds more slowly than its preceding one. Bhaumik et al. (1997

and 1998) also reported that the denitration of GMN to glycerol was the slowest step, and other studies with pure cultures were not able to demonstrate conversion of GMN to glycerol (White, Snape, and Nicklin 1996; and Blehert et al. 1997). Due to the kinetics, intermediates should accumulate during biodegradation of NG, and they have been confirmed, as shown in Table 14. Since useable carbon and electrons can be released only from degradation of glycerol, it is difficult for the bacteria to use NG as a sole carbon and electron source.

Another kinetic aspect of NG degradation is its regiospecificity during denitration. Figure 56 shows that NG can be degraded to glycerol via three paths: NG \rightarrow 1,2-GDN \rightarrow 1-GMN; NG \rightarrow 1,2-GDN \rightarrow 2-GMN; or NG \rightarrow 1,3-GDN \rightarrow 1-GMN. In most cases, the majority of NG was converted through the third path (White, Snape, and Nicklin 1996; Blehert et al. 1997; Christodoulatos, Bhaumik, and Brodman 1997; Bhaumik et al. 1997, 1998). The enzymes have a strong regioselectivity for the C-2 position. However, Blehert et al. (1997) also reported that one of the two strains studied, *P. putida* II-B, attacked the three nitrate groups randomly, while the other strain, *P. fluorescens* I-C, attacked the C-2 location preferably.

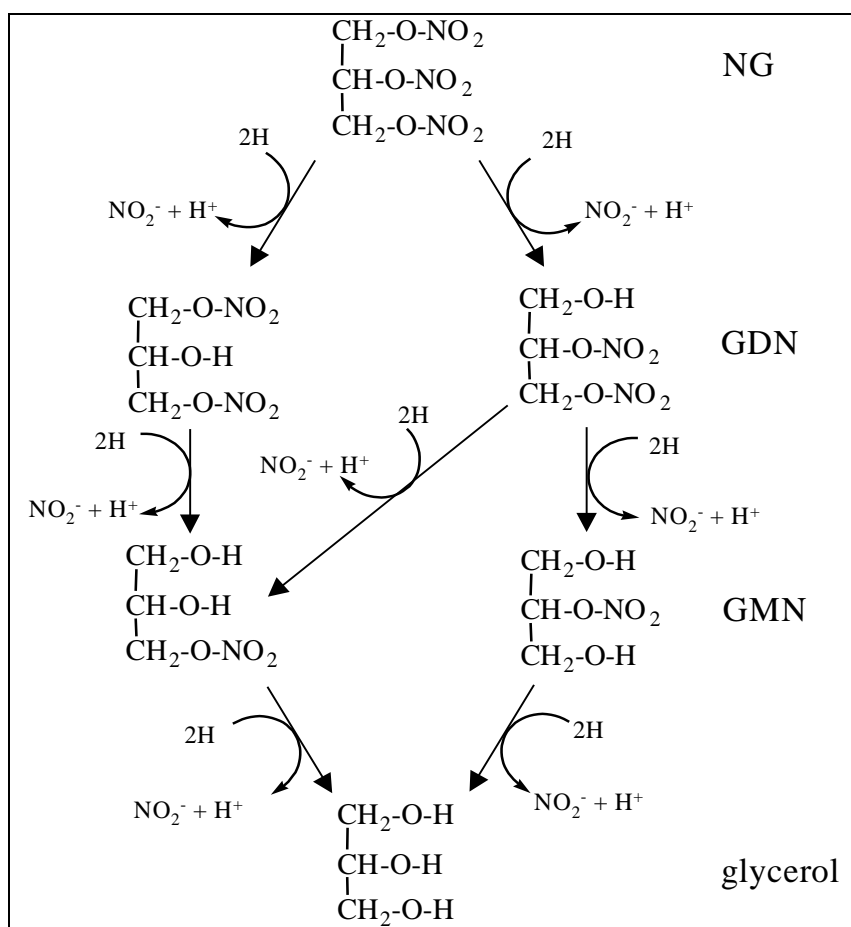


Figure 56. Potential biological pathway of NG denitration.

Two types of denitration reactions, illustrated in Figure 57, have been proposed for the removal of the nitrite group from NG. Direct reductive denitration is shown in the bottom part of the figure and is the consensus pathway. This same mechanism is found in fungal denitration reactions (Servent et al. 1991 and 1992). White, Snape, and Nicklin (1996) and Blehert et al. (1997) reported that adding NAD(P)H to the system accelerated the rate of denitration reactions. However, Meng et al. (1995) found NADH or other cofactors were not required for denitration. They did, however, observe that nitrite, instead of nitrate, was formed during denitration reaction. Thus, Meng et al. (1995) proposed a hydrolytic reaction followed by nitrate reduction as the denitration mechanism. Because two electrons are required in each proposed pathway, the net outcome is the same: NAD(P)H is required, and $\text{NO}_2^- + \text{H}^+$ are produced.

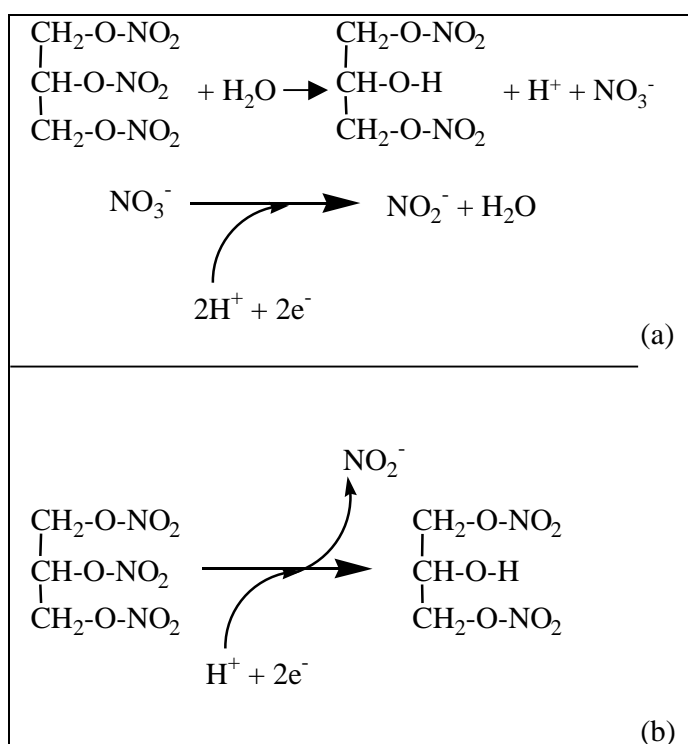


Figure 57. Possible denitration mechanisms. (a), hydrolytic reaction followed by nitrate reduction; (b) direct reductive reaction.

Experiments

The study of NG removal from the circulating-bed biofilm reactor was conducted after the experiments of BTX removal from gas streams were completed. The VOC in the gas stream was returned to 100 percent toluene, and the reactor loading was set to the same value as Steady State 3 (i.e., $15.5 \text{ mol/m}^3\text{-day}$ [Table 9]). The total gas and liquid flowrates were at 532-537 mL/min and 42.2 mL/min, re-

spectively, the same as those for the original Steady State 3. When the NG-degradation experiments began 2 wk later, the biofilm reactor was performing similarly to the original Steady State 3. Averages of the measurements of several variables on three consecutive days were all in good agreement with the values at the original Steady State 3, which also were averages of three days' data (Table 15). Since the second Steady State 3 for NG removal was developed 2 mo after the first one, data in Table 15 indicate that the same amount of biomass was maintained in the reactor, and its activity was not permanently affected during the periods of multi-substrate loading.

The NG-removal experiments were designed similarly to the experiments described in Chapter 3. Once the reactor achieved steady state for degrading toluene, NG stock solution was fed into the reactor through an independent liquid influent line connected to one of the liquid sampling ports. NG stock solution (500 mg/L) was prepared by dissolving 4 grams of pure NG into 8 L of minimum mineral media. The flowrate of NG stock was 0.422 mL/min, giving an overall NG feed concentration of 5 mg/L (22.0 μ M). Throughout the experiments, the flowrate and loading conditions of toluene and nutrients were not changed. All the variables shown in Table 15 and the concentrations of NG/GDN/GMN were monitored until the concentrations of NG/GDN/GMN in the effluent reached steady states.

The constant NG feed was maintained for 1 wk and monitored every 2 days. Two short-term pseudo-steady-state experiments similar to those described in Chapter 3 were conducted 1 wk later. The NG feed concentrations for the short-term experiments were 10 and 15 mg/L (44 and 66 μ M), respectively. The same measurements done during the dynamic experiments were performed. The reactor was returned to toluene-only condition after the short-term experiments.

Table 15. Circulating-bed reactor performance during two identical steady states.

	SS3, original	SS3, 65 days later
Toluene Loading (mol/m ² -day)	0.059	0.059
Suspended Biomass (mg/L)	42	44
Fixed Biomass (mg/carrier)	2.0	2.1
Toluene in Liquid Effluent (mg/L)	1.2	1.4
Toluene in Gas Effluent (mg/L)	0.54	0.36
COD in Liquid Effluent (mgCOD/L)	9.5	6.8
Dissolved Oxygen (DO) (ppm)	3.1	3.2
Toluene Removal (%)	88	91

Results and Discussion

Figure 58 shows the dynamic responses of NG, GDN, and GMN (estimated by mass balance assuming it is not reduced to glycerol) in the liquid-effluent after the reactor started receiving 5 mg/L (22.0 μM) of NG. The reactor had a liquid retention time of 1.1 h. Figure 58 shows that it took three to five liquid-retention times for the concentrations of NG/GDN/GMN to reach steady states. NG was transformed immediately after entering the reactor, as shown by the detection of GDN in the effluent. The GMN concentration is plotted only for the last three data points, where it was at steady state. The total amount of NG, GDN, and GMN equals the NG in the influent after all three components reach steady state, because the concentration of GMN was calculated by mass balance. The biomass attached to the carriers (2.08 mg biomass/carrier, or 4.34 g biomass/L of reactor volume) was able to degrade 46 percent of the influent NG to its intermediates with a liquid detention time of 1.1 h.

The effluent concentrations of NG/GDN/GMN during the week of steady-state operation are shown in Figure 59. They stayed nearly constant during the period, although that the NG concentration increased slightly after the first day, causing the concentration of GMN to dip slightly, and the product removal of NG to decline to 40 percent. Figures 58 and 59 show the (estimated) steady-state concentration of GMN was roughly equal to that of GDN, although a significant amount of NG was still in the liquid phase. This phenomenon was different from what was observed in the batch reactors, in which the concentration of GDN was much higher than GMN when NG was present.

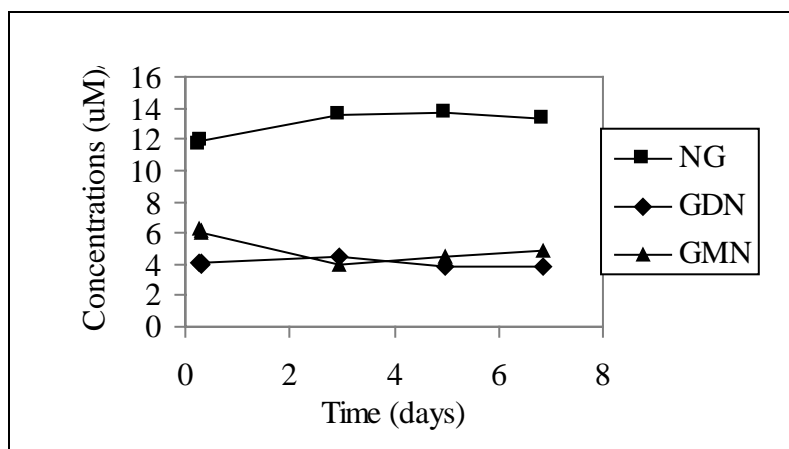


Figure 58. Dynamic responses of NG, GDN, and GMN (estimated) in the liquid effluent of circulating-bed biofilm reactor fed with 22.0 μM of NG.

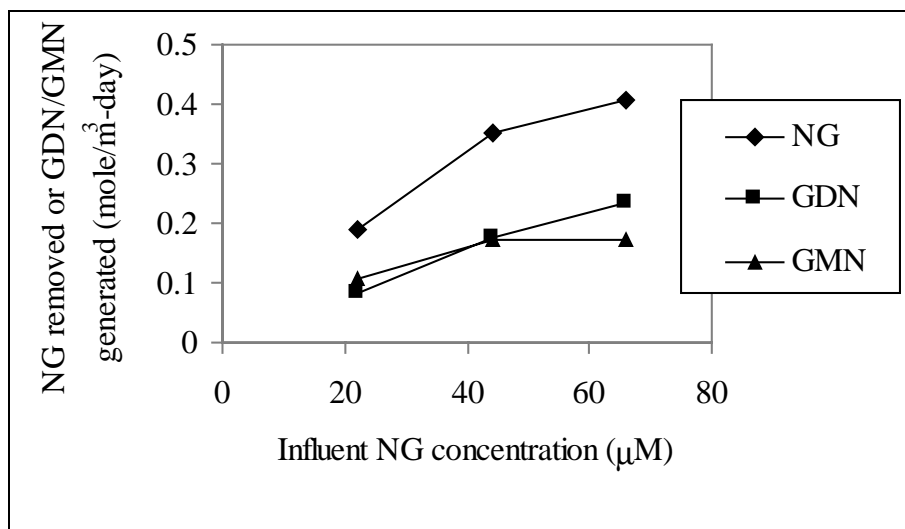


Figure 59. Steady-state concentrations of NG, GDN, and GMN (estimated) in the liquid effluent of the circulating-bed biofilm reactor fed with 22.0 μM of NG.

The increased formation of GMN in the circulating bed probably is caused by the thick biofilm accumulation inside the carriers. In the circulating-bed, most of the biomass was immobilized inside the carriers, where it used most of the primary substrate, toluene, to produce the electrons for cometabolism. Because NG is degraded much more slowly than toluene, it diffuses deeper into the biofilm before being reduced to GDN. The GDN produced in the biofilm then diffuses outward through the biofilm, at which time it is further reduced to GMN. Since the toluene concentration is the highest near the biofilm surface, the amount of electrons available for the reductive denitration reaction is high along the path of GDN diffusion, where further reduction of GDN to GMN occurs. Thus, the large biofilm accumulation in the carriers of the circulating-bed biofilm reactor favored reduction of GDN to GMN.

The removals of NG during the steady state and the two pseudo-steady states are shown in Figure 60. When the concentration of NG in the liquid influent was increased from 22.0 to 66.1 μM , the NG transformed in the reactor increased from 0.19 to 0.41 $\text{mole}/\text{m}^3\text{-day}$. However, the rate of increase of NG removal slowed for the higher NG loading. The percentages of NG transformation are shown in Figure 61. When the NG loading in the liquid was increased, the NG removal as a percentage of that in the influent dropped from 40 to 28 percent. The percentage of transformation from NG to GDN only decreased slightly (~1 percent) throughout the loading range, but the percentage of transformation to GMN dropped from 22 to 12 percent, almost parallel to the decrease of overall NG removal. The slowed NG conversion to GMN suggests a limit on how many electrons are available for cometabolism for a fixed toluene-loading rate. Electron limitation should favor the transformation of NG to GDN, due to its faster rate. Thus, reduction of GDN to GMN did not increase at all when the NG concentration increased from 40 to 60 μM .

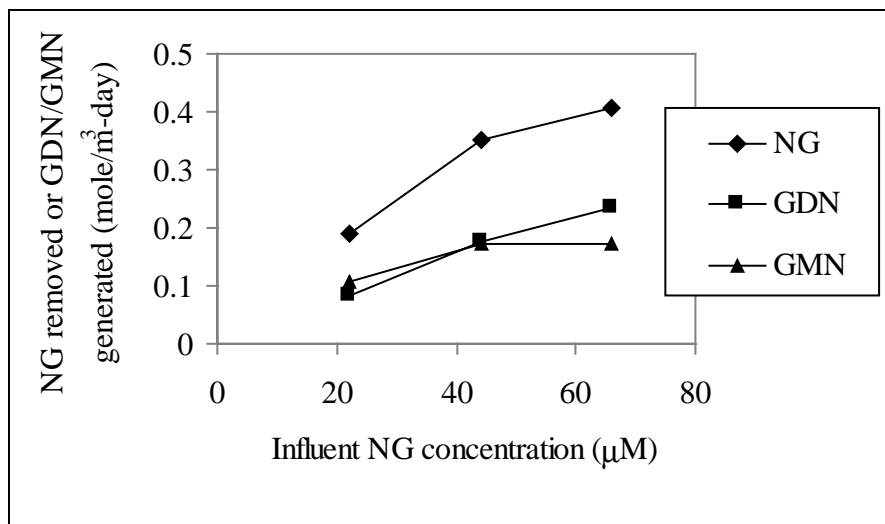


Figure 60. NG removal and GDN/GMN production in the circulating-bed biofilm reactor during the steady state and pseudo-steady-states experiments.

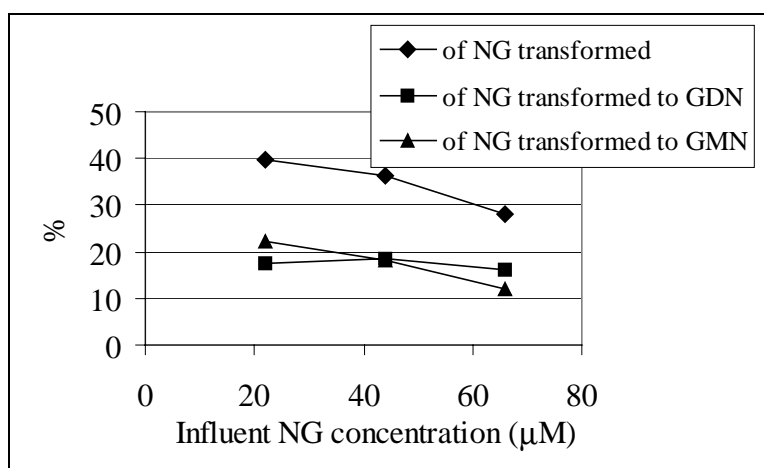


Figure 61. Transformation of NG during the steady state and pseudo-steady-states experiments.

Other aspects of reactor performance are shown in Table 16. For comparison, data in the first column are steady-state results without NG loading, which was shown in Table 15. Table 16 shows that the reactor performance for removing toluene was only minimally affected by NG for the amount of NG treated. This minimal impact probably occurred because only two electrons are needed to transform NG to GDN, while every molecule of toluene can generate 36 electrons when completely oxidized to CO_2 . Since the total NG loading was small compared to the toluene loading, the number of electrons used by cometabolism of NG was only a small portion of the total number of electrons released from toluene. Table 16 shows that only 0.23 percent of the electrons released from toluene was needed to reduce NG to GDN and GMN.

Table 16. Circulating-bed reactor performance during NG-removal experiments.

NG in Liquid Feed (μM)	None	22.0	44.1	66.1
Toluene Loading ($\text{mol}/\text{m}^2\text{-day}$)	0.059	0.059	0.059	0.059
Suspended Biomass (mg/l)	44	44	48	36
Toluene in Liquid Effluent (mg/l)	1.4	1.6	1.0	1.6
Toluene in Gas Effluent (mg/l)	0.36	0.39	0.37	0.40
COD in Liquid Effluent (mgCOD/l)	6.8	8.7	12	14
Dissolved Oxygen (DO) (ppm)	3.2	3.2	3.1	3.0
Reactor Liquid Temperature ($^{\circ}\text{C}$)	21	21	21	21
Toluene Removal (%)	91	90	91	90
% of electrons used by denitration reaction to GDN and GMN	0.00	0.12	0.21	0.23

The increase of COD in the reactor effluent was primarily caused by the increase of NG loading. Based on their molecular formula, the COD for NG, GDN, and GMN are 0.28 mgCOD/mgNG, 0.44 mgCOD/mgGDN, and 0.70 mgCOD/mgGMN, respectively. Using the measured steady-state COD value when no NG was fed (6.8 mgCOD/L) and the concentrations of NG/GDN/GMN in the effluent at the three NG loading rates, the effluent total CODs were calculated to be 8.3 mgCOD/L, 9.8 mgCOD/L, and 11 mgCOD/L, respectively. These values are only 0.34 mgCOD/L, 1.8 mgCOD/L, and 2.9 mgCOD/L lower than the measured COD values in the effluent, respectively. The differences in COD may have been caused by small increases in toluene intermediates in the effluent because of the cometabolic reactions or inhibition effects.

Table 16 also shows that the DO concentration decreased slightly when the NG loading increased. Since the toluene removal hardly changed at these loading rates and NG denitration did not require oxygen as a cosubstrate, the lowered DO values at higher NG loading rates suggest that an additional source of electrons might be present. One possibility was that glycerol might be formed from GMN denitration in the circulating bed and subsequently oxidized. Because the biomass in the circulating-bed reactor had been fed with NG for 1 wk when the pseudo-steady-state experiments began, the biomass might have adapted to degrade NG completely. However, the soluble COD values computed using the estimated GMN concentration suggest that the GMN remained undegraded.

Summary

In summary, prior studies of NG denitration by various bacterial cultures suggest that many organisms have the ability to degrade the xenobiotic compound NG and its denitrated intermediates. Most of the bacterial cultures did not use NG as a carbon and electron source, but used it cometabolically. The nitrite released from NG degradation could serve as a nitrogen source for biomass growth.

The circulating-bed biofilm reactor inoculated with *P. putida* F1 could remove NG immediately upon its addition, and steady-state removal was approximately 28 to 40 percent, depending on the NG loading rates. Only about one half of the NG transformed accumulated as GDN, and the large biofilm accumulation in the carrier is implicated as the reason that significant transformation occurred beyond GDN.

7 Conclusions and Practical Implications

Using biofilm reactors to treat VOC-contaminated waste gas streams has gained tremendous attention in recent years. However, the kinetic fundamentals of the process are still being explored, particularly because of the complex nature of the biodegradation reactions involved and the interactions among the VOCs being removed. Using BTX as the model VOCs and *P. putida* F1 as the model bacterial culture, this study investigated the removals of BTX from gas streams in a three-phase circulating-bed biofilm reactor. The following main conclusions can be drawn from the results of this study.

Hydrodynamic experiments of the circulating-bed reactor confirmed that the carriers and bulk liquid were well mixed in the reactor. The characteristic of oxygen gas-liquid mass transfer in the reactor was similar to that in other similarly designed circulating-bed reactors. DO concentrations in the liquid indicated that oxygen in the gas and liquid was not at equilibrium. The VOCs (BTX) in the gas and liquid phases, on the other hand, were at equilibrium throughout the study. Therefore, although the removals of BTX and oxygen in the reactor drive their gas-liquid mass transfers, the gas-liquid mass transfer of BTX was fast relative to their removals, while potentially the gas-liquid mass transfer of oxygen could be rate limiting to the BTX removals.

The suspended biomass was subjected to short-term loading shocks because it was not protected from washout, but it was always less than 1 percent of the total biomass in the reactor. The biofilm accumulation in the carriers increased proportionally to the COD loading rates during the first three steady states, and was near constant in the next five steady states when the COD loading was constant. In this study, higher biofilm accumulation in the carriers showed adverse effects on reactor performance. A reduction in toluene and COD removal can be attributed to the increased oxygen demand due to biomass respiration.

When toluene was the sole substrate in the circulating-bed biofilm reactor, its removals were most strongly controlled by oxygen. When oxygen loading was insufficient or toluene was overloaded, the toluene removals decreased dramatically, and significant concentrations of toluene and its intermediates accumulated in the effluent. On the other hand, the removals of the toluene intermediate were most strongly controlled by noncompetitive inhibition from toluene.

Consequently, lowered oxygen or increased toluene loading in the reactor caused accumulation of toluene in the bulk liquid phase, which in turn forced more toluene intermediate to be removed inside the biofilm, where inhibition from toluene was relieved. A change in direction for the intermediate mass flux from out of to into the biofilm demonstrated the biofilm's protection role. The suspended biomass contributed to the removals of toluene and its intermediate, therefore, could not be neglected. The suspended biomass played its most important role when oxygen limitation was significant, because the suspended biomass was less affected by diffusion limitation.

When toluene and benzene or toluene and *p*-xylene were removed simultaneously in the circulating-bed biofilm, their inhibition to each other forced more VOCs to be removed inside the biofilm. In this case, biofilm provided protection for metabolism of the VOCs and their intermediates from substrate inhibition at higher concentrations. Because the inhibition among BTX was truly competitive, the compound present at the lower concentration was affected more by the stronger inhibition from the compound at higher concentration. Consequently, a higher fraction of the low-concentration VOC was removed in the biofilm than the high-concentration one. Because the *p*-xylene intermediate was not degraded in the reactor, the removal efficiencies for COD were worse than that for the VOCs. Because of these complex interactions among the substrates, intermediates, and total COD, the concentrations of COD and individual VOCs should be monitored.

In this study, a removal "capacity" was observed in the reactor above which the reactor performance did not increase with increased loading rates. For example, when toluene was used as the sole substrate and the gas stream was 100 percent air, the highest removal toluene fluxes into the biofilm (surface removal rate) were 0.080, 0.058, and 0.051 mol/m²-day for Ss1-Ss3, respectively. In units of g/m³-h, the biofilm removal capacities were 81, 58, and 52 g/m³-h for Ss1-Ss3, respectively. Since some toluene also was removed in the liquid phase, the total removals in the reactor were slightly higher. These capacities were in the upper range of values found in many fixed-bed biofilters treating toluene. Pedersen and Arvin (1997) summarized the toluene removal capacities for nearly a dozen fixed-bed biofilters published in literature and found the toluene removal capacities varied from 9 to 80 g/m³-h. Compared with fixed-bed biofilm reactors, the circulating-bed design offers great advantages of no bed clogging due to excess biomass growth and easy management of biofilm surface area, both of which are important in maintaining long-term stable and consistent operation of the biofilm system.

Lowering the biofilm accumulation and/or increasing the total surface area of the carriers can enhance the removal capacity of the circulating-bed biofilm reactor. Compared to fixed-bed biofilters, one significant advantage to the circulating-bed is that the total biofilm surface can be easily controlled by the carrier size and amount of carriers loaded. In a fixed-bed biofilter, excess growth of biomass can clog the spaces among the carriers and lower the total biofilm surface area available. Because the biofilm surface was a constant in this study, the biofilm activity in the reactor was stable and behaved consistently during the several months of continuous operation with periodic short-term loading shocks of single or dual substrates. Therefore, the reactor design used in this study is suitable for studying the biofilm kinetics or removing VOC-contaminated gas streams in practice.

In practice, the contaminated gas streams seldom contain a single substrate. BTX degradation is a good example in which the substrates are of different types, either electron donating or cometabolic, and interact with each other during reaction. The results of this study provide the insights needed on how these different types of compounds are removed and the critical issues for improvements in reactor performance. Since the removal efficiencies for each compound are usually different and some compounds may not degrade completely, removals of both COD and individual substrates should be monitored to better assess the reactor performance.

The bacterial culture used in this study, *P. putida* F1, can reduce NG with the presence of a primary electron donor substrate, such as toluene. During the denitration of NG, its partially denitrated compounds of GDN and probably GMN accumulated in the reactors. In the circulating-bed biofilm reactor, NG was degraded immediately upon its addition, and steady-state removal was approximately 28 to 40 percent, depending on the NG loading rates. NG degradation consumed only a small fraction of the electrons released by toluene degradation. Only about one-half of the NG transformed accumulated as GDN, and the large biofilm accumulation in the carrier is implicated as the reason that significant denitration reduction occurred beyond GDN.

References

- American Public Health Association (APHA) *Standard Methods for the Examination of Water and Wastewater*, 19th ed. A.D. Eaton, L.S. Cleseri, and A.E. Greenberg, eds. (APHA, Washington, DC 1995).
- Bae, W., "Modeling Dual-Limitation Kinetics Incorporating Intracellular Cofactor Responses," Ph.D. Thesis (University of Illinois at Urbana-Champaign, 1992).
- Bhaumik, S., C. Christodoulatos, G.P. Korfiatis, and B.W. Brodman, "Aerobic and anaerobic biodegradation of nitroglycerin in batch and packed bed bioreactors," *Wat. Sci. Technol.*, Vol. 36 (1997), pp 139-146.
- Bhaumik S., C. Christodoulatos, B.W. Brodman, and N. Pal, "Biodegradation of glycerol trinitrate by activated sludge: Cosubstrate requirements, inhibition, and kinetics," *J. Environ. Sci. Heal. A*, Vol 33 (1998), pp 547-571.
- Blehert, D.S., K.L. Knoke, B.G. Fox, and G.H. Chambliss, "Regioselectivity of nitroglycerin denitration by flavoprotein nitroester reductases purified from two *Pseudomonas* species," *J. Bacteriol.*, Vol 179 (1997), pp 6912-6920.
- Bohn, N., "Consider biofiltration for decontaminating gases," *Chem. Eng. Prog.*, Vol 88, No 4 (April 1992), pp 34-40.
- Chisti, M.Y. and M. Moo-Young, "Airlift reactors: characteristics, applications and design considerations," *Chem. Eng. Commun.*, Vol 60 (1987), pp 195-242.
- Chisti, M.Y., B. Halard, and M. Moo-Young, "Liquid circulation in airlift reactors," *Chem. Eng. Sci.*, Vol 43 (1988), pp 451-457.
- Christodoulatos, C., S. Bhaumik, and B.W. Brodman, "Anaerobic biodegradation of nitroglycerin," *Wat. Res.*, Vol 31 (1997), pp 1462-1470.
- Deckwer W.-D., R. Burckhar, and G. Zoll, "Mixing and mass transfer in tall bubble columns," *Chem. Eng. Sci.*, Vol 29 (1974), pp 2177-2188.
- Doran, P.M., *Bioprocess Engineering Principles* (Academic Press, London, 1995).
- Ducrocq, C., C. Servy, and M. Lenfant, "Bioconversion of glyceryl trinitrate into mononitrates by *Geotrichum candidum*," *FEMS Microbiol. Let.*, Vol 65 (1989), pp 219-222.

- Ducrocq, C., C. Servy, and M. Lenfant, "Formation of glyceryl 2-mononitrate by regioselective bio-conversion of glyceryl trinitrate: efficiency of the filamentous fungus *Phanerochaete chrysosporium*," *Biotech. Appl. Biochem.*, Vol 12 (1990), pp 325-330.
- Fan, L.-S. *Gas-Liquid-Solid Fluidization Engineering* (Butterworths, Boston, 1989).
- Fouhy, K. "Cleaning waste gas, naturally," *Chem. Eng.* (McGraw-Hill, New York, 1992), pp 41-46.
- Goto, S., Y. Matsumoto, and P. Gaspillo, "Mass transfer and reaction in bubble column slurry reactor with draft tube," *Chem. Eng. Commun.*, Vol 85 (1989), pp 181-191.
- Heijnen, J.J., M.C.M. van Loosdrecht, R. Mulder, R. Weltevrede, and A. Mulder, "Development and scale-up of an aerobic biofilm air-lift suspension reactor," *Wat. Sci. Technol.*, Vol 27 (1993), pp 253-261.
- Jaeger, B. and J. Jager, "Geruchshekaempfung in Kompostwerken am Beispiel Heidelberg," *Muell und Abfall* (February 1978), pp 48-52.
- Jutras, E.M., C.M. Smart., R. Rupert, I.L. Pepper, and R.M. Miller, "Field-scale biofiltration of gasoline vapors extracted from beneath a leaking underground storage tank," *Biodegradation*, Vol 8 (1997), pp 31-42.
- Koide, K., H. Sato, and S. Iwamoto, "Gas holdup and volumetric liquid-phase mass transfer coefficient in bubble column with draught tube and with gas dispersion into annulus," *J. Chem. Eng. Japan*, Vol 16 (1983a), pp 407-413.
- Koide, K., H. Sato, and S. Iwamoto, "Gas holdup and volumetric liquid-phase mass transfer coefficient in bubble column with draught tube and with gas dispersion into tube," *J. Chem. Eng. Japan*, Vol 16 (1983b), pp 413-419.
- Leson, G. and A.M. Winer, "Biofiltration: an innovative air pollution control technology for VOC emissions," *J. Air Waste Manag. Assoc.*, Vol 41 (1991), pp 1045-1054.
- Malmstead, M.J., F.J. Brockman, A.J. Valocchi, and B.E. Rittmann, "Modeling biofilm biodegradation requiring cosubstrates: the quinoline example," *Wat. Sci. Technol.*, Vol 31 (1995), pp 71-84.
- Meng, M., W.Q. Sun, L.A. Geelhaar, G. Kumar, A.R. Patel, G.F. Payne, M.K. Speedie, and J.R. Stacy, "Denitration of glycerol trinitrate by resting cells and cell extracts of *Bacillus thuringiensis/cereus* and *Enterobacter agglomerans*," *Appl. Environ. Microbiol.*, Vol 61 (1995), pp 2548-2553.
- Miyahara, T., M.S. Lee, and T. Takahashi, "Mass transfer characteristics of a three-phase fluidized bed containing low-density and/or small particles," *Int. Chem. Eng.*, Vol 33 (1993), pp 680-686.
- Moretti, E.C. and N. Mukhopadhyay, "VOC control: current practices and future trends," *Chem. Eng. Prog.*, Vol 89, No. 7 (1993), pp 20-26.

- Muroyama K., Y. Mitani, and A. Yasunishi, "Hydrodynamic characteristics and gas-liquid mass-transfer in a draft-tube slurry reactor," *Chem. Eng. Commun.*, Vol 34 (1985), pp 87-98.
- Nore, O., C.L. Briens, A. Margaritis, and G. Wild, "Hydrodynamics, gas-liquid mass transfer and particle-liquid heat and mass transfer in a three-phase fluidized bed for biochemical process applications," *Chem. Eng. Sci.*, Vol 47 (1992), pp 3573-3580.
- Ottengraf, S.P.P. "Biological systems for waste gas elimination," TIBTECH, Vol 5 (1987), pp 132-136.
- Parsons, F., G. Barrio-Lage, and R. Rice, "Biotransformation of chlorinated organic solvents in static microcosm," *Environ. Toxicology Chem.*, Vol 4 (1985), pp 739-742.
- Pedersen, A.R. and E. Arvin, "Removal of toluene in waste gases using a biological trickling filter," *Biodegradation*, Vol 6 (1995), pp 109-118.
- Pedersen, A.R. and E. Arvin, "Toluene removal in a biofilm reactor for waste gas treatment," *Wat. Sci. Technol.*, Vol 36 (1997), pp 69-76.
- Pesari, H. and D. Grasso, "Biodegradation of an inhibitory nongrowth substrate (nitroglycerin) in batch reactors," *Biotechnol. Bioeng.*, Vol 41 (1993), pp 79-87.
- Rittmann, B.E., and P.L. McCarty, "Substrate flux into biofilms of any thickness," *J. Environ. Eng. ASCE*, Vol 107 (1981), pp 831.
- Ruddy, E.N., and L.A. Carroll, "Select the best VOC control strategy," *Chem. Eng. Prog.*, Vol 89, No. 7 (July 1993), pp 20-26.
- Seagren, E., "Quantitative Evaluation of Flushing and Biodegradation for Enhancing in situ Dissolution of Nonaqueous-phase Liquids," PhD Thesis, Department of Civil Engineering (University of Illinois at Urbana-Champaign, 1994).
- Servent, D., C. Ducrocq, Y. Henry, A. Guissani, and M. Lenfant, "Nitroglycerin metabolism by *Phanerochaete chrysosporium*: evidence for nitric oxide and nitrite formation," *Biochem. Biophys. Acta*, Vol 1074 (1991), pp 320-325.
- Servent, D., C. Ducrocq, Y. Henry, C. Servy, and M. Lenfant, "Multiple enzymatic pathways involved in the metabolism of glyceryl trinitrate in *Phanerochaete chrysosporium*," *Biotechnol. Appl. Biochem.*, Vol 15 (1992), pp 257-266.
- Shields, M.S., S.O. Montgomery, P.J. Chapman, S.M. Cuskey, and P.H. Pritchard, "Novel pathway of toluene catabolism in the trichloroethylene-degrading bacterium G4," *Appl. Environ. Microbiol.*, Vol 55 (1989), pp 1624-1629.

- Shishido, M. and M. Toda, "Apparent zero-order kinetics of phenol biodegradation by substrate-inhibited microbes at low substrate concentrations," *Biotechnol. Bioeng.*, Vol 50 (1996), pp 709-717.
- Smet, E., VanLangehove H. and Verstraete W. "Long-term stability of a biofilter treating dimethyl sulphide," *Appl. Microbiol. Biotechnol.*, Vol 46 (1996), pp 191-196.
- Standefer, S., and C. van Lith, "Biofilters minimize VOC emissions," *Environ. Protection* (March 1993), pp 48-58.
- Swanson, W.J., and R.C. Loehr, "Biofiltration: fundamentals, design and operations principles, and applications," *J. Environ. Eng.*, Vol 123 (American Society of Chemical Engineers, 1997), pp 538-546.
- Tchobanoglous, G., and F. Burton, *Waste Water Engineering: Treatment, Disposal, and Reuse*. (McGraw-Hill Inc., New York, 1991).
- Vaart, D.R., van der, M.W. Vatauvuk, and A.H. Wehe, "The Cost Estimation of Thermal and Catalytic Incinerators for the Control of VOCs," *J. Air Waste Mgmt. Assn.*, Vol 41, No. 4 (April 1991), pp 497-501.
- Webster, T.S., J.S. Devanny, E.M. Torres, and S.S. Basrai, "Biofiltration of odors, toxic and volatile organic compounds from publicly owned treatment works," *Environ. Prog.*, Vol 15, No. 3 (March 1996), pp 141-147.
- Wendt, T.M., J.H. Cornell, and A.M. Kaplan, "Microbial degradation of glycerol nitrates," *Appl. Environ. Microbiol.*, Vol 36, No.5 (1978), pp 693-699.
- White, G.F., and J.R. Snape, "Microbial cleavage of nitrate esters: defusing the environment," *J. General Microbiol.*, Vol 139 (1993), pp 1947-1957.
- White, G.F., J.R. Snape, and S. Nicklin, "Biodegradation of glycerol trinitrate and pentaerythritol tetranitrate by *Agrobacterium radiobacter*," *Appl. Environ. Microbiol.*, Vol 62 (1996), pp 637-642.
- Yu, H., "Kinetics of Removing Volatile Organic Compounds from Gas Streams Using Three-Phase Biofilm Reactors," Ph.D. dissertation (Northwestern University, Evanston, IL, 1998).
- Zhang, Y.Z., S.T. Sandaram, A. Sharma, and B.W. Brodman, "Biodegradation of glyceryl trinitrate by *Penicillium corylophilum* Dierckx," *Appl. Environ. Microbiol.*, Vol 63 (1997), pp 1712-1714.

CERL Distribution

Chief of Engineers

ATTN: CEHEC-IM-LH (2)
ATTN: HECSA Mailroom (2)
ATTN: CECC-R
ATTN: CERD-L
ATTN: CERD-M

Commander ERDC, Vicksburg, MS

ATTN: Coastal and Hydraulics Lab, Vicksburg
ATTN: Cold Regions Research, Hanover, NH
ATTN: Environmental Lab, Vicksburg
ATTN: Geotechnical Lab, Vicksburg
ATTN: Information Technology Lab, Vicksburg
ATTN: Structures Lab, Vicksburg
ATTN: Topographic Engineering Center, Alexandria, VA

Defense Tech Info Center 22304

ATTN: DTIC-O (2)

17
1/00

REPORT DOCUMENTATION PAGE

Form Approved
OMB No. 0704-0188

Public reporting burden for this collection of information is estimated to average 1 hour per response, including the time for reviewing instructions, searching existing data sources, gathering and maintaining the data needed, and completing and reviewing the collection of information. Send comments regarding this burden estimate or any other aspect of this collection of Information, including suggestions for reducing this burden, to Washington Headquarters Services, Directorate for Information Operations and Reports, 1215 Jefferson Davis Highway, Suite 1204, Arlington, VA 22202-4302, and to the Office of Management and Budget, Paperwork Reduction Project (0704-0188), Washington, DC 20503.

1. AGENCY USE ONLY (Leave Blank)		2. REPORT DATE April 2000	3. REPORT TYPE AND DATES COVERED Final		
4. TITLE AND SUBTITLE Treatment of Volatile Organic Compounds From Gas Streams Using a Three-Phase Circulating-Bed Biofilm Reactor			5. FUNDING NUMBERS 62720 D048 U29		
6. AUTHOR(S) Byung Kim, Haibo Yu, and Bruce E. Rittman					
7. PERFORMING ORGANIZATION NAME(S) AND ADDRESS(ES) U.S. Army Construction Engineering Research Laboratory (CERL) P.O. Box 9005 Champaign, IL 61826-9005			8. PERFORMING ORGANIZATION REPORT NUMBER TR 00/9		
9. SPONSORING / MONITORING AGENCY NAME(S) AND ADDRESS(ES) U.S. Army Corps of Engineers (USACE) ATTN: CERD 20 Massachusetts Avenue, NW Washington, DC 20314-1000			10. SPONSORING / MONITORING AGENCY REPORT NUMBER		
9. SUPPLEMENTARY NOTES Copies are available from the National Technical Information Service, 5385 Port Royal Road, Springfield, VA 22161.					
12a. DISTRIBUTION / AVAILABILITY STATEMENT Approved for public release; distribution is unlimited.			12b. DISTRIBUTION CODE		
13. ABSTRACT (<i>Maximum 200 words</i>) This study focuses on the biofilm kinetics of removing benzene, toluene, and ρ -xylene (BTX) from gas streams in a three-phase circulating-bed reactor using porous carriers. In the biofilm reactor, gas-liquid equilibrium existed for BTX, but not for oxygen. Oxygen was consumed as a cosubstrate in the oxygenation reactions and the terminal electron acceptor during respiration. When toluene was the sole substrate, oxygen mostly controlled its removals, and toluene inhibition mostly controlled the removals of the toluene intermediate. With increased toluene or decreased oxygen loading, more toluene intermediate was removed inside the biofilm, and the intermediate mass flux changed in direction from out-of to into the biofilm. The mass transfer resistance in the biofilm relieved the intermediate from toluene inhibition. However, higher biofilm accumulation showed adverse effects on reactor performance due to increased demand for oxygen for respiration. The suspended biomass contributed to the removals of toluene and its intermediate and played its most important role when oxygen limitation was significant. When toluene/benzene or toluene/ ρ -xylene were removed simultaneously, their inhibition forced more volatile organic compounds to be removed inside the biofilm, where mass transfer resistance relieved the inhibition effects. The removal efficiencies for the lower-concentration compound were smaller.					
14. SUBJECT TERMS volatile organic compounds emissions Clean Air Act			15. NUMBER OF PAGES 100		
			16. PRICE CODE		
17. SECURITY CLASSIFICATION OF REPORT Unclassified			18. SECURITY CLASSIFICATION OF THIS PAGE Unclassified	19. SECURITY CLASSIFICATION OF ABSTRACT Unclassified	20. LIMITATION OF ABSTRACT SAR